Inaugural dissertation

Elucidating the Functional Relevance of BAP1 in the Liver

Submitted to the
Combined Faculty of Mathematics, Engineering and Natural Sciences
of the Ruprecht – Karls – University Heidelberg
for the degree of
Doctor of Natural Sciences

Olatunji Oluwole Gege, M Sc.

2021

Inaugural dissertation

for

obtaining the doctoral degree

of the

Combined Faculty of Mathematics, Engineering and Natural Sciences

of the

Ruprecht – Karls – University

Heidelberg

Presented by

M. Sc., Olatunji Oluwole Gege

Born in: Ori-Opo, Ondo State, Nigeria

Oral Examination: 14th March 2022

Elucidating the Functional Relevance of BAP1 in the Liver

Referees: Prof. Dr. Michael Boutros

Prof. Dr. Darjus Felix Tschaharganeh

For Bamijoko

My mother, an immovable pillar of support.

Summary

Prognosis for primary liver cancer remain poor due to a combination of factors including late presentation of disease, genetic heterogeneity and ineffective therapies. Therefore, there is an urgent need to disentangle genetic heterogeneity by characterizing individual mutations and investigating potential vulnerabilities that these mutations may harbor. *BAP1* inactivation is one of the most common genetic alterations in liver cancer with prevalence up to 25% in intrahepatic Cholangiocarcinoma (iCCA) and up to 7% in Hepatocellular Carcinoma (HCC), indicating a potential role in these diseases. BAP1 is an epigenetic modifier that deubiquitinates the mono-ubiquitinated K119 residue on histone 2A. In addition to its deubiquitinase activity, BAP1 also contains a HBM motif that mediates the interaction with host cell factor-1 (HCF-1), O-linked N-acetylglucosamine transferase (OGT), and the polycomb group proteins ASXL1 and ASXL2 and thus is a central point for epigenetic regulation. However, despite its functional properties and mutational prevalence in liver cancer, the role of BAP1 in the liver remains unknown. In order to dissect the functional relevance of BAP1 in the liver, I employed Tet-regulatable shRNA mouse strains and *in-vivo* CRISPR/Cas9 technology as well as *in-vitro* models of *BAP1* depletion in this study.

Surprisingly, liver specific *Bap1* depletion (using shRNAs) in dietary models of metabolic distress (CD-HFD and HFD) led to acute fatality and severe hepatic injury characterized by elevated serum transaminases (ALT and AST) and Bilirubin, as well as TUNEL positive hepatocytes. Conversely, endogenous restoration of *Bap1* rescued fatality and attenuated liver damage, thereby highlighting the importance of BAP1 in this process. Transcriptional profiling and lipidomics analyses revealed elevated unfolded protein response pathway and dysregulated fatty acid metabolism upon *Bap1* depletion under metabolic stress.

Moreover, to elucidate the role of BAP1 in liver tumorigenesis and liver plasticity, I combined *Bap1* loss with other prevalent oncogenic events in liver cancer *in-vivo* by hydrodynamic tail vein injection. In contrast to the observations in non-tumorigenic livers, *Bap1* loss accelerated liver tumorigenesis in combination with *Pten*-deficiency and enforced YAP expression (YAP^{S127A}) resulting in HCC like tumors. Furthermore, *Bap1* loss also co-operated with YAP^{S127A} alone to drive liver tumorigenesis, thereby reinforcing the notion that BAP1 is a bonafide liver tumor suppressor. Similarly, a cocktail comprising *Bap1* loss in combination with *Arid1a* loss and YAP^{S127A}, delivered to murine hepatocytes resulted in a phenotypic switch and liver cancer lineage reprograming exemplified by tumors bearing hallmarks of iCCA, thereby implicating BAP1 in liver cancer plasticity. Additionally, BAP1

deficiency (in tumorigenic and non-tumorigenic livers) was demonstrated to inversely correlate with strong CHOP (ER stress sensor) expression, thus providing a molecular hallmark and point of convergence for BAP1 deficiency in liver pathologies.

Finally, using *in-vivo* and *in-vitro* models, I identified BAP1 deficiency as a therapeutic vulnerability in *TP53* depletion driven tumors. This highlighted the unexpected utility of a tumor suppressor as a genotype specific therapy in liver cancer.

Together, the results from this study implicate BAP1 as a critical determinant of hepatic survival in metabolic distress states, as well as a bonafide liver tumor suppressor. Furthermore, BAP1 deficiency was unraveled as a therapeutic vulnerability in *TP53* null tumors. Thus, this study unveils previously undiscovered context dependent functions of BAP1 in the liver.

Zusammenfassung

Die Prognosen für primären Leberkrebs sind nach wie vor schlecht, was auf eine Kombination von Faktoren wie das späte Auftreten der Krankheit, genetische Heterogenität und unwirksame Therapien zurückzuführen ist. Daher ist es nötig diese genetische Heterogenität aufzuklären, indem wiederkehrende Mutationen charakterisiert werden und potenzielle Schwachstellen zu untersuchen, die diese Mutationen mit sich bringen. *BAP1*-Inaktivierung ist eine der häufigsten genetischen Veränderungen bei Leberkrebs mit einer Prävalenz von bis zu 25 % beim intrahepatischen Cholangiokarzinom (iCCA) und bis zu 7 % beim hepatozellulären Karzinom (HCC), was auf eine wichtige Rolle von BAP1 bei diesen Erkrankungen hinweist. BAP1 ist ein epigenetischer Modifikator, der den mono-ubiquitinierten K119-Rest auf Histon 2A deubiquitiniert. Neben seiner Deubiquitinase-Aktivität enthält BAP1 auch ein HBM-Motiv, das die Interaktion mit dem Wirtszellfaktor-1 (HCF-1), der O-gebundenen N-Acetylglucosamin-Transferase (OGT) und den Polycomb-Gruppenproteinen ASXL1 und ASXL2 vermittelt und somit einen zentralen Punkt für die epigenetische Regulierung darstellt. Trotz seines funktionellen Profils und der Häufigkeit von Mutationen bei Leberkrebs ist die Rolle von BAP1 in der Leber jedoch nach wie vor unbekannt. Um die funktionelle Bedeutung von BAP1 in der Leber zu untersuchen, habe ich in dieser Studie Tet-regulierbare shRNA-Mausstämme und in-vivo CRISPR/Cas9-Technologie sowie in-vitro-Modelle der *BAP1*-Depletion eingesetzt.

Überraschenderweise führte die leberspezifische *Bap1*-Depletion (mit shRNAs) in Ernährungsmodellen mit Fettstoffwechselstörungen (CD-HFD und HFD) zu akuter Morbidität und schweren Leberschäden, die durch erhöhte Serumtransaminasen (ALT und AST) und Bilirubin sowie TUNEL-positive Hepatozyten gekennzeichnet waren. Umgekehrt konnte durch die endogene Reaktivierung von BAP1 diese Morbidität reversiert werden und die Leberschädigung abgeschwächt werden, was die Bedeutung von BAP1 in diesem Prozess unterstreicht. Transkriptionelles Profiling und Lipidomics-Analysen zeigten eine verstärkte Aktivierung des Unfolded-Protein-Response-Signalweges und einen dysregulierten Fettsäurestoffwechsel nach *Bap1* Depletion, welche ursächlich für den Leberschaden waren.

Um die Rolle von BAP1 bei der Lebertumorentstehung und der Leberplastizität aufzuklären, wurde der BAP1-Verlust mit anderen onkogenen Ereignissen bei Leberkrebs in-vivo durch eine hydrodynamische Schwanzveneninjektion kombiniert. Im Gegensatz zu den Beobachtungen in nicht-tumorigenen Lebern beschleunigte *Bap1* in Kombination mit *Pten*-Knockout und YAP-Überexpression (YAP^{S127A}) die Lebertumorigenese. Zudem führte der

Verlust von *Bap1* mit YAPS127A Überexpression auch zur Lebertumorentstehung, was die Vermutung untermauert, dass BAP1 ein Tumorsuppressorgen in der Leber ist. In ähnlicher Weise führte die Kombination aus dem Verlust von *Bap1* mit dem Verlust von *Arid1a* und YAP^{S127A} Überexpression zu einer phänotypischen Veränderung der Lebertumore, die nun Merkmale von iCCA aufwiesen. Diese Beobachtung deutet darauf hin, dass BAP1 an der Plastizität von Leberkrebs beteiligt ist. Darüber hinaus wurde nachgewiesen, dass ein BAP1-Mangel (in tumorigener und nicht-tumoriger Leber) mit einer starken CHOP-Expression(ER-Stress-Sensor) korreliert, was ein molekulares Merkmal für einen BAP1-Mangel in den jeweiligen Leberpathologien darstellt.

Darüber hinaus habe ich mit Hilfe von In-vivo- und In-vitro-Modellen festgestellt, dass der Mangel an BAP1 eine therapeutische Schwachstelle in *TP53*-depletierten Tumoren darstellt. Dies zeigt den unerwarteten Nutzen eines Tumorsuppressors als genotypspezifische Therapie bei Leberkrebs.

Insgesamt weisen die Ergebnisse dieser Studie darauf hin, dass BAP1 ein entscheidender Faktor für die Homöostase der Leber bei Stoffwechselstörungen und als Tumorsupressor in der Leber fungiert. Darüber zeigt diese Studie, dass der Verlust von BAP1 die Spezifizierung der Tumordifferenzierung in Kombination mit bestimmten genetischen Veränderungen beeinflusst. Schließlich konnte überraschenderweise BAP1 als eine therapeutische Schwachstelle in *TP53*-defizienten Tumoren aufgedeckt werden. Somit enthüllt diese Studie bisher unentdeckte kontextabhängige Funktionen von BAP1 in der Leber.

Table of Contents

List of Tables

List of Figures

List of Abbreviations

Abbreviation	Full meaning
ALB	Albumin
ALD	Alcoholic liver disease
ALT	Alanine transaminase
AST	Aspartate transaminase
ASXL1/2	Additional sex combs-like proteins
Atf3	Activating transcription factor 3
BAP1	BRCA1 associated protein 1
BAP1-TPDS	BAP1 tumor predisposition syndrome
BARD1	BRCA1 associated ring domain protein1
BCLC	Barcelona clinic liver cancer
CCL4	Carbon tetrachloride
CD-HFD	Choline deficient high fat diet
CHOP	C/EBP homologous protein
CK19	Cytokeratin 19
CMCP	Center for model system and comparative pathology
CRISPR	Clustered regularly interspaced short palindromic repeats (CRISPR)
CTD	The C-terminal domain
CTNNB1	B-catenin
DAG	Diacylglycerols
DEN	N-nitrosodiethylamine
DGAT2	Diacylglycerol o-acyltransferase 2
DMEM	Dulbecco’s modified eagle medium
Dox	Doxycycline
DUB	Deubiquitinase
ECM	Extracellular matrix
EGF II	Epidermal growth factor

ER	Endoplasmic reticulum
ES	Embryonic stem cells)
FBS	Fetal bovine serum
FDA	The food and drug administration
FGF	Fibroblast growth factor
FGFR2	Fibroblast growth factor receptor 2
GEMMs	Genetically engineered mouse models
GFP	Green fluorescence protein
GS	Gomori methenamine silver stainings
GSEA	Gene set enrichment analysis
H&E	Hematoxylin and eosin
HBV	Hepatitis B virus
HCC	Hepatocellular carcinoma
HCF-1	Host cell factor
HCV	Hepatitis C virus
HDTVI	Hydrodynamic tail vein injection
HFD	High fat diet
HGF	Hepatocyte growth factor
HNF4α	Hepatocyte nuclear factor 4 alpha
HSCs	Hepatic stellate cells
iCCA	Intrahepatic cholangiocarcinoma
IGF	Insulin-like growth factor
IHC	Immunohistochemistry
IL-4	Interleukin 4
IL-6	Interleukin 6
IPA	Ingenuity pathway analysis
LB	Luria Bertani
LSECs	Liver sinusoidal endothelial cells
MALFD	Metabolic associated fatty liver disease
MMPs	Matrix metalloproteinases

MPM	Malignant pleural mesothelioma
MRI	Magnetic resonance imaging
myrAKT	Myristoylated AKT
NAFLD	Non-alcoholic fatty liver disease
NASH	Non-alcoholic steatohepatitis
NICD	Notch intracellular domain
NLS	Nuclear localization signal
OGT	O-linked N-acetylglucosamine transferase
PcG	Polycomb group proteins
PDGF	Platelet-derived growth factor
PEI	Polyethylenimine
PFA	Paraformaldehyde
PNK	T4 polynucleotide kinase
PR-DUB)	Polycomb group repressor deubiquitinase
PTEN	Phosphatase and tensin homolog
RFA	Radiofrequency ablation
RPM	Revolutions per minute
RNAseq	RNA sequencing (rnaseq)
RT qPCR	Real time Quantitative PCR RT qpcr
rtTA	Reverse tet-transactivator
SB	Sleeping beauty
sgRNAs	Short guide rnas (sgrnas)
shRNA	Short hairpin RNA)
TAG	Triacylglycerol
TBS	Tris buffered saline)
TBS-T	Tris buffered saline with tween 20
TERT	Telomerase reverse transcriptase
TNF	Tumor necrosis factor
TP53	Tumor protein 53
TRE	Tetracycline regulatory element

Trp53	Transformation related protein
TSGs	Tumor suppressor genes
TUNEL	Terminal deoxynucleotidyl transferase (tdt) dutp Nick-End Labeling
UCH	Ubiquitin C-terminal hydrolase
UM	Uveal melanoma
UPR	Unfolded protein response (UPR)
VEGF	Angiogenesis (Vascular endothelial growth factor
VEGFR	Vascular endothelial growth factor receptor
VLDL	Very low-density lipoprotein
WB	Western blot
WD	Western diet
WT	Wild-type
YAP	Yes associated protein
YY1	Ying yang 1

1 Introduction

1.1 Functional anatomy of the liver

The largest internal organ of the body, the cone shaped liver is an important node of control for metabolic (anabolic and catabolic) processes and excretion of toxic metabolites[1]. Critically, it functions in the control, regulation and detoxification of absorbed substances from the digestive tract before onward distribution to the systemic circulation[2]. Aside its parenchymal cells, the hepatocytes and cholangiocytes, the liver comprises a plethora of other cells types such as kupffer cells, stellate cells and liver sinusoidal endothelial cells (LSECs)[1].

1.1.1 Parenchymal and non-parenchymal cells of the liver

Hepatocytes, are considered the basic structural component of the liver[3].They constitute the bulk of cells resident in the liver by total cell count (>60%) and by volume (80%). They mediate the canonical liver functions of metabolism and detoxification as well as protein synthesis and innate immunity. They are uniquely equipped to function as cellular factories, possessing mitochondria and endoplasmic reticulum in abundance, which enables them to produce large quantities of albumin, clotting factors, and other serum proteins. [2]. Hepatocytes are also critical in the production of bile, a complex molecular soap that functions in the emulsification and digestion of fats as well as the removal of xenobiotics and endogenous wastes[4]. As part of its detoxification functions, hepatocytes contain a vast arsenal of the P450 family of enzymes that modifies chemicals and other harmful substances and enabling their elimination via urine or bile[2].Hepatocytes are also key mediators of energy metabolism with their metabolic functions ranging from fatty acid metabolism to gluconeogenesis[2, 5]. The role of hepatocytes in innate immunity is characterized by secretion of innate immunity proteins such as the coagulation factor fibrinogen, which helps in activation of the innate immune system and bactericidal proteins, which directly kill bacteria[6].

Cholangiocytes, also known as biliary epithelial cells are specialized cells that function primarily in the modification of hepatocytic canalicular bile by basal and hormone-controlled events as it moves along the biliary tree[7, 8]. Cholangiocytes are quiescent in homeostatic conditions but they respond to liver injury through a number of compensatory responses such as enhanced proliferation, ductular reaction and biliary hyperplasia in order to restore homeostatic balance[9]. Aside the bile modification function, cholangiocytes also function

in liver regeneration, especially in the context of impaired hepatocyte regeneration[10]. While less metabolically active than hepatocytes, cholangiocytes regulate metabolic processes such as bicarbonate synthesis[2].

Kupffer cells, which are liver resident macrophages acts are the largest population of tissue resident macrophages in the body[11]. Critical in the innate immune response, their privileged location in the hepatic sinusoids allows them to scavenge and phagocytose pathogens present in the bloodstream (entering from the portal or arterial circulation) [11] . Kupffer cells also function in the clearance of particles and dead erythrocytes from the hepatic parenchyma. Their role in the liver can vary in different pathological states[11]. While they have a protective function in drug induced liver injury and toxin-induced fibrosis[12, 13], they can contribute to the pathogenesis of chronic inflammatory liver conditions such as non-alcoholic steatohepatitis (NASH)[14].

Hepatic mesenchymal cells, called Stellate cells, are quiescent in the homeostatic liver environment and function as a reservoir of Vitamin A lipid droplets. During liver injury, stellate cells become activated and transdifferentiate into proliferating myofibroblast-like cells[15, 16]. In their activated state, stellate cells become a major source of extracellular matrix production ,generating a temporary scar at the site of liver injury to forestall further damage, thus acting as a key regulator of hepatic fibrogenesis[16]. Additionally, they function in hepatic regeneration by secreting cytokines and growth factors

LSECs are the most abundant non-parenchymal cells in the liver forming 15-20% of all hepatic cells[17].As highly specialized cells, they constitute a distinctive vascular interface in the liver, facilitating the porto-central blood flow and mainly mediate hepatic homeostatic, filtration, and endocytic functions[17, 18]. LSECs location in the liver as well as the expression of numerous endocytic and scavenger receptors make them a very powerful scavenging system[17, 18]. LSECs also function in the regulation of hepatic blood pressure by producing vasodilatory mediators in response to shear stress[17] .Collectively, these cells regulate and mediate hepatic function[19].

1.1.2 Structural organization of the liver

Structurally, hepatic resident cells (parenchymal and non-parenchymal cells) are organized into hexagonal units called lobules which comprises of cords of hepatocytes with a central vein in the middle[20]. The corners of the lobules are formed by the portal triad (with contributions from the hepatic artery, portal vein and bile ducts)[21]. Within the cords,

interconnected hepatocyte membranes face sinusoids, which are unique circulatory channels, allowing perpetual access to the blood stream[22]. These sinusoids are wrapped in fenestrated epithelial cells (LSECs) and also harbour *kupffer* cells. The space of Disse forms a separation between endothelial cells and the apical membrane of hepatocytes and is the residence niche of *stellate* cells. Additionally, it accommodates a collagen and proteoglycan rich extracellular matrix which acts as a scaffolding structure for hepatocytes and the lobules[21]. This structural organization allows for a unique blood composition where incoming flow differs from outgoing flow in the lobule due to the mixture of nutrient rich portal vein flow and oxygen rich hepatic artery flow. This distinct feature forms the basis of hepatic zonation[1, 22]. Zone 1 hepatocytes also called periportal hepatocytes are rich in blood supply and play a critical role in oxidative metabolic processes. Zone 2 hepatocytes (pericentral hepatocytes) are situated just after the periportal hepatocytes while Zone 3 hepatocytes, the least perfused of all zones (due to its distance from the portal triad) are essential in detoxification processes[21]. Apical membrane of adjacently placed hepatocytes, sealed by tight junctions forms the hepatic bile secretory unit called the 'bile canaliculi'[23].Bile flow through the bile canaliculi (outgoing) is in opposite direction to blood flow (incoming) into the liver **(Figure 1.1)** [21]. Interactions between hepatic cells (parenchymal and non-parenchymal cells) in this carefully laid out architecture enables efficient functionality of the liver **(Figure 1.1)**

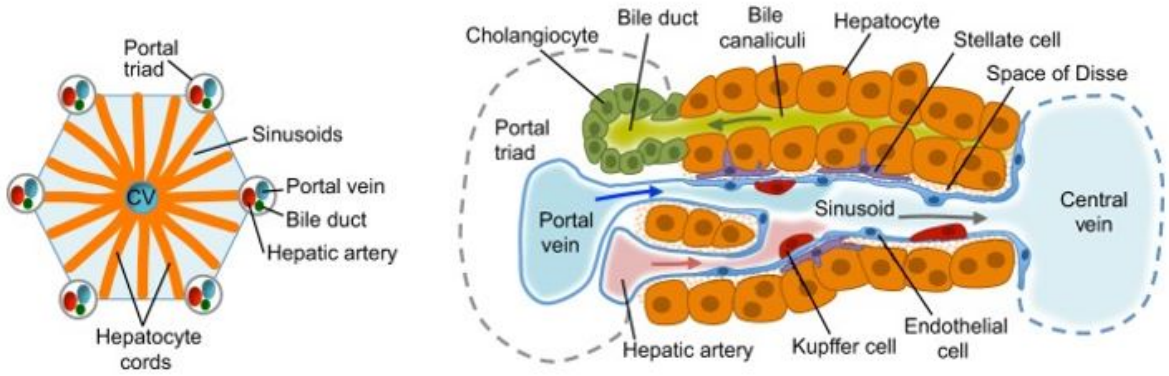

Figure 1.1: Cytoarchitecture of the liver: A schematic showing the cells of the liver in relation to the unique hepatic architecture. Unmodified from [12].

1.2 Pathologies of the liver

Due to its unique physiology and status as the central node of homeostatic metabolism in the body[1], the liver could can present various pathologies, chief among them being the inter-connected conditions such as non-alcoholic fatty liver disease (NAFLD) and non-alcoholic steato-hepatitis (NASH), as well as alcoholic liver disease (ALD), fibrosis, cirrhosis, and liver cancer[24, 25]. These pathologies can have different sources and they are often accompanied by chronic liver damage[26]. Annually, liver diseases account for about 2 million deaths globally, thereby constituting a major public health concern[24].

1.2.1 ALD

Alcoholic liver disease is the most prevalent form of chronic liver disease worldwide[27]. It refers to a progressive spectrum of disease encompassing fatty liver alcoholic hepatitis and cirrhosis, occasioned by heavy alcohol consumption[28, 29]. Steatosis develops in mostly binge drinkers and chronic alcohol abusers[30], with 90% of this population developing alcohol abuse related steatosis[29]. While simple steatosis in itself is reversible, chronic steatosis may lead to fibrotic liver disease presumably due to lipid peroxidation and oxidative damage[29, 31]. It is believed that alcohol consumption leads to steatosis via alteration of cellular redox processes and increased hepatic lipid synthesis.[29] However, this development is likely multifactorial due to rapid onset of steatosis[29]. In support of this notion, recent studies have highlighted other mechanisms including impaired very low-density lipoprotein (VLDL) secretion, deceleration of hepatic lipid oxidation and influx of fatty acid from adipose tissue[29]. Alcoholic hepatitis refers to a severe necro-inflammatory liver condition characterized by neutrophilic infiltration and accumulation of Mallory-Denk bodies (aggregate of insoluble proteins)[29]. Cirrhosis, the terminal stage of fibrosis completes the ALD spectrum[27].

1.2.2 NAFLD and NASH

Non-alcoholic fatty liver disease (NAFLD) is a general term for liver diseases that presents with fat deposition without an underlying alcoholic etiology, thus encompassing conditions from simple steatosis to progressive diseases such as NASH[32]. NAFLD is considered a spectrum comprising of non-alcoholic fatty liver (NAFL), non-alcoholic steatohepatitis (NASH) and cirrhosis[33, 34]. While NAFL characterizes liver steatosis involving 5% or more of the liver parenchyma without accompanying liver injury[32], NASH refers to a necro-

inflammatory liver condition exemplified by hepatic injury with a steatotic background[35, 36].

NAFLD cases are increasing globally with an estimated prevalence of 25%, a portion of whom will develop into full blown NASH, cirrhosis and eventually result into liver cancer[34, 35, 37]. This increase in prevalence owes principally to a sedentary lifestyle[32, 37]. Metabolic syndrome associated obesity and type II diabetes constitute a major risk factor for NAFLD with a sizeable proportion of patients suffering from it being obese or diabetic[26, 34].

Although there are calls to rename the disease to metabolic associated fatty liver disease (MALFD), the exact mechanism responsible for the pathogenesis of NAFLD/NASH is yet to be fully understood[38]. The development of NAFLD has previously been described in a “two-hit” hypothesis[39, 40]. The first hit is characterized by hepatic lipid accumulation while the second hit is described in terms of cytokine infiltration and oxidative stress[39]. However, it is likely influenced by multiple synergistic parallel pathologies[41, 42]. Studies have shown relevant metabolic co-morbidities in NAFLD patients such as obesity and insulin resistance[43, 44], while others have linked NAFLD/NASH to the emergence of other metabolic pathologies such as cardiovascular and kidney diseases[42, 45].Moreover, genetic pre-disposition, de-novo lipogenesis, dietary intake as well as hepatic endoplasmic reticulum (ER) stress have all been linked to NAFLD/NASH pathogenesis[46]. Dietary overload overwhelms the ER thereby leading to ER stress and reactive oxygen species production as well as fat droplet accumulation in the form of Triacylglycerols, consequently leading to insulin resistance[47] **(Figure 1.2)**. Additionally, the gut microbiota may influence NAFLD pathogenesis by indirect regulation of hepatic inflammation[48] **(Figure 1.2)**. Together, this highlights the complex crosstalk between NAFLD/NASH and its multiple parallel influences and renders the previously described two-hit hypothesis obsolete[46, 49].

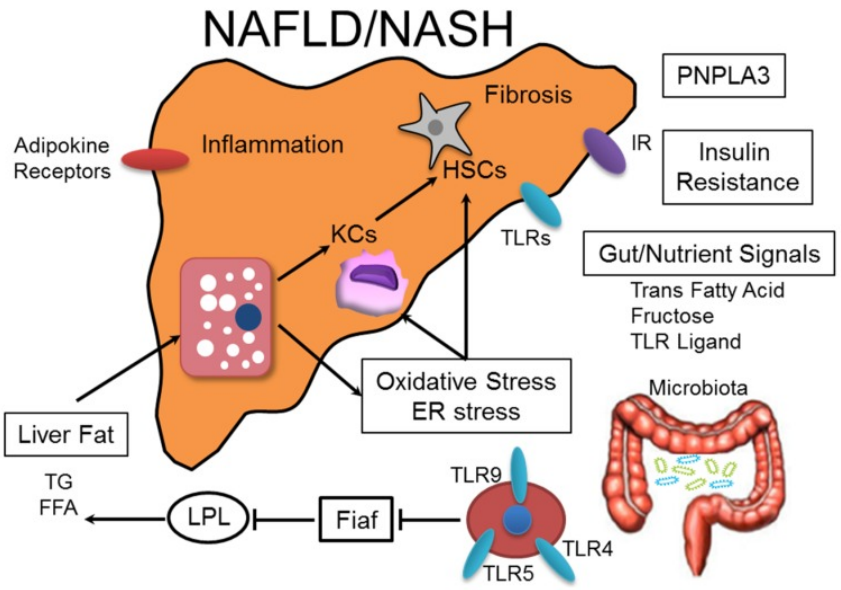

Figure 1.2: Multi-parallel hypothesis of NAFLD/NASH evolution: The pathogenesis of NASH which involves contribution from separate but complementary factors such as dietary overload oxidative stress and insulin resistance is depicted in the schematic. Unmodifed from[49].

1.2.3 Hepatic fibrosis and cirrhosis

Chronic and persistent hepatic injury leads to fibrosis and subsequently cirrhosis, an advanced, near irreversible condition[50]. Cirrhosis may ultimately lead to liver cancer[50] and is therefore a pre-cancerogenic state of the liver. Hepatic fibrosis commences with fibrogenesis, replacement of normal tissue with extracellular matrix (ECM), especially collagen I and III, and forming a fibrous scar[50, 51]. This primarily results from either hepatotoxic injury such as hepatitis B infection, chronic alcohol intake and NASH or from cholestatic injuries obstructing bile flow such as biliary atresia and biliary cholangitis[51, 52]. Hepatic cirrhosis on the other hand is considered the end stage of fibrosis and characterized by profound disruption of hepatic cytoarchitecture, ultimately leading to portal hypertension and eventual liver failure[53-55].The pathogenesis of fibrosis and cirrhosis usually spans multiple decades [55]. It is characterized by a complex cross-talk of several players such as platelets, inflammatory cells, hepatocytes, portal fibroblasts and stellate cells[51, 53]. The development of fibrosis and cirrhosis regardless of etiology share common hallmarks[51]. These include chronic hepatic injury, release of inflammatory cytokines, production of TGFβ by liver resident macrophages, excessive extracellular matrix production and ultimately fibrous scar formation[51, 52]. Myofibroblasts, derived from hepatic stellate cells or portal fibroblasts, are activated in response to hepatic insults and are the primary source of ECM in fibrotic livers. In response to injury, activated hepatic stellate cells (HSCs) upregulate the

expression of α-smooth muscle actin, migrate to the site of injury to deposit ECM and generate a fibrous scar[52]. The response of hepatic stellate cells is potentiated by pro-fibrogenic cytokines such as TGFβ and IL-17[56, 57]. These cytokines help stimulate collagen type 1 transcription in activated HSCs[51]. While fibrosis is generally considered reversible by removal of the underlying etiology, cirrhosis is considered “a point of no return”[51, 58]. Consequently, advance fibrosis and cirrhosis represent a major risk factor in hepatocellular carcinoma[59]

1.2.4 Primary liver cancer

Cirrhosis - the end stage of all chronic liver diseases, is a prerequisite for liver cancer[60]. Liver cancer refers to two major cancer types, Hepatocellular carcinoma (HCC) and intrahepatic cholangiocarcinoma (iCCA)[61]. HCC derives from hepatocytes and constitutes approximately 80% of all liver malignancies[35]. Conversely, intrahepatic cholangiocarcinoma primarily arises from liver resident cholangiocytes and accounts for around 10-15% of liver cancers[62]. Both present with very poor prognosis and account for one of the most common cancer related mortalities globally.[26, 61, 63, 64].

1.2.4.1 Epidemiology and etiology of HCC

Hepatocellular carcinoma, the most dominant form of primary liver cancer has increased progressively in incidence over the past decades. It is currently the sixth most frequently occurring cancer[65]. Its upward trajectory is most pronounced in Africa and Asia, which together accounts for the bulk of new cases. Conversely, most European countries and the USA have recently reported stagnation or reduction in new cases[66]. Gender has been shown to be a risk factor in HCC development, with incidence rate among men 2 to 4-fold when compared to women[67]. Also, age is correlated with incidence as most new cases occur in >60 yr olds. HCC prognosis is poor worldwide, resulting in incidence (9.3 per 100k) almost equalling mortality (8.5 per 100k)[64].

Etiologically speaking, most HCC cases have an underlying virus-related cause (over 50%), with >30 % of all cases being associated with hepatitis B virus (HBV) infections and a further 21% being related to hepatitis C virus (HCV) infections[65, 68]. HCC largely occurs in cirrhotic livers, with non-cirrhotic liver setting contributing less than 20% of all cases[69] **(Figure 1.3)**. Other principal risk factors of HCC development include carcinogens such as food and environmental toxins (e.g., aflatoxins) as well as lifestyle and dietary factors including excessive alcoholic intake (AFD), excessive calorie intake (leading to

NAFLD/NASH) and metabolic syndrome (related to diabetes and obesity)[66, 70]. Virus related causes of HCC are most common in Asian and African countries where HCV/HBV are prevalent while HCC with underlying dietary and lifestyle etiology are more common in western countries where individuals are more likely to lead a sedentary lifestyle[65]. Less common HCC risk factors include genetic factors and autoimmune disorders[68].

1.2.4.2 Pathogenesis of HCC

The pathogenesis of HCC involves the intricate interplay of multiple mechanisms and is thus not yet fully understood. However, it is generally accepted that HCC development occurs mainly in a complex multistep process involving molecular and cellular events spanning liver injury, hepatic inflammation and fibrosis. Chronic injury to hepatocytes and consequent cyto-architectural disruption of the liver ultimately leads to cirrhosis which precedes 80 to 90 % of all HCCs[71]. As liver damage and injury progresses, formation of lesions with increasingly decipherable histological features occurs, from well differentiated pre-malignant lesions to poorly differentiated clinically advanced cancer. Histomorphologically, HCC typically arises from dysplastic nodules, abnormal precancerous lesions formed from hepatocytes within a cirrhotic background. The progression from pre-cancerous lesions to poorly differentiated HCC is typified by strong stroma invasion, development of aberrant vascularization, clearly decipherable tumour nodules and metastasis[71]. These characteristics form the basis of the aggressiveness and poor prognosis of HCC.

Molecularly, the tumour microenvironment, as well as genetic and epigenetic alterations play a critical role in hepatocarcinogenesis. Recent sequencing efforts have unveiled a complex and heterogenous mutational landscape in HCC[72]. Common somatic genetic events in HCC include mutations in the telomerase (TERT) promoter, tumour suppressor gene *TP53* and in the WNT/ β-catenin family member, β-catenin (CTNNB1)[71, 72]. Other less common but potentially important somatic mutations in HCC involve the chromatin remodellers *ARID1A*, the deubiquitinase *BAP1*, the RAS/MAPK pathway signalling component *RPS6KA3* among others **(Figure 1.3)**. Interestingly, it has been noted that the underpinning aetiology might affect the frequency of specific HCC mutations. For example, HCV associated HCCs have increased frequency of *TP53* and *CTNNB1* gene mutations while HBV -induced HCCs display TERT activation by integration of HBV sequences into the TERT gene locus[71]. Conversely, dietary exposure to aflatoxin gives rise to a specific and recurrent *TP53* mutation at codon 249[73].

Aside somatic mutations, widespread chromosomal instability has also been reported in HCC. This is commonly manifested as amplifications (gain of genomic DNA occurring in approximately 32% of HCC), allelic loss or deletions (loss of heterozygosity, 40% prevalence in HCC) and chromosomal re-arrangements[74]. These structural alterations drive carcinogenesis by disrupting the expression of cancer relevant genes in the affected genomic regions with amplification leading to increased expression of oncogenes and deletions resulting in muted expression of tumour suppressor genes (TSGs)[71]. Similarly, epigenetic events play a key role in carcinogenesis. DNA methylation and the consequent silencing of TSGs, histone modifications and chromatin remodelling have all been associated with HCC pathogenesis.

The tumour microenvironment plays an important role in HCC progression. Fibrotic, cirrhotic as well as inflammatory changes in the liver leads to dramatic changes in the microenvironmental milieu with increased expression of extracellular matrix remodelling factors, such as matrix metalloproteinases (MMPs) and production of platelet-derived growth factor (PDGF)[75]. Consequently, critical signalling pathways become dysregulated, probably as an adaptive response to the changing tumour microenvironment and ensuring tumour survival. The most commonly perturbed signalling pathways in HCC include those regulating growth (fibroblast growth factor (FGF) and hepatocyte growth factor (HGF) signalling), differentiation and development (WNT/ β-catenin, NOTCH signalling etc), angiogenesis (Vascular endothelial growth factor (VEGF) signalling), cell survival and proliferation (PI3K/AKT axis), and cell cycle regulation (p53/p21 signalling)[72]. In addition, immuno-suppressive events, such as aberrant expression of cytokines (tumour necrosis factor (TNF), interleukin 6 (IL-6), interleukin 4 (IL-4), and dysregulated metabolism (presence of hypoxia, glycolytic switch) also contribute to HCC pathogenesis and aggressiveness.[72, 76].

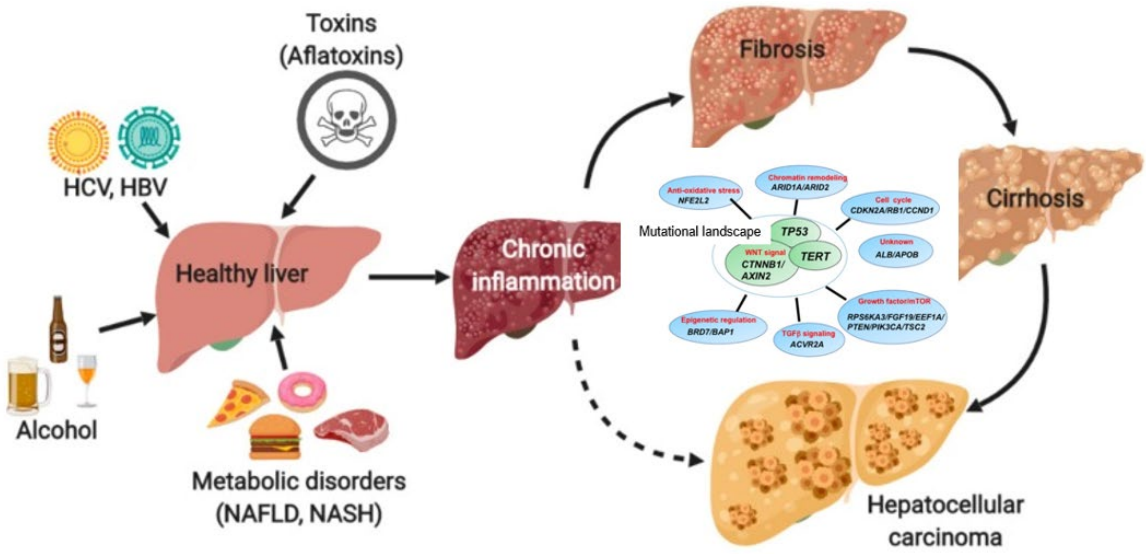

Figure 1.3: Natural history and pathogenesis of HCC: Schematic showing the multi-step process leading to HCC. The major risk factors (Metabolic disorders, toxins and hepatitis virus infection), its transitional pathological states (e.g., liver inflammation, cirrhosis) and common genetic alterations are depicted. Modified from[77, 78].

1.2.4.3 Epidemiology and etiology of iCCA

Intrahepatic cholangiocarcinoma (iCCA) is the second most common type of primary liver cancer accounting for 10-20% of cases. Due to certain histological similarities, it is frequently misdiagnosed as HCC. It is a relatively rare form of cancer, accounting for only 3% of all gastrointestinal malignancies and 10% of all cancers of the biliary tract[79]. It is epidemiological and patho-physiologically distinct from other cholangiocarcinomas (extra hepatic and peri-hilar cholangiocarcinoma). While iCCA is most prevalent in eastern Asian countries, there is a global increase in incidence over the past two decades[80]. It occurs mostly in later stages of life with the majority of cases being reported in individuals over >50 years of age[81]. Unlike HCC, prevalence according to sex is not as dramatic with male cases only 1.5-fold higher than female cases[80]. Survival rates are poor (similar to HCC) likely due to late diagnosis and limited therapeutic options.

The etiologies contributing to iCCA are less well established as compared to HCC, several risk factors are considered to predispose to it, chief among them being chemical and environmental toxins (such as exposure to asbestos, radon etc), liver flukes' infections as well as biliary tract diseases such as primary sclerosing cholangitis[80]. Well established HCC risk factors have also been implicated in iCCA. Several studies have linked viral hepatitis (HBV and HCV) infections with development of iCCA. Liver cirrhosis, metabolic

syndrome, NASH and alcohol abuse have also been associated with iCCA, thus raising the possibility (at least in part) of sharing similar pathogenesis with HCC[80, 82].

1.2.4.4 Pathogenesis of iCCA

The pathogenesis of iCCA is complex and involves yet to be fully understood mechanisms with contributions from biliary injury, epigenetic and genetic alterations and stroma[83-85]. Although it is widely accepted that iCCA arise from Cholangiocytes, recent evidence suggests that iCCA can also arise from trans-differentiation and de-differentiation of hepatocytes and hepatic progenitor cells[86-88]. The most common type of iCCA are the adenocarcinomas, forming over 95% of iCCA. iCCA can be categorized based on histopathological and macroscopic features. These includes mass forming iCCA (>75%) characterized by central fibrotic changes as well as invasion of surrounding blood vessels. Periductal iCCA are characterized by stenosis and periductal infiltration (>16%), with the third and least common being intraductal iCCA, with a papillary tumour mass arising from the lumen of a dilated bile duct[83]. In general, iCCAs appear firm and hard, and possess an accompanying desmoplastic stroma.

Regardless of aetiology, iCCA arises in a backdrop of chronic bile injury and inflammation or cholestasis. Classically, chronic biliary inflammation leads to the release of pro-tumorigenic cytokines such as IL-6 and TNFα and transcription of nitric oxide synthase. This enzyme leads to the production of Nitric oxide and the subsequent induction of cyclooxygenase-2 expression providing the platform for impaired DNA repair, cholestasis and eventual mutagenesis.[85] Consequently, this is believed to lead to cholangiocyte growth as a result of the aberrant expression epidermal growth factor receptor[85]. These events coupled with additional genetic and epigenetic events confer limitless replicative potential on the impaired cholangiocytes, thus completing iCCA pathogenesis[84, 85].

Common somatic mutations in iCCA include activating mutations in KRAS and loss of *TP53* [83]. Mutations in epigenetic modifiers are also notably present in iCCA with inactivating mutations in *BAP1*, *PBRM1* and *ARID1A* as well as oncogenic point mutations in isocitrate dehydrogenase 1 and 2 (IDH) among the most common ones, albeit with varying degree of frequency depending on the cohort[89-91]. Studies have also reported chromosomal instability events such as deletions and amplifications in iCCA although their importance is difficult to access due to very low sample sizes [85]. Several signaling pathways are deregulated in iCCA, chief among them being those related to inflammation (IL6/STAT signaling), growth and angiogenesis (EGF, VEGF signaling) proliferation (AKT,

KRAS/MAPK signaling) and survival and development (WNT, Hedgehog/Notch signaling)[84, 85].

Importantly the desmoplastic stroma typical of all iCCAs plays a critical role in its pathogenesis. Cell survival and invasion promoting changes typified by ECM alteration and fibroblast recruitment occurs in the stroma[84, 85]. In addition, cytokines, chemokines and other tumor promoting factors (IL-6 and TGFB3) were found to be uniquely enriched in the stroma, thus forming the stroma signature which is associated with poor outcomes in iCCA[84, 85, 92].

1.2.5 Therapies of liver cancer

HCC is a fatal diagnosis. Despite well documented advances in therapies, the patient outcome remains bleak[93]. For example, the 5 year survival rate for HCC is under 20%[94]. The reason for the poor outcome is likely multifactorial. One of the widely stated reasons for the poor outcome is due to late presentation of disease [61]. Other possible reasons for poor prognosis in HCC includes genetic heterogeneity and advanced cirrhosis[93, 95].

It is important to properly stage and grade HCC to determine the course of treatment[96]. Many HCC staging algorithms have been proposed, with the Barcelona Clinic Liver Cancer (BCLC) system the most prominent one. It takes into account hepatic function; tumour spread and provides treatment and prognosis advice. It sub-classifies tumours from 0 (very early) to D (terminal stage).

While radiofrequency ablation (RFA), liver transplantation and surgical resection have curative potential, they are only indicated for early stage diseases, thus covering only a fraction of HCC patients[61]. Underlying cirrhosis and extensive liver damage in intermediate to advance tumours make surgery generally ineffective for patients[97].

At the time of clinical presentation (usually at an advanced stage without option of curative treatments such as surgery), advance stage HCC is unresponsive to chemotherapy and resistant to radiation therapy [108]. Recently approved molecular therapies, such as the first line multi-kinase inhibitor Sorafenib and the second line Regorafenib, have shown promise; however their benefits remain minimal[108]. Novel therapies including oncolytic viruses and immunotherapy (PDL1 and CTLA4 antibodies) are currently in clinical trials, however their utility is yet to be fully ascertained[108] **(Figure 1.4).**

Similar to HCC, iCCA is also diagnosed with advanced disease presenting with similarly poor prognosis. Surgical resection is the only curative modality available for iCCA, although only a limited number of patients (with early-stage disease) qualify[61]. Limited surgical success in advance disease is compounded by difficulties in obtaining negative margins due to intraductal and periductal invasion[98, 99].

Unlike HCC, iCCA is slightly responsive to systemic treatments. Currently, combination of gemcitabine and platinum-derived chemotherapy is commonly utilized as first line treatment for unresectable iCCA, with median survival less than 1 yr. Advances in molecular therapies represent a ray of light in the treatment of this disease. Recently, the FGFR inhibitor pemigatinib was approved by the food and drug administration FDA for iCCA[100] **(Figure 1.4)**. Specifically, it shows promise in the treatment of iCCA with FGFR2 fusion or rearrangement[101]. This has led to the development of other targeted therapies for iCCA. For example isocitrate dehydrogenase 1/2 (IDH1/2) and vascular endothelial growth factor receptor (VEGFR) inhibitors are currently being evaluated for efficacy[61] **(Figure 1.4)**.

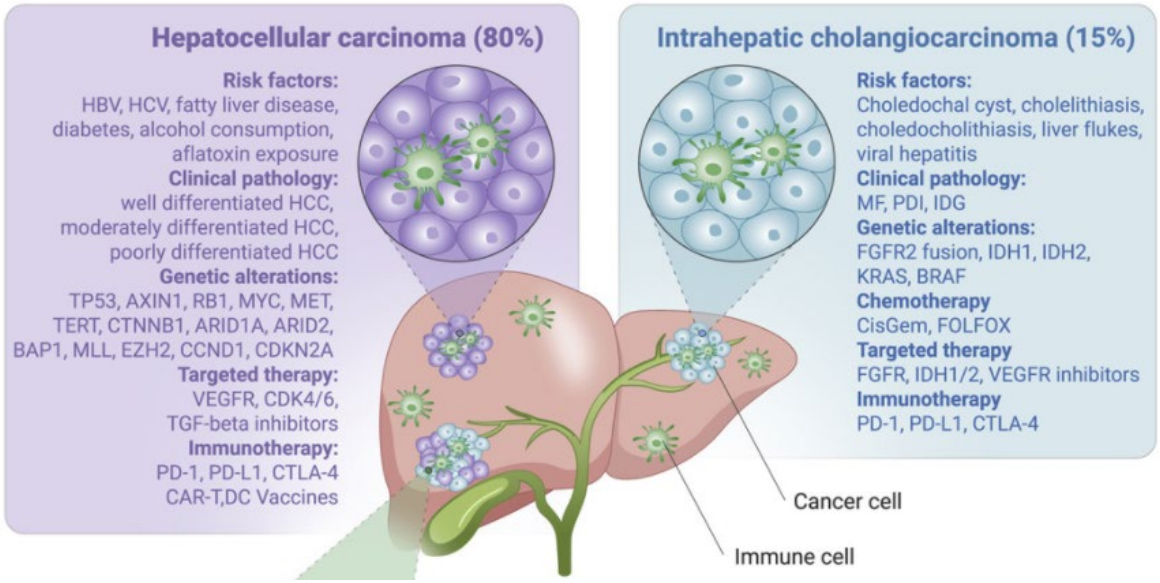

Figure 1.4: **Genetic mutational landscape and therapies of liver cancer:** Illustration of the genetic mutational landscape as well as current therapeutic possibilities in primary liver cancer. Modified from [61].

Despite the promise of different therapeutic options in HCC/iCCA the prognosis for advance disease remains dismal. This is probably due to genetic heterogeneity and acquired drug resistance in the tumour[61]. Hence there remains an urgent need to better understand the genetic basis of primary liver cancer in order to develop effective therapy. The relative success of the FGFR inhibitor pemigatinib suggests targeting recurrent and specific genetic alterations in liver cancer might represent a winning strategy. To this end, it will be important

in the future to Identify and functionally characterize driving mutations in HCC and iCCA and to investigate potential vulnerabilities that these drivers generate in order to make liver cancer therapy more specific and effective.

1.2.6 Mouse models of liver cancer

In order to study the molecular underpinnings and therapeutic opportunities in liver cancer, a multitude of strategies have been described to induce liver cancer in mouse, especially HCC. These models can be broadly categorized into chemically induced models, dietary models (as described above) and genetic models [93]. These mouse models should recapitulate the cascade of events that leads to liver cancer.

Hepatotoxins used to induce liver cancer normally causes DNA damage and/or promote the generation of cancer-promoting alterations. The most widely employed ones include N-nitrosodiethylamine (DEN) and Carbon tetrachloride (CCL4) models. Tumor incidence in these models is usually very high (around 100%) albeit with long latency[93]. Dietary models such as Western diet (WD) and choline deficient high fat diet (CD-HFD) are also commonly used to generate HCCs. One major drawback of such models is the low incidence (25% to 40%) and the relatively long latency (12 to 15 months)[35, 93].

Genetic models of liver cancer (HCC and iCCA) that captures disease progression are very critical in the identification and understanding of disease relevant genetic alterations. Genetically engineered mouse models (GEMMs), particularly transgenic mouse models, used to model disease states such as oncogene activation and tumor suppressor gene loss has been generated in both iCCA and HCC[102-104]. Liver tissue specific expression of relevant transgenes via the albumin (ALB) promoter further adds to the elegance and sophistication of these models. For example, transgenic mouse model of iCCA involving oncogenic KRAS activation and heterozygous phosphatase and tensin homolog (PTEN) loss (Cre-loxP system) has been reported[102]. While for HCC, mouse models mimicking C-myc activation and *Trp53* loss has been described[104, 105]. Recent advances in genetic manipulation techniques, such as the above mentioned Cre-LoxP system and doxycycline regulated control of genetic elements have allowed for improved precision and conditional spatio-temporal regulation of genes expression. Although useful, the use of GEMMs can be resource intensive, technically demanding and time consuming[106].

A robust yet simple and inexpensive alternative to traditional *in-vivo* genetic manipulation is hydrodynamic tail vein injection (HDTVI). It allows efficient transfection of adult mice hepatocytes with naked plasmid DNA by utilizing the venous circulatory system[107]. It

involves rapid injection of 2ml (approximately 10% of adult mice body weight) saline solution containing plasmid DNA via the lateral tail vein[108, 109]. This result in a temporary heart dysfunction and accumulation of the fluid in the inferior vena cava. The resultant hydrodynamic force then directs the fluid into the liver, followed by compensatory enlargement of the liver and subsequent absorption of the injected solution and its contents, thus transiently transfecting the liver[103, 110]. Combination of HDTVI with sleeping beauty (SB) transposase, allows for stable integration and continuing expression of the injected genetic cargo[103, 111]. HDTVI allows for combination of multiple genetic modifications in a mosaic fashion, thus opening up a world of possibilities in accessing the relevance and consequence of different genetic alterations[103].

1.3 BAP1 and its complexes

The *BAP1* (BRCA1 associated protein 1) gene is located on the short arm of chromosome 3(specific position 3p21.1). It comprises of 17 exons which codes for the 729 amino acids making up the 90 kDA BAP1 protein[112]. It is a widely expressed protein deubiquitinase (DUB) that belongs to the ubiquitin C-terminal hydrolase (UCH) domain-containing family of deubiquitinase [113]. Structurally, the UCH and the C-terminal domain (CTD) are evolutionarily conserved. In its N-terminal domain, BAP1 possesses a functional nuclear localization signal (NLS) that ensures efficient nuclear positioning. Its catalytic domain allows it to canonically alter ubiquitin signaling and consequently affecting a range of cellular processes[112]. BAP1 interacts with numerous proteins forming integral complexes, especially with chromatin regulators. It forms a central complex with the polycomb group proteins ASXL1/2 (additional sex combs-like proteins), Host cell factor (HCF-1) and O-linked N-acetylglucosamine transferase (OGT) via its centrally located HBM binding motif[113]. Additionally, BAP1 has been demonstrated to interact with the transcription factors FOXK1/2 and Ying yang 1 (YY1) as well as the chromatin modifiers HAT1 and KDM1B[112] [113] **(Figure 1.5)**. Thus, BAP1 is likely involved in diverse cellular processes not only because of its central role in ubiquitin modification but also as a result of its interaction with regulators of important biological processes[112, 113].

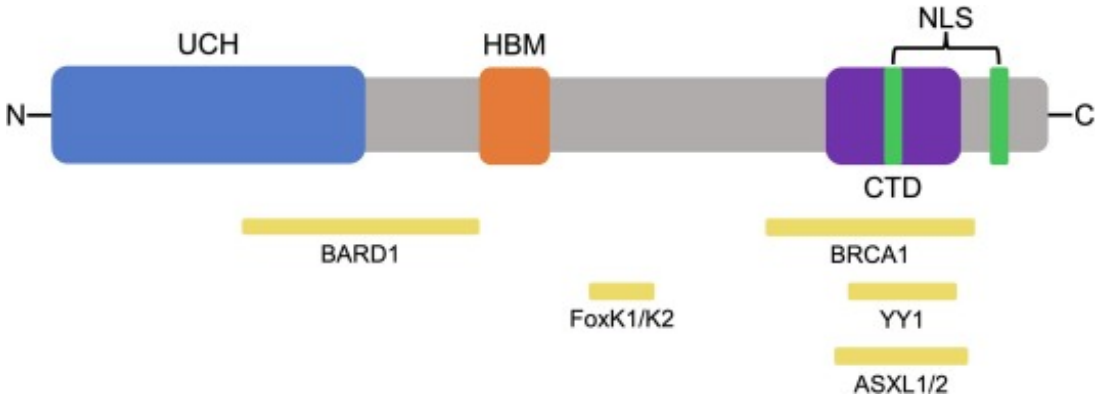

Figure 1.5: BAP1 structure: Structural schematic of BAP1 showing its relevant structures (UCH domain, HBM domain etc.) and the relative interaction sites of its partners Unmodified from [112].

1.3.1 Functions of BAP1

Functionally, BAP1 deubiquitinates the mono-ubiquitinated K119 residue on histone 2A, a transcriptional repressive mark catalyzed by Polycomb group proteins (PcG). Through its central complex with ASXL1/2, BAP1 forms the polycomb group repressor deubiquitinase (PR-DUB). PR-DUB opposes the gene silencing effect of PcG by deubiquitinating histones[113].BAP1 is considered a transcriptional co-activator, at least in part due to its opposition of the PcG and removal of H2Aub ubiquitination[114, 115]. However, BAP1 role in transcriptional regulation is likely more complex due to its relationship with several chromatin- associated proteins[113]. Nonetheless, its recruitment to histones and the exact mechanism of its functional interaction with member of its complexes as well as its associated proteins remain insufficiently understood [113]. It is also an important component of the DNA damage signaling cascade, as it binds to and deubiquitinates BRCA1 associated ring domain protein1 (BARD1), thereby regulating the E3 ligase activity of the BRCA1/BARD1 complex[116] **(Figure 1.6)**.

Aside its chromatin associated functions in the nucleus, BAP1 has been implicated in cytoplasmic localization relevant functions such as regulation of calcium signaling and consequently apoptosis[117]. Additionally, several studies have implicated BAP1 in cell death regulation (apoptosis and ferroptosis), [112, 113] **(Figure 1.6)**. However, BAP1 role in cell death processes may be context dependent. For example, BAP1 has been shown to safeguard glucose starved cells from ER stress mediated apoptosis by restricting expression of C/EBP homologous protein (CHOP)[118]. In another context, BAP1 was demonstrated to have a pro-apoptotic role[117] .BAP1 is also involved in cell proliferation

metabolism and development. Consistent with its role in embryonic development, *Bap1* gene ablation leads to embryonic fatality[119].

Taken together, these studies highlight the complex cellular context that BAP1 is involved in and positions it as an emerging regulator of critical cellular processes.

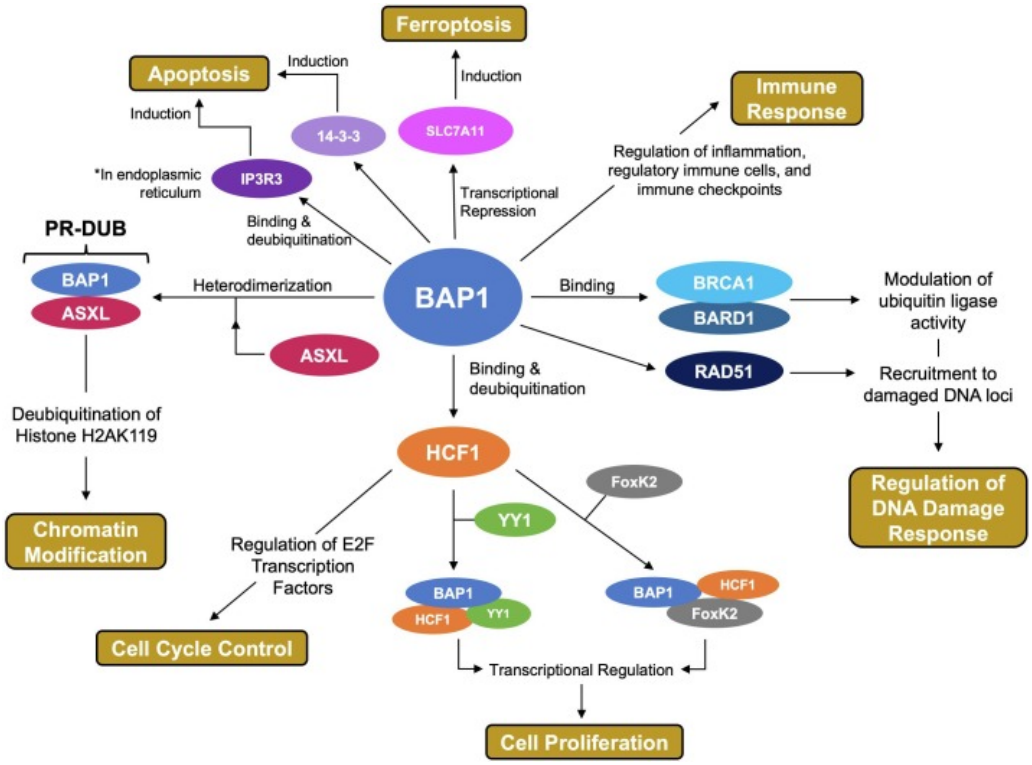

Figure 1.6: BAP1 is involved in diverse cellular processes: Aside its canonical role in deubiquitylation, BAP1 is also involved in other processes such as DNA damage response and cell cycle regulation. Unmodified from[112].

1.3.2 BAP1 as a tumor suppressor

BAP1 is an emerging tumor suppressor. Accordingly, BAP1 inactivating mutations has been identified in several cancers. *BAP1* alterations in human cancer predominantly follow the Knudson two hit hypothesis of tumor suppression[113]. Importantly, both somatic and germline BAP1 mutations have been identified in many human tumors. *BAP1* is predominantly inactivated in in uveal melanoma (UM) and malignant pleural mesothelioma (MPM). In fact, heterozygous germline mutations of *BAP1* have been associated with the so called BAP1 tumor predisposition syndrome (BAP1-TPDS) a familial predisposition to multiple tumors including uveal melanoma, malignant mesothelioma and renal cell carcinoma[113]. *BAP1* inactivation has also been observed in cutaneous melanoma and liver cancer (HCC and iCCA)[78, 89], thus underlying the importance of *BAP1* as a tissue

agnostic tumor suppressor gene. There is no consensus on the prognostic implication of *BAP1* loss in human cancers. Accordingly, malignant mesothelioma patients with *BAP1* somatic mutations show drastically higher overall survival rates when compared to *BAP1* WT patients[120]. Conversely, *BAP1* mutations are associated with grimmer outcomes in renal cell carcinoma[121]. Despite its function in important cellular processes and its mutational prevalence in multiple tumor entities, the role of BAP1 in many tissues, especially the liver, is not fully understood yet.

2 Study objectives

Primary liver cancer remains very difficult to treat primarily due to late presentation of disease and the genetic heterogeneity of tumors. Thus, it is critical to better understand the functional relevance of frequently observed genetic events in liver cancer (HCC and iCCA).

Inactivating mutation in BAP1 is a frequent genetic event in liver cancer (cholangiocarcinoma and hepatocellular carcinoma). The recurrent mutational profile of BAP1 in iCCA and HCC and its reported role in various physiological processes such as DNA repair and metabolism suggest it is an important player in these tumor entities and may play a role in liver homeostasis. Yet functional analyses regarding the relevance of BAP1 in liver homeostasis and liver cancer (iCCA and HCC) remain elusive. Thus, this thesis aims to provide a methodical and mechanistic understanding of the role of BAP1 in liver homeostasis, pathophysiology and carcinogenesis. This is envisioned to be achieved by providing answer to the following questions:

I. What is the role of BAP1 in normal liver physiology?
II. What role does BAP1 play in liver metabolic distress?
III. What molecular signatures (transcriptomics, lipidomic etc.) are associated with *BAP1* loss in liver metabolic pathologies?
IV. What role does *BAP1* loss play in liver tumorigenesis and what are its co-operating genetic events?
V. What is the mechanism of BAP1 role in tumor suppression?
VI. Does BAP1 deficient tumors share the identified molecular attributes in BAP1 deficient liver metabolic pathologies?

3 Materials and Methods

3.1 Materials

3.1.1 Consumables

Needles used in this study were sourced from BD and Henke-SaaS, Wolf. Cell scrappers, 15ml centrifuges tubes and strippetes were sourced from corning. Cryovials, falcons and cell culture dishes were sourced from Sarstedt. Other consumables were sourced from the suppliers listed in the table below.

Table 3.1: Consumables

Item	Manufacturer	Catalog Number
BeadBlaster 24	Biozym	55D1032-15
Disposable scalpel	Feather Safety Razor	19100815
GOT/AST P-III	Fujifilm	9903140
GPT/ALT P-III	Fujifilm	9903150
PVDF membrane (0.45µm)	Carl Roth	T830.1
QIA shredder	Qiagen	79656
Solofix Blood lancets	B.Braun	170-19-107
Sterile virus-filter 0.45µm	VWR International	514-0063
TBIL-P	Fujifilm	9903240
Tissue grinderMK28-R/2ml	Bertin Corp	50-154-2937
Tissue-Tek Cryomold	Sakura	32571
Tissue-Tek OCT	Sakura	2022602832
Whatman paper	Cytiva	3003-917

3.1.2 Equipment

The equipment used in this thesis are listed in table below

Table 3.2: Equipment

Equipment	Class and Model	Manufacturer
Benchtop flow cytometer	11HT	Guava
Centrifuge	Fresco 17	Thermo Scientific
Centrifuge	Pico 17	Thermo Scientific
Centrifuge	Megafuge 16R	Thermo Scientific

CO_2 incubator	Heracell VIOS 250i	Thermo Scientific
Electrophoresis system	E861	Consort
Flat plate shaker	UNITWIST-RT	Kisker Biotec
Fume Hood	Secuflow	Waldner
Gel and WB imager	FluorChem M	ProteinSimple
Heat block	Dri-Block	BioStep
Heat block	QBD2	Grant Instruments
High speed imaging system	Cell Observer HS	Zeiss
Homogenizer	Precellys 24	Bertin Instruments
Incubation Hood/Shaker	CERTOMAT H	B.Braun
Laminar flow hood	HERAsafe	Heraus
Microplate reader	FLUOstar Omega	BMG LABTECH
Microscope	Axiovert 40 C	Carl Zeiss
Microscope with camera	BX51 / XC30	Olympus
Modular stereo microscope	MZ10 F	Leica
pH meter	pH210	Hanna Instruments
Pipette set	Discovery comfort	HTL Lab solutions
Rolling shaker	CAT RM5	Neolab
RT-qPCR system	QuantStudio 3	Thermo Scientific
Serum analyzer	DRI-CHEM NX500	Fujifilm
Sonicator	Transsonic T460/H	Elma
Spectrophotometer	NanoDrop ND-100	Thermo Scientific
Thermal cycler	Arktik	Thermo Scientific
Thermal cycler	Peltier Thermal Cycler	Bio-Rad
Thermal cycler	PTC-200	Bio-Rad laboratories
Thermo Shaker	Thermomixer C	Eppendorf
Thermo Shaker	PHMT	Grant-Bio
Vortex	Vortex Genie 2	Scientific Industries
Water bath	SW22	Julabo
Western immunoblotting chambers	Mini protean system	Bio-Rad laboratories

3.1.3 Reagents and chemicals

All chemicals were sourced from Carl Roth, Serva electrophoresis, AppliChem and Sigma-Aldrich. Restriction enzymes and buffers for molecular cloning were sourced exclusively from New England Biosciences. Luria Bertani (LB) medium preparation components were sourced from BD biosciences. Saline solution for hydrodynamic tail vein injection was sourced from B. Braun. All other reagents and chemicals were sourced from:

Table 3.3: Reagent and Chemicals

Reagent/chemical	Manufacturer	Catalog Number
10 mM dNTPs	Thermo Scientific	R0191
10X Cell Lysis Buffer	Cell Signaling Technology	9803S
Bradford reagent	Bio-Rad	5000006
BSA	New England Biolabs	B9000S
Clarity Western ECL Substrate	Bio-Rad Laboratories	170-5060
Collagenase D	Sigma-Aldrich	11088866001
Dispase II	Sigma-Aldrich	4942078001
DMEM	Sigma-Aldrich	D6429
Doxycycline hyclate	Alfa Aesar	J60579-22
Ethanol	Honeywell	52603.000001
Ethidium bromide	Thermo Fisher Scientific	E/P800/03
FBS	Gibco	10270-106
Hoechst dye	Thermo Fisher Scientific	62249
IGF- II protein	R&D systems	792-MG-050
Methanol	VWR Chemicals	20847.307
Mouse EGF	PeproTech	315-09
Murine HGF	PeproTech	315-23-20ug

NEB Stable Competent E. Coli	New England Biolabs	C3040
NEBuffer 2	New England Biolabs	B7002
NEBuilder HiFi DNA Assembly Master Mix	New England Biolabs	E2621
Oleic Acid	Sigma-Aldrich	O1383-1G
Page Ruler protein ladder	Thermo Fisher Scientific	26616
Palmitic Acid	Sigma-Aldrich	P5585-10G
PBS	Sigma-Aldrich	D8537
Penicillin-Streptomycin	Sigma-Aldrich	P0781
Polybrene	Sigma-Aldrich	107689
Polyethylenimine (PEI)	Polysciences Europe GmbH	23966-1
Protease inhibitor mix	Sigma-Aldrich	11836170001
Proteinase K	Sigma-Aldrich	3115852001
PureCol	CellSystems	5005
Puromycin	Thermo Fisher Scientific	BP2956-100
Q5 DNA Polymerase	New England Biolabs	M0593
REDTaq ReadyMix	Sigma-Aldrich	2648-20RXNR
rSAP	New England Biolabs	M0371L
SYBR Green PCR Master Mix	Thermo Fisher Scientific	4367659
T4 DNA Lligase Buffer	New England Biolabs	B0202S
T4 ligase	New England Biolabs	M0202M
T4 Polynucleotide Kinase (PNK)	New England Biolabs	M0201
T7 Endonuclease I	New England Biolabs	M0302L
Trypsin/EDTA	Sigma-Aldrich	T4049

β-Mercaptoethanol	Thermo Fisher Scientific	M3148

3.1.4 Commercial kits

The commercial kits used in this study are as follows:

Table 3.4: Commercial kits

Kit	Manufacturer	Catalog Number
Puregene Core Kit A	Qiagen	158445
QIAGEN Plasmid Plus Midi Kit	Qiagen	12945
QIAprep Spin Miniprep Kit	Qiagen	27106
QIAquick Gel Extraction Kit	Qiagen	28706X4
QIAQuick PCR Purification Kit	Qiagen	28106
RNeasy Mini Kit	Qiagen	74106
TaqMan Reverse Transcription	Applied Biosystems	N808023
Triacylglycerols quantification kit	Sigma-Aldrich	MAK266-1KT

3.1.5 Solutions and buffers

Table 3.5: Solutions and Buffers

Solution/buffers	Components
10X MGB (10 mL)	6.7 mL 1 M Tris pH 8.8 830 µL 2 M $(NH_4)_2SO_4$ 650 µL 1 M $MgCl_2$ 1.82 mL water
50X Phosphatase Inhibitor	5 mM sodium fluoride 1 mM sodium orthovanadate 1 mM sodium pyrophosphate 1 mM β-glycerophosphate
Antigen retrieval buffer (pH 6, 1 L)	22.94 g tri-sodium citrate 5 mL Tween 20
Doxycycline water (1 L)	2 g Doxycycline hyclate 10 g saccharose 1 L water

Crystal violet staining solution (1 L)	0.5g Crystal Violet 27 mL 37% Formaldehyde 100 mL 10X PBS 10 mL Methanol
Genotyping lysis solution (10 mL)	1 mL 10X MGB 500 µL 10% Triton X 100 µL β-mercaptoethanol 200 µL Proteinase K (20 mg/mL)
Lysis buffer (protein extraction)	10% 10X lysis buffer 10% 10X protease inhibitors 2% 50X phosphatase inhibitors in distilled water
SDS-PAGE Running buffer (10X, 2L)	60.6 g 0.25 M Trizma base 288.5 g 1.92 M Glycine 20 g 1% SDS
TBS (Tris buffered saline)	20 mM Tris-HCL 140 mM NaCl pH 7.6
TBS-T	0.1% Tween-20 in TBS

3.1.6 Antibodies

Table 3.6: Antibodies

Antibody	Manufacturer	Catalog no	Application/Dilution	
Actin-HRP	Sigma-Aldrich	A3854	WB	1:20000
Alexa Fluor 488-DAC	Jackson ImmunoResearch Laboratories	AB2340375	IF	1:200
Alexa Fluor 568-DAG	Invitrogen	A11058	IF	1:250
Alexa Fluor 594-DAR	Invitrogen	A21207	IF	2 drops/ml
BAP1	Bethyl Laboratories	A302-243A	IF WB	1:100 1:1000
BAP1	Cell Signalling Technology	13271S	IF	1:100

			WB	1:1000
CHOP	Cell Signalling Technology	5554S	WB	1:1000
GFP	Abcam	ab13970	IF	1:500
GFP (D5.1)	Cell Signalling Technology	2956	WB	1:1000
HNF4α	Santa Cruz	sc-6556	IF	1:50
			IHC	1:100
Ki67	Abcam	ab15580	IHC	1:100
KRT19	Abcam	ab52625	IF	1:100
			IHC	1:100
tRFP	Evrogen	AB233	WB	1:1000

3.1.7 Oligonucleotides

3.1.7.1 RT-qPCR primers

The RT-qPCR primers used in this study are listed below. All primers were designed for murine genes. They were sourced/designed using PrimerBlast or PrimerBank internet resources.

Table 3.7: RT-qPCR primers

Primer	Sequence (5'- 3')
Atf3 1 for	AGAGTGCCTGCAGAAAGAGTC
Atf3 1 rev	GAGGTTCCTCTCGTCTTCCG
Bap1 1 for	CACTCACAGAGGGTGGGAAG
Bap1 1 rev	CTCCACTCAAGGGCTCACTG
Bap1 2 for	CTCCTGGTGGAAGATTTCGGT
Bap1 2 rev	GAGTGGCACAAGAGTTGGGAA
Ddit3 1 for	CCTGAGGAGAGAGAACCTGGTC
Ddit3 1 rev	AGGTGCCCCCAATTTCATCT
Ddit3 2 for	CTGGAAGCCTGGTATGAGGAT
Ddit3 2 rev	CAGGGTCAAGAGTAGTGAAGGT
Dgat2 1 for	ACACCTTCTGCACAGACTGC
Dgat2 rev	TGCGATCTCCTGCCACCTTT
Fabp1 for	ATGAACTTCTCCGGCAAGTACC

Fabp1 for	CTGACACCCCCTTGATGTCC

3.1.7.2 PCR primers

All PCR primers used in this study were designed sourced/designed using CHOPCHOP or PrimerBlast internet resources.

Table 3.8: PCR primers

Primer	Sequence (5'- 3')
Col1a1.1	TTCAGACAGTGACTCTTCTGC
Col1a1.2	AATCATCCCAGGTGCACAGCATTGCGG
Col1a1.3	CTTTGAGGGCTCATGAACCTCCCAGG
Cre for	TGCCACGACCAAGTGACAGC
Cre rev	CCAGGTTACGGATATAGTTCATG
pX330_gib_sgrev	AAGGAATCATGGGAAATAGGCCCTCACAT GAAAAAAGCACCGACTCGGTG
pX330_gib_U6	GTTCCTGGCCTTTTGCTGGCCTTTTGCTCA GAGGGCCTATTTCCCATGATT
Rosa26.1	AAAGTCGCTCTGAGTTGTTAT
Rosa26.2	GCGAAGAGTTTGTCCTCAACC
Rosa26.3	CCTCCAATTTTACACCTGTTC
sgArid1a 1 for (murine)	GGGGAATTTGACTATGTGGTGT
sgArid1a 1 rev (murine)	GAATCTAAGGGTGACGTTTTGC
sgArid1a 2 for (murine)	GGAATGGAGACTTGCTAGGAGA
sgArid1a 2 rev (murine)	CAGTATTAATCTCCCCTTTGCG
sgArid1a 3 for (murine)	AAGCTCACTGAACCTAACAGCC
sgArid1a 3 rev (murine)	CTCAGTCTCCCTTTTCTCCTCA
sgArid1a 4 for (murine)	CTTTTAACCCAGCCGTTAACAC
sgArid1a 4 rev (murine)	GTTCAGTGAGCTTGTCCTTGTG
sgBAP1 1 for (human)	ACCTGCTCAAGGGTCTCTACCT
sgBAP1 1 rev (human)	TCTCCAGCTGGGACTATTCAGT
sgBAP1 2 for (human)	CATAAGGAGACTGGGTGGACTC
sgBAP1 2 rev (human)	CATCAATCACGGACGTATCATC
sgBAP1 3 for (human)	GATATCTGCCTCAACCTGATGG

sgBAP1 3 rev (human)	AGCTGAAGCCCAGATCTACAAG
sgBap1.1 for (murine)	AACTCTTGCCATGGTTTCATCT
sgBap1.1 rev (murine)	CTTCCATCTTACCTGCATAGGG
sgBap1.2 for (murine)	AACTCTTGCCATGGTTTCATCT
sgBap1.2 rev (murine)	CTTCAGGTACTGGGATTTCAGG
sgBap1.3 for (murine)	ACTCTTGCCATGGTTTCATCTT
sgBap1.3 rev (murine)	CTTCAGGTACTGGGATTTCAGG
sgBap1.4 for (murine)	GTACTCATAGGCCCCAACAGAG
sgBap1.4 rev (murine)	GTCACCCACCTTGAACTTCTTC
sgDDIT3 1 for (human)	CAGGAGAATGAAAGGAAAGTGG
sgDdit3 1 for (murine)	GGTTTGTATGCCTCTCCTGAAC
sgDDIT3 1 rev (human)	GAGACTGGACAAGCTGAATCCT
sgDDIT3 2 for (human)	AAACGGAAACAGAGTGGTCATT
sgDdit3 2 for (murine)	GGTTTGTATGCCTCTCCTGAAC
sgDDIT3 2 rev (human)	ATCTTAGGGAAACATTGTCCGA
sgDdit3 2 rev (murine)	TGAGAGGCTGTTGACACAAAGT
sgDdit3 2 rev (murine)	AAGTGAGAGGCTGTTGACACAA
sgPten for 1 (murine)	ACAATTCCCAGTCAGAGGCG
sgPten for 2 (murine)	GATTACAGACCCGTGGCACT
sgPten pan rev (1 and 2) (murine)	ACAATTCCCAGTCAGAGGCG

3.1.7.3 Short hairpin RNAs

The shRNAs employed in this study are listed below. All shRNA were generated using splashRNA internet resource.

Table 3.9: Short hairpin RNAs

shRNA	Sequence (5'- 3')
shBAP1.1299 (human)	TGCTGTTGACAGTGAGCGACGGCCTTTCTAGACAATCAC ATAGTGAAGCCACAGATGTATGTGATTGTCTAGAAAGGC CGGTGCCTACTGCCTCGGA
shBAP1.1399 (human)	TGCTGTTGACAGTGAGCGACCAGCAGTACTCAGATGAT GATAGTGAAGCCACAGATGTATCATCATCTGAGTACTGC TGGGTGCCTACTGCCTCGGA

shBAP1.1409 (human)	TGCTGTTGACAGTGAGCGATCAGATGATGAGGATGACT ATTAGTGAAGCCACAGATGTAATAGTCATCCTCATCATC TGAGTGCCTACTGCCTCGGA
shBAP1.370 (human)	TGCTGTTGACAGTGAGCGCCCTGTTCAAATGGATCGAA GATAGTGAAGCCACAGATGTATCTTCGATCCATTTGAAC AGGATGCCTACTGCCTCGGA
shBAP1.434 (human)	TGCTGTTGACAGTGAGCGATCCGTGATTGATGATGATAT TTAGTGAAGCCACAGATGTAAATATCATCATCAATCACG GACTGCCTACTGCCTCGGA
shBAP1.442 (human)	TGCTGTTGACAGTGAGCGCTGATGATGATATTGTGAATA ATAGTGAAGCCACAGATGTATTATTCACAATATCATCATC AATGCCTACTGCCTCGGA
shBAP1.466 (murine)	TGCTGTTGACAGTGAGCGACCGAATGAAGGATTTCACC AATAGTGAAGCCACAGATGTATTGGTGAAATCCTTCATT CGGCTGCCTACTGCCTCGG
shBAP1.2092 (murine)	TGCTGTTGACAGTGAGCGCAAGGAAGAAGTTCAAGATT GATAGTGAAGCCACAGATGTATCAATCTTGAACTTCTTC CTTTTGCCTACTGCCTCGGA
shREN	TGCTGTTGACAGTGAGCGCAGGAATTATAATGCTTATCT ATAGTGAAGCCACAGATGTATAGATAAGCATTATAATTC CTATGCCTACTGCCTCGG

3.1.7.4 Short guide RNAs

The sgRNAs used in this study are listed in the table below. sgRNAs were designed using CHOPCHOP internet resource.

Table 3.10: Short guide RNAs

sgRNA	sequence (5'- 3')
sgArid1a 1 (murine)	GGGGATCAGGGTCTATGCAG
sgArid1a 2 (murine)	GCGGCGATCAGTAGCAGCGG
sgARID1A 3 (murine)	GCAGGAGAGCCAACAGGGGA
sgARID1A 4 (murine)	GGACAGATGCACTCGGGCGT
sgBAP1 1 (human)	GGCAGAACATCTCCGTGCGG
sgBAP1 2 (human)	GCAAATGGATCGAAGAGCGC

sgBAP1 3 (human)	GGACCGCAGGATCAAGTATG
sgBap1.1 (murine)	GCCCTGCCCCTATTGTCCAG
sgBap1.2 (murine)	GGGTCTCATACTTAATCCTG
sgBap1.3 (murine)	GTGTGGGTCTGAATCAGCTC
sgBap1.4 (murine)	TTGGACCCCACAGATACAAG
sgDdit3 1 (human)	GCATTCGGTCAATCAGAGCT
sgDdit3 1 (murine)	GTCGATCAGAGCCCGCCGTG
sgDdit3 2 (human)	GGAGAATGAACGGCTCAAGC
sgDdit3 2 (murine)	GATCGAGCGCCTGACCAGGG
sgDdit3 3 (murine)	GGAAATCGAGCGCCTGACCA
sgGFP	GGGCGAGGAGCTGTTCACCG
sgPten (murine)	GTTTGTGGTCTGCCAGCTAA
sgTrp53 (murine)	GACCCTGTCACCGAGACCCC

3.1.8 Plasmids

Table 3.11: Plasmids

Plasmid	Description	Source
CMV-SB13	Plasmid expression Sleeping Beauty transposase	AG Tschaharganeh, DKFZ, Heidelberg
LentiCRISPR V2	Lentiviral backbone expressing SpCas9 and sgRNA under U6	AG Tschaharganeh, DKFZ, Heidelberg
MLPe (pMSCV-LTR-miR-E-PGK-Puro-IRES-GFP)	Retroviral vector for shRNA expression	AG Tschaharganeh, DKFZ, Heidelberg
pLVX-M-Flag-BAP1	Lentiviral vector expressing human wild type BAP1	Addgene, 125840
pLVX-M-Flag-BAP1-C91A	Lentiviral vector expressing human mutant BAP1-C91A	Addgene, 125841
pLVX-M-Flag-BAP1-H169Q	Lentiviral vector expressing human mutant BAP1-H169Q	Addgene, 125847
pLVX-M-puro	Lentiviral vector backbone	Addgene, 125839
pMD.2G	VSV-G envelope expressing plasmid	Addgene, 12259
psPAX2	Viral packaging plasmid	Addgene, 12260

pT3-cMYC-IRES-rtTA3	Transposon based plasmid expressing c-MYC and rtTA3	AG Tschaharganeh, DKFZ, Heidelberg
pT3-EF1a-KRASG12D	Transposon based plasmid expressing human KRAS-G12D	AG Tschaharganeh, DKFZ, Heidelberg
pT3-EF1a-MYC	Transposon based plasmid expressing c-MYC	AG Tschaharganeh, DKFZ, Heidelberg
pT3-EF1a-myrAKT	Transposon based plasmid expressing myristoylated AKT	AG Tschaharganeh, DKFZ, Heidelberg
pT3-EF1a-YAPS127A	Transposon based plasmid expressing human YAP-S127A	AG Tschaharganeh, DKFZ, Heidelberg
pT3-TRE-tRFP-miR-E	Transposon based plasmid for doxycycline inducible shRNA expression	AG Tschaharganeh, DKFZ, Heidelberg
pX330-U6-Chimeric_BB-CBh hSpCas9	SpCas9 and chimeric guide RNA expression plasmid	Addgene, 42230

3.1.9 Cell lines

Table 3.12: Cell lines

Cell line	Tissue of origin	Source
HEK293T	Kidney	ATCC
HEK293T-gp	Kidney	ATCC
Hep3B	Liver	ATCC
HepG2	Liver	ATCC
HuH7	Liver	ATCC
NIH/3T3	Embryonic fibroblasts	ATCC

3.1.10 Mouse lines

Table 3.13: Mouse lines

Mouse line	Source
C57BL/6N mouse	Charles River laboratory
shBAP1.2092 mouse line	In-house generation
shBAP1.416 mouse line	In-house generation
shREN mouse line	In-house generation

3.1.11 Mouse diets

Table 3.14: Mouse diets

Diet	Composition	Vendor	Catalog no
CD-HFD	Rodent diet with 45 kcal% fat without added choline	Research Diets	D05010402
Doxycycline diet	6.25% doxycycline hyclate	Envigo	TD.08541
HFD	Rodent diet with 45 kcal% fat	Research Diets	D12451

3.1.12 Software

Table 3.15: Software

Software	Vendor	Use
Aperio ImageScope	Leica Biosystems	IHC image viewer
EndNote 20	Clarivate	Citation manager
Fiji (ImageJ)	Open source	Image processing
Gimp	Gimp Development Team	Image editing
Ingenuity Pathway Analysis	Qiagen	RNAseq Analysis
Inkscape	Inkscape Project	Making figures
Microsoft office 2019	Microsoft	General productivity
Prism 8	GraphPad	Generating graphs
SnapGene	GSL Biotech LLC	Molecular cloning aid

3.1.13 Internet Resources

Table 3.16: Internet sources

Internet resource	URL	Use
cBioportal	https://www.cbioportal.org/	Cancer genomics data analysis
CHOPCHOP	http://chopchop.cbu.uib.no/	sgRNA design
GSEA	https://www.gsea-msigdb.org/gsea/index.jsp	RNAseq data analysis
Heat mapper	http://www.heatmapper.ca/	Heatmap generation
HUGO database	https://www.genenames.org/	Human Gene nomenclature resource
Mouse Nomenclature database	http://www.informatics.jax.org/mgihome/nomen/	Mouse gene nomenclature
NEBio Calculator	https://nebiocalculator.neb.com/#!/ligation	Calculation for molecular methods
Primer Bank	https://pga.mgh.harvard.edu/primerbank/	Primer repository
Primer Blast	https://www.ncbi.nlm.nih.gov/tools/primer-blast/	Primer generation
PubMed	https://pubmed.ncbi.nlm.nih.gov/	Publication repository
splashRNA	http://splashrna.mskcc.org/	Designing shRNA

3.2 Methods

3.2.1 Molecular cloning

3.2.1.1 sgRNA cloning

To enable CRISPR/Cas9 mediated *in-vivo* genome editing, the Cas9 expressing vector px330 (pX330-U6-Chimeric_BB-CBh-hSpCas9) was used to express sgRNAs, targeting genes of interest. Briefly, 2µg of px330 vector was digested with BbsI at 37°C for 4hours. Next 1µl of rSAP was added to the digested vector for 45 minutes to enable dephosphorylation of the DNA ends. Subsequently PCR purification was performed using the QiaQuick PCR purification kit.

Next, the sgRNA oligonucleotide and its reverse complement counterpart were annealed in an annealing mixture comprising: 0.5 µL PNK, 1 µL T4 ligase buffer, 1µL 10 µM top sgRNA, 1µL 10 µM bottom sgRNA, 6.5 µL water. The oligos were then annealed using the thermal cycler viz; 37°C for 30 minutes, 95°C for 5 minutes, - 2°C/sec until 85°C, -0.1°C/sec until 25°C, and held at 4°C. The annealed products were diluted 1:250 and cloned into the digested px330 vector.

To enable CRISPR/Cas9-mediated genome editing in a cell culture setting, the Cas9 expressing lentiviral expression vector, LentiCRISPR V2 was utilized. The vector was digested at 55° with BsmBI. All other steps were the same as specified for px330.

To enable simultaneous expression of two sgRNAs (sgBap1 and sgDdit3), px330 vector expressing sgBap1 was digested with PciI for 4 hours and dephosphorylated with rSAP. The digested vector was run in a gel and the backbone was excised and gel purified. Next, Q5-based PCR was performed on Ddit3 sgRNA insert using U6 (pX330_gib_U6) and px330 (pX330_gib_sgrev) primers designed for HiFi assembly. The amplicon was purified using QiaQuick PCR purification kit. Afterwards, the vector and insert (1:2) were added to HiFi assembly mix and incubated for 1 h at 50°C.

3.2.1.2 shRNA cloning

shRNA oligos in 97 mers format were PCR amplified with miRE-xhoI and miRe -EcoR1 primers viz: 35.75 µL water, 10 µL 5X Her II Pol Buffer, 1.25 µL dNTPs (10 µM), 1.25 µL mirE-XhoI primer, 1.25 µL mire-EcoRI primer, 0.5 µL Herculase II polymerase, 1 µL 97- mer (0.05 ng/µL). PCR program: 95°C for 2 minutes, 30 cycles of 95°C for 20 seconds, 54°C for 20 seconds, 72°C for 30 seconds and finally 72°C for 3 minutes. The PCR product was

subsequently digested with XhoI and EcoRI-HF enzymes and purified. Simultaneously, the retroviral shRNA expression MLPe vector (pMSCV-LTR-miR-E-PGK-Puro-IRES-GFP) was digested with XhoI and EcoRI-HF. The purified PCR product was then ligated into the digested vector.

To assess the potency of the shRNAs, target cells were transduced and subsequently selected with puromycin for 4 days. Afterwards, cells were harvested, protein extracted and WB performed. The most potent shRNAs (as compared to shRNA targeting Renilla) were then selected and used for subsequent experiments.

For *in-vivo* shRNA mediated repression of *Bap1*, two potent shRNAs were cloned into pT3-TRE vector (pT3-TRE-tRFP-miR-E). This was done by digesting the vector with XhoI and ECORI-HF and ligating it with digested shRNA PCR product referenced above.

3.2.1.3 PCR purification

The PCR product to be purified is added to 5x its' volume worth of binding buffer (Buffer PB). The mix was transferred to the supplied QIAquick column and centrifuged for a minute at highest speed (13300 rpm). Afterwards, 750µl of Buffer PE was added to the column in order to wash it and centrifuged for 1 minute at 13300 rpm. The Buffer PE flowthrough was discarded and column was centrifuged again to remove any residual volume. Next, 40 µl of pre-warmed (62°C) elution buffer (Buffer EB) was added to the column and incubated at room temperature for 10 minutes. The eluate was collected in a 1.5 ml tube by centrifuging at 13300 rpm for 1 minute.

3.2.1.4 Gel purification

In order to maintain the fidelity and purity of certain DNA fragments that were subjected to agarose gel electrophoresis, and subsequently excised from agarose gels, gel purification is necessary. Gel purifications in this study were carried out using the QIAquick gel extraction kit. **(See table 3.4)**.

3.2.1.5 Ligation

Ligations of DNA fragments were perfomed using a simple ligation setup that consist of T4 ligase (0.5µl), T4 ligase buffer (1 µl) as well as the digested target vector and the annealed insert (1µl each) topped up with water to reach 10µl. The ligation mix was incubated for 2 hours at room temperature. A ligation mix without the insert was utilized as control. Subsequently, 3 µl of the ligation mix was used for bacterial transformation.

3.2.1.6 Bacterial transformation

Bacteria used for transformations were sourced from New England Biosystems. Briefly, 3µl of ligation mix was gently mixed with 25 µl of bacteria and incubated on ice for 10 minutes. The stable bacteria underwent heat shock at 42°C for 45 second to enable take up of the ligated genetic material. The bacteria were incubated on ice for 3 minutes to enable recovery. Subsequently, bacteria were placed on ampicillin-laden agar plates and incubated overnight at 32°C to allow bacterial colony growth.

3.2.2 Extractions

3.2.2.1 Protein extractions

In this study, proteins were either extracted from cells or from liver tissue. For extraction of proteins from cells, plates/dishes containing cells were placed on ice and the cells were washed twice with cold PBS. Protein lysis buffer were added to the cells (100µl/well for 6 well plates or 500µl/well for 10 cm dishes) and incubated briefly. Cells were scrapped using the cell scrapper and placed in 1.5 ml tubes. The lysates were then sonicated for 30 seconds, vortexed vigorously and incubated on ice for 1 minute. This was done twice. Finally, the samples were centrifuged at 4°C for 10 minutes at 13300 rpm and protein supernatant collected in 1.5 ml tubes.

Protein extraction from tissue was done using a mortar and pestle or a Beadblaster tube placed in Precellys homogenizer for homogenization of 3-4 mm^3 of liver tissue. After homogenization, the samples were transferred to 1.5 ml tubes and the rest follows the protocol specified for protein extraction for cells.

3.2.2.2 mRNA extraction

The mRNA extraction was done using RNeasy Mini Kit (Qiagen), following supplied instructions with slight modifications. Liver tissue was first lysed in 600 µl buffer RLT (β-mercaptoethanol) and homogenized using a mini pestle and mortar or the Precellys homogenizer. Afterwards, the tissue lysate was transferred into the QIAshredder and centrifuged at 13300 rpm for 2 minutes. From here, the protocol supplied in the kit was followed judiciously.

3.2.2.3 gDNA extractions

All gDNA extractions from cell lines and tissues with potential downstream applications (such as T7 assays) were performed using Puregene Core Kit A (Qiagen) DNA isolation kit.

For DNA isolation from mouse tail and ears for genotyping, 200µl of genotyping lysis buffer mix (comprising 196µl genotyping lysis buffer and 4µl proteinase K) were added to each sample. The sample and lysis mix combination were incubated overnight at 56°C. Samples were heated at 95°C for 15 minutes to inactivate proteinase K and subsequently centrifuged at 13000rpm for 5 minutes.

3.2.2.4 Plasmid DNA extraction

Plasmid DNA extractions in this study were carried out using the QIAprep Spin Miniprep Kit and Plasmid Plus Midi Kit from QIAGEN. The supplied protocols were followed judiciously.

3.2.3 Cell and molecular biological assays

3.2.3.1 Museum techniques

For this study, all post fixation assays such as embedding of tissues in paraffin and transfer of tissue slices onto glass slides were performed by the center for model system and comparative pathology (CMCP) & the histology laboratory of the Pathology Institute, Heidelberg, unless stated otherwise.

3.2.3.2 Immunofluorescence

Slides containing tissue slides of interest were deparaffinized in xylol for 5 minutes (3x). Afterwards the slides were placed in Ethanol of decreasing dilutions viz; 5 minutes in 100% EtOH (2x), 5 minutes in 96% EtOH (2x) and finally in 70% EtOH to complete deparaffinization. Slides were immediately rehydrated by placing them in distilled water for 5 minutes. Slides were subsequently placed in antigen retrieval buffer and heated with pressure cooker for 8 minutes to facilitate antigen retrieval. Next slides were cooled down by placing them in running water. The cooled slides were dried and tissues borders were delineated with a hydrophobic pen. The slides were blocked with blocking solution (5% BSA in PBS + 0.05% Triton X) for 1 hour at room temperature. The blocking solution was discarded and 150µl of primary antibody combinations (in blocking solution) was added (uniformly spread) on the slides and incubated overnight in a humid slide chamber at 4°C.

Next, the slides were washed in cold PBS for 5 minutes (3x) and incubated with 300µl of secondary antibody (in blocking solution) for 1 hour at room temperature in a dark slide chamber. The slides were then washed thoroughly in PBS by gentle rocking for 5minutes (x3). Next the slides were incubated for 2 minutes with DAPI or Hoechst solution to facilitate nuclear staining. Subsequently, the slides were dried, one drop of mountant was added and covered with coverslips.

3.2.3.3 Tissue staining and immunohistochemistry

Tissue stainings (such as hematoxylin and eosin (H&E) and Gomori methenamine silver stainings (GS) as well as immunohistochemistry were performed by the CMCP & the histology laboratory of the Pathology Institute, Heidelberg. IHC and other tissue stainings not covered by the CMCP laboratory was performed by the histology facility of Professor Dr Mathias Heikenwaelder (AG Heikenwaelder, F180, DKFZ, Heidelberg).

3.2.3.4 Real-time quantitative PCR (RT-qPCR)

mRNAs isolated using the RNeasy Mini Kit from Qiagen were converted to cDNA using the TaqMan Reverse transcription kit following manufacturer provided protocols. Afterwards, the synthesized cDNA was diluted 1:20. Next, 1 µl of the diluted cDNA was mixed into a cocktail containing SYBR Green Master Mix and primers designed for specific genes. The qPCR reaction was laid out in triplicates and performed using the QuantStudio 3 system from Thermo Fisher. GAPDH was employed as the housekeeping gene in all reactions. Finally, relative gene expression was obtained using the ΔΔCt method.

3.2.3.5 Genotyping PCR

For genotyping PCR, a master mix comprising of 1 µl of sample, 1 µl of primers, 12.5 µl of RedTag mix and 8.5 µl of water was constituted. Genotyping PCR program (denaturation at 95°C for 5 minutes, 35 amplification cycles of 95°C for 30 seconds, 58°C for 30 seconds, 72°C for 1 minute, and finally 72°C for 3 minutes) was then applied to the cocktail. Following amplification, the samples were loaded in 2% agarose (with ethidium bromide diluted at 1:20000) and finally imaged with the ProteinSimple imager to validate the genotype of each mouse.

3.2.3.6 Immunoblotting

Following protein extraction and quantification, 30µg of protein per sample was added to 4µl of protein loading buffer and filled with water until 20µl. The mix containing the samples were then heated in a heat block at 95°C to ensure sample denaturation. The denatured samples were loaded into acrylamide gels and separated by SDS-PAGE. Afterwards, transblotting onto PVDF membrane was performed at 120V for 90 minutes. Next, the membrane was blocked in 5% milk diluted in TBS-T. Primary antibodies were diluted in the blocking solution (5% milk in TBS-T) and incubated on the membrane at 4°C overnight on the rolling shaker. The blots were subsequently thoroughly washed with TBS-T for 5 minutes (repeated 3x). Afterwards, the membranes were incubated with the appropriate secondary antibodies for 1 hour at room temperature. Following another thorough wash (4x 5minutes), signal detection was carried out by incubating the membrane in ECL solution and developing it under the ProteinSimple imager.

3.2.3.7 T7 endonuclease assay

T7 assay was used to test for the potency of sgRNAs or for mutation detection after CRISPR/Cas9-mediated editing. Briefly, 3T3 Hras cells transfected with the target sgRNA were harvested 4 days post transfection (allowing enough time for genome editing after transfection). Next, genomic DNA was isolated using the Puregene Core Kit A supplied by Qiagen. High fidelity primers designed to amplify the region immediately surrounding the CRISPR/Cas9-targeted region was tested and verified to produce a single band of the expected product size. The targeted area was amplified using the Q5 polymerase with the reaction mix comprising: 10 µL 5X Q5 Buffer, 2.5 µL 10 µM forward primer, 2.5 µL 10 µM reverse primer, 1 µL 10 mM dNTPs, 0.5 µL Q5 Hot Start DNA Polymerase, 250 ng gDNA and nuclease-free water until 50µl. The amplicon was PCR purified and re-annealed. The melt-anneal hybridization mixture comprised of 200 ng amplicon, 2 µl of 10x NEB 2 buffer in a reaction volume totaling 19 µl (supplemented with water if necessary). The melt-anneal hybridization program was as follows: 95°C for 5 minutes, -2°C/sec until 85°C, -0.1°C/sec until 25°C, 4°C forever. Subsequently, 1 µl of T7 endonuclease (which cleaves mismatches and heteroduplexes) is added to the annealed product and incubated at 37°C for 35 minutes. T7 cleavage was then analyzed by loading the reaction mix on a 2% agarose gel and imaged on the ProteinSimple imager.

3.2.3.8 Nucleic acid and macromolecule quantification

Nucleic acids (RNA and DNA) were quantified using the Nanodrop spectrophotometer.

Triacylglycerol quantification was performed by following the instructions provided in the Triacylglycerols Quantification Kit from Sigma.

Protein quantification was performed using Bradford protein assay. Briefly, the reagent was prepared by diluting the Bradford concentrated in water (1:5). BSA standards of known concentrations corresponding to 0, 5, 10, 15, 20 and 25 µg/µl was prepared and 1 ml of diluted Bradford reagent added and vortexed. Next, 1 µL of protein samples of unknown concentration were added to 1 ml of the diluted Bradford reagent, vortexed vigorously and incubated at room temperature for 10 minutes. 150 µl each of sample and standard were transferred in triplicates to 96 well and absorbance measured at 595 nm using the plate reader. Protein concentration was determined by using Excel to extrapolate samples' protein concentration from the absorbance data.

3.2.4 Cell culture related methods

3.2.4.1 General cell culture

In the course of this study, all cells were maintained at 37°C in 5% CO_2. Cells were sustained in complete DMEM (Dulbecco's Modified Eagle Medium) and nourished with 10% FBS (fetal bovine serum) and 1% Pen-Strep. Cells were split 1:3 whenever they attained 90% confluency. In order to ensure adherence, mouse cell lines were cultured on collagen coated plates.

3.2.4.2 Primary cell line derivation from liver tumors

Liver tumors were harvested using sterile animal surgical instruments. Approximately 10 mg of tumor was minced with a disposable scalpel and incubated in 2 ml of collagenase dispase solution (consisting of 4mg/ml collagenase IV and dispase medium dissolved in DMEM without supplements). Next, cells were centrifuged at 1500 rpm for 5 minutes and the supernatant replaced with supplemented DMEM. Supplemented DMEM was further nourished with 40 ng/ml EGF II (epidermal growth factor) and 8ng/ml IGF (insulin-like growth factor) to enable more efficient establishment of the cell lines. Primary cell lines were passaged until other cell type contaminants were absent. Once established, routine mycoplasma checks were carried out on the cell lines.

3.2.4.3 Virus production and transduction

Two types of viruses were produced in this study, namely lenti- and retroviruses. For lentivirus production, the kidney embryonic cells, HEK293T, were plated at about 40% confluency in 10cm plates a day before transfection such that it attains around 80% confluency on transfection day. The transfection mix (1 mL DMEM, 8 µg psPAX2,2.5 µg pMD.2G, 10 µg of vector and 60 µL of PEI (1 µg/µL) was vortexed for 30 seconds and incubated at room temperature for 30 minutes. The mixture was then added to the near confluent (80%) HEK293T cells in a dropwise manner. 24 hours following transfection, the medium was replaced with fresh supplemented DMEM. At 48 hours post transfection, lentiviral supernatant was collected and filtered by passing them through purpose fit 0.45µm µm cellulose acetate membrane filters from VWR international.

Retroviral production was performed using HEK293T-gp cells. The plating protocol was followed as described for lentiviral production. The transfection mix here differs slightly from that for lentiviral production. It comprises of 1 mL DMEM, 2.5 µg pMD.2G, 20 µg of vector and 60 µL of PEI (1 µg/µL). Following transfection, the protocol as described for lentivirus production applies.

Prior to transduction, recipient cells were plated at about 30% confluency. Next, the target cells were transduced with viral supernatant containing polybrene (4 µg/ml). 4hours days post-transduction, cells were plated at 40% confluency and challenged with puromycin (2 µg/ml) to eradicate untransduced cell populations.

3.2.4.4 Proliferation assay

In order to evaluate proliferation trajectory in cells of interest, proliferation assay was performed viz: 50,000 to 100,000 (depending on cell type and growth rate) cells per well were seeded in triplicates in 6-well plates. Cells were maintained in culture and split just before reaching confluency, with their concentration being measured with the Guava flow cytometer. This is repeated until at least 4 time points were measured.

3.2.4. Fatty acid challenge assay

The free fatty acids, palmitic acid and oleic acid, were dissolved in ethanol, aliquoted and frozen at -20˚C. Cells were plated in triplicates at a concentration of 2000 cells per well in 6-well plates. Pre-warmed fatty acids were added directly to the medium at a 1:1 ratio to

yield 500 µm fatty acid concentration (250 µm each). The fatty acid-supplemented medium was exchanged every 3 to 4 days until the end of the assay.

3.2.4.6 Colony formation assay

For colony forming assay (CFA), cells were plated in 6-well plates at a concentration of 1000-2000 depending on the cell line growth rate. The cells were left to grow for 7 to 12 days. Afterwards, the colonies were washed with PBS to remove traces of cell culture medium and stained with 0.5 ml of crystal violet solution (see table 3.5), followed by incubation for 30 minutes on a flat plate shaker. The crystal violet solution was then removed and the colonies washed with PBS. The plates were subsequently imaged using the ProteinSimple imager.

Indirect quantification of colony number via intensity of the crystal violet staining was done by dissolving the colonies in solubilization buffer (50% methanol, 5% acetic acid, 0.1% SDS) and incubating at room temperature for 1 hour. Afterwards, absorbance of the dissolved colonies was measured at 570 nm using a plate reader.

3.2.5 Transcriptomics and lipidomics analyses

For transcriptomics analyses, RNA was isolated from mouse liver tissue using the RNeasy Kit from Qiagen. RNA seq was performed by the DKFZ sequencing facility. After aligning of the RNAseq counts, subsequent analysis was perfomed using the HUSAR platform of the DKFZ. Briefly, genome-wide transcript count was performed using the HUSAR program HTSeq count to generate FPKM (fragments per kilobase of transcripts per million) data. Next, differentially expressed genes were identified by using the HUSAR program COMPARNA which integrates different statistical tools including DEseq2. The files generated using DEseq2 were exported and used for downstream analysis such as Ingenuity Pathway Analysis (IPA) and Gene Set Enrichment Analysis (GSEA).

For lipidomics analysis, liver tissues were prepared on dry ice. Briefly, around 50 ng of liver tissue was cut out and kept in MK28-R/2ml in frozen conditions for subsequent lysis. The samples were delivered to Prof. Britta Brueger's lab (Heidelberg University Biochemistry Center (BZH) where lipidomic assay was performed.

3.2.6 Animal experiments

All animal experiments were performed at the DKFZ animal facilities. Animal experiments were approved by the regional board in Karlsruhe.

3.2.6.1 Hydrodynamic tail vein injection (HDTVI)

For hydrodynamic tail vein injections, 7-week-old female female C57BL/6N mice were obtained from Charles River laboratories. Upon attaining 8 weeks of age, the animals were injected with 2ml of sterile saline solution (10% of body weight) containing naked DNA plasmids. Overexpression or gene depletion can be achieved depending on the plasmid used. For sgRNA- and shRNA-mediated gene disruption, 20 µg of plasmid (px330 or pT3-TRE, respectively) was used. For overexpression 5 µg (c-MYC expressing plasmids) or 10 µg (myrAKT or YAP^{S127A}) of plasmids were used. Sleeping Beauty transposase-carrying plasmid was injected at a 1:5 ratio of the corresponding transposon-based plasmid. All HDTVIs were performed by Lena Wendler, Kai Volz and Prof. Dr. Darjus Tschaharganeh. For HDTVI experiments, the number of animals in each experimental group were at least 5.

3.2.6.2 Mouse dietary experiments

In this study, mice were fed with CD-HFD, HFD or doxycycline diet. For simultaneous doxycycline and CD-HFD/HFD intervention, mice were administered doxycycline water (2 g doxycycline, 10 g saccharose in 1 L of water). Blood was collected from mice using sub-mandibular bleeding. Serum was subsequently isolated from the blood samples, unless otherwise specified. The number of animals in each experimental group were at least 4.

3.2.6.3 Handling of mouse tissue

In the event of tumor detection by palpation or following the end of an experiment, the animals were sacrificed by cervical dislocation, liver tissue was harvested and snap frozen for eventual genetic material (DNA, RNA) and macromolecule (protein) extraction. Another liver piece was designated for freezing in OCT medium. The bulk of the liver tissue was fixed in 4% paraformaldehyde (PFA) for 5 days for downstream tissue processing.

3.2.6.4 Magnetic resonance imaging (MRI)

MRI used in this study was performed by the small animal imaging facility of the DKFZ.

3.2.7 Statistical analysis

All statistical analysis in this study was performed using GraphPad Prism 8. Error bars indicate standard deviation. The statistical analysis used in any given figure is specified in the figure caption. Statistical significance levels (i.e rejection of the null hypothesis) are depicted as follows; *: $p < 0.05$, **: $p < 0.01$, ***: $p < 0.001$, ****: $p < 0.0001$. Non-significant results were left empty with no particular designation. Results close to significance are written out with the p-value shown.

4 Results

4.1 Unravelling the functional relevance of BAP1 in liver homeostasis and metabolic pathologies

4.1.1 Generation and validation of a doxycycline regulatable BAP1 transgenic mouse model

In order to investigate the functional relevance of BAP1 in liver homeostasis and pathogenesis, a novel, temporally regulatable shRNA based transgenic mouse strain was developed. To enable robust and efficient modelling of BAP1 functions in the liver, a previously described technology developed for producing transgenic mice harboring tetracycline responsive shRNA constructs was employed[122, 123]. The technology utilizes embryonic stem (ES) cells containing a frt-hygro-pA "homing" cassette downstream of the *ColA1* gene on mouse chromosome 11, and a reverse tet-transactivator (rtTA) targeted into murine *Rosa26* locus. This system allows for the generation of a powerful knockdown mouse model by taking advantage of potent shRNAs with silencing efficiency akin to a genetic knockout. Two powerful shRNAs targeting *Bap1* were cloned into a targeting vector, which comprises of Tetracycline regulatory element (TRE), a doxycycline (Tetracycline analog) inducible promoter, (TRE-promoter) and green fluorescence protein (GFP). This was subsequently introduced into ES cells and positive clones were used to generate *Bap1* shRNA chimeras. Upon generation, *Bap1* shRNA chimeras were crossed with Albumin-Cre mice to generate doxycycline inducible, liver specific shBAP1 mice. The expression of the reverse tetracycline trans-activator (rtTA3) alongside the far-red fluorescent gene mKate2 is made possible by Cre-Lox recombination in the Rosa26 locus. Conceptually, mKate2 serves as an analog for Cre recombination and rtTA3 expression while GFP expression on the other hand serves as a reporter for rtTA3 binding and activation of the TRE promoter which drives the expression of the shRNAs targeting *Bap1* upon administration of doxycycline. A complementary mouse model with the same system targeting Renilla luciferase was also developed and was utilized to control for any potential doxycycline and unspecific shRNA induced effects. A visual overview of the system is depicted in **Figure 4.1.1A**. The two *Bap1* strains will henceforth be referred to shBAP1.1 and shBAP1.2 while Renilla mouse strain will be referred to as shRenilla. For the presentation of results utilizing this mouse strains, control (off dox) cohort will be depicted as Co while experimental (on dox) animals will be depicted as the shRNA it induces (e.g., shBAP1.1 or shRenilla). The mouse models described here were generated by Prof Dr. Darjus Tschaharganeh.

To test the integrity of the system and to validate whether tissue specificity and correct expression of the reporter system was achieved, I placed shBAP1 and shRenilla transgenic mice on Dox chow for one week to allow for efficient activation of the Dox regulatable system. Afterwards, mice were sacrificed and vital organs (liver, heart, kidneys, spleen, lungs and intestine) were collected and imaged under the dissectoscope to check for GFP and mKate2 expression. As expected, livers taken from mice placed on Dox expressed both mKate2 and GFP while those from off Dox mice expressed only mKate2 **(Figure 4.1.1B).** All other organs showed no expression of the fluorescent reporter genes.

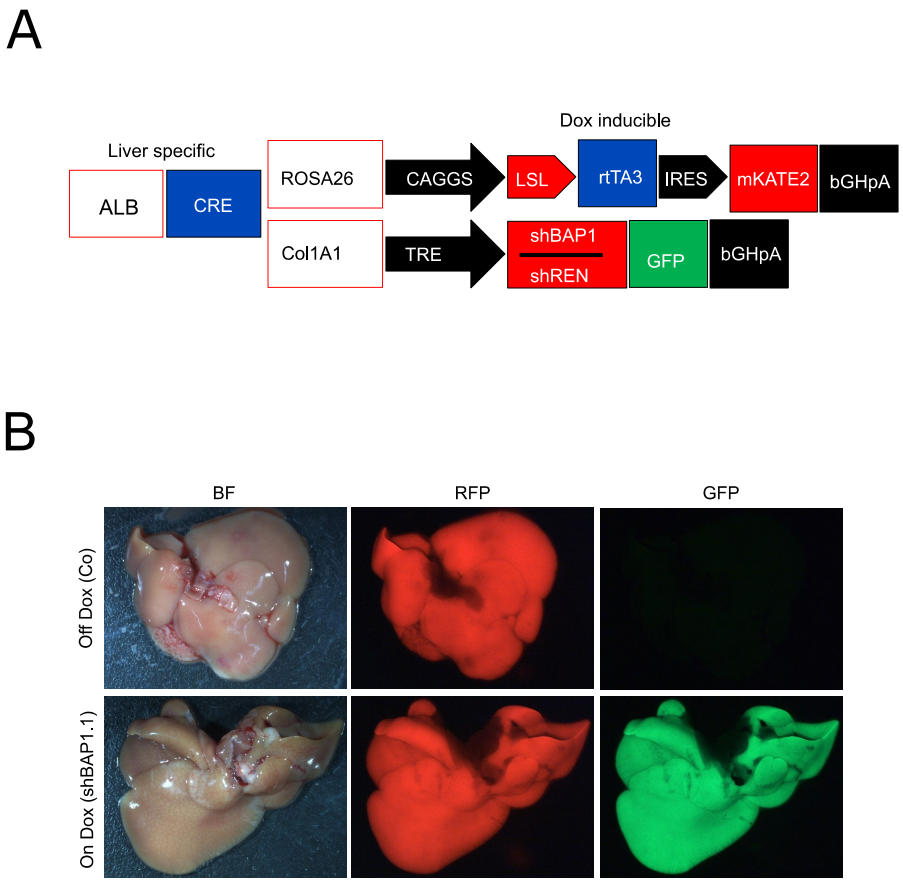

Figure 4.1.1: Conditional shBAP1 and shRenilla mouse strains. **(A)** Illustration of the transgenic composition of the strain that enables liver tissue specificity and dox dependent expression of shRNAs. **(B)** Dissectoscope image of the traffic light reporter system (red and green). mKate2 expression is observed with and without Dox while GFP expression is observed only after Dox administration

4.1.2 Expression of shBAP1 transgene potently represses BAP1 *in-vivo*

Upon validation of the reporter system and liver specificity of the shBAP1 and shRenilla mouse strains, I proceeded to probe whether the transgenic mouse system indeed targeted the relevant liver resident cells (hepatocytes and cholangiocytes). To achieve this, I placed

shBAP1 and shRenilla mice on Dox (to allow for expression of the shRNA transgene) for one week. The animals were sacrificed, the liver tissues were harvested and subsequently processed for immunofluorescence. Afterwards, double immunofluorescence staining was performed for liver parenchymal cells specific markers, hepatocyte nuclear factor 4 alpha (HNF4α) for hepatocyte and cytokeratin-19 (CK19) for cholangiocytes, (reported by red fluorescence) in combination with GFP staining. Immunofluorescence staining revealed that the *Bap1* mouse strains (shBAP1.1 and shBAP1.2) express GFP (a surrogate for shBAP1 expression), which colocalizes with both CK19-positive and HNF4α-positive cells and thus is expressed in cholangiocytes and hepatocytes, respectively **(Figure 4.1.2A).**

After confirming that the shBAP1 transgene is expressed in hepatocytes and cholangiocytes, I proceeded to interrogate the *in-vivo* potency of the shRNAs targeting *Bap1*. Firstly, I performed double immunofluorescent staining for BAP1 and GFP. Next, analysis of the immunofluorescence staining suggested potent repression of BAP1 *in-vivo* as exemplified by markedly reduced nuclear expression in on Dox mice. Off Dox mice maintained strong BAP1 nuclear expression. Expectedly, on Dox (shBAP1.1) mice showed strong expression of GFP while off dox (co) mice did not **(Figure 4.1.2B)**.

To further corroborate the finding regarding the *in-vivo* potency of *Bap1* shRNAs, shBAP1 and shRenilla mice were placed on normal diet or Dox chow for one week. Afterwards, RNA and proteins were isolated from liver tissues of the respective mouse strains. Western blot analysis revealed strong knockdown of BAP1 in the shBAP1 mouse strains (shBAP1.1 and shBAP1.2) for mice administered Dox chow **(Figure 4.1.2C&D)**, whereas no such reduction in BAP1 protein levels was observed in shRenilla mice **(Figure 4.1.2E).** Strong expression of GFP in Dox administered animals was observed in all mouse strains, as expected **(Figure 4.1.2C-E).** Additionally, quantitative real time polymerase chain reaction (qRT-PCR) analysis showed potent and significant reduction in BAP1 gene expression for mice placed on Dox chow in shBAP1.1 and shBAP1.2 strains as compared to mice placed on normal diet. **(Figure 4.1.2C&D)**. Of note, shRenilla mice placed on Dox chow showed no difference in *Bap1* gene expression when compared to mice on normal diet **(Figure 4.1.2E)**

Taken together, these results show that the transgenic mouse strain described here potently represses *Bap1 in-vivo*.

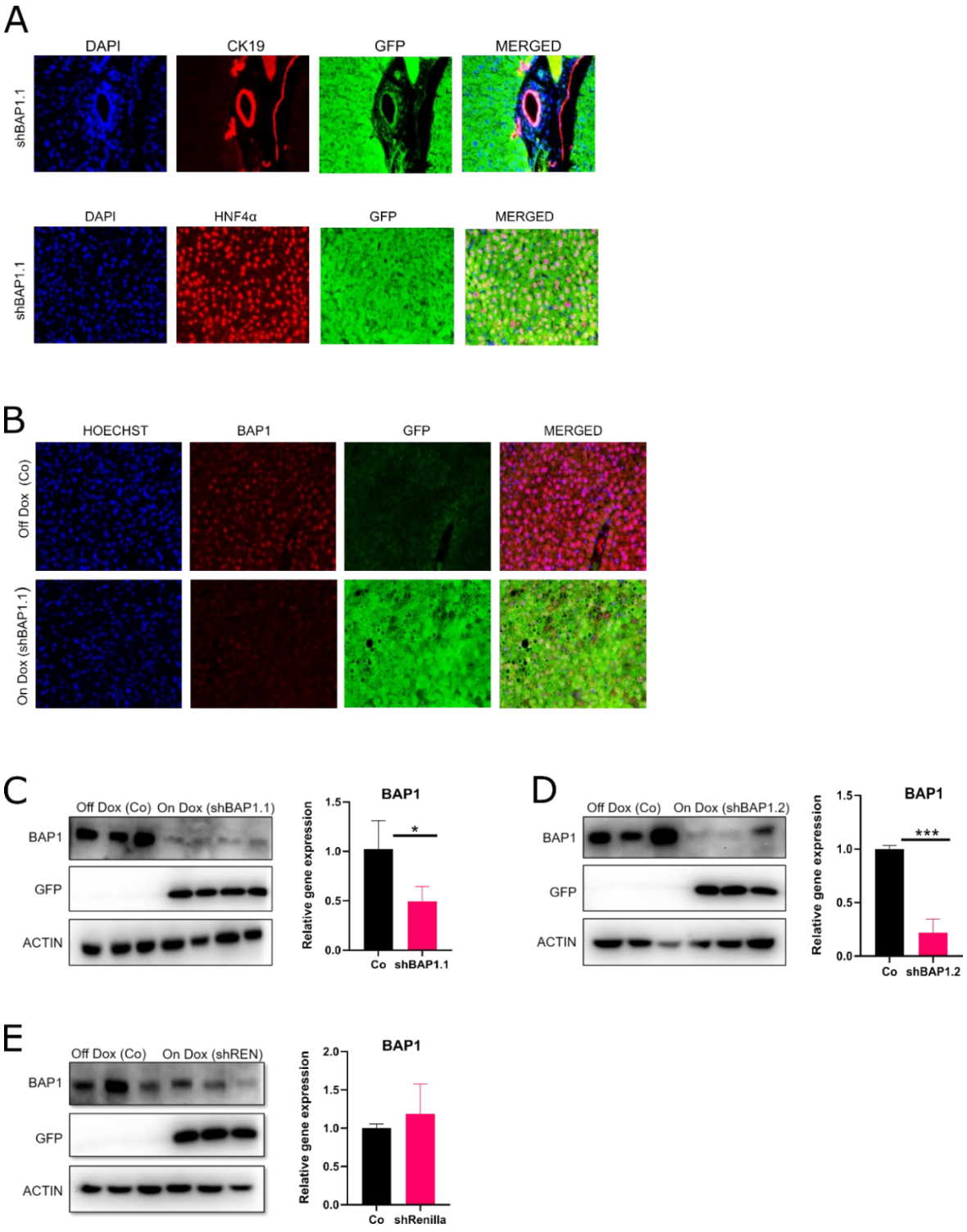

Figure 4.1.2: Short hairpin RNA targeting *Bap1* potently represses its expression *in-vivo*: (A) Representative Immunofluorescence image depicting the co-localization of GFP and hence expression of shBAP1 in cholangiocytes (CK19) (upper panel) and hepatocytes (HNF4α) (Lower panel). **(B)** Immunofluorescence image showing the loss of BAP1 nuclear expression in Dox fed shBAP1 mice. **(C&D)** Western blot image and qRT-PCR quantification (n=3) showing loss of BAP1 protein expression and reduced *Bap1* gene expression in dox fed shBAP1.1 and shBAP1.2 mouse strains. **(E)** Western blot image and qRT- PCR (n=3) quantification of shRenilla mouse strain which shows no changes in BAP1 expression in Dox fed mice. Statistical test: Student's t- test.

4.1.3 Long term suppression of *Bap1* leads to mild pathological changes in the liver

To understand the potential effect of long-term suppression of BAP1 in the liver, I utilized the previously described shBAP1 and shRenilla mouse strains. Briefly, animals were divided into two broad groups, one receiving normal diet (control cohort) while the other group was challenged with dox chow (experimental cohort). The animals were further subdivided in timed groups namely: 6, 12, 24 and 36-weeks' time points. This grouping and experimental setup enabled an easy-to-follow regimented time-limited experimental course **(Figure 4.1.3A).** At the end of each time point, I took animal weight and collected blood serum as well as the respective livers **(Figure 4.1.3A)**. Analyses of data obtained on animal weight during the course of the experiment indicated a gradual increase in weight as the animals aged. However there were no significant differences in weight between the experimental and the control groups themselves **(Figure 4.1.3B)**. The animals remained generally healthy throughout the duration of the experiment with no signs of becoming moribund. These data indicate that the animals could tolerate long term loss of BAP1 under homeostatic conditions.

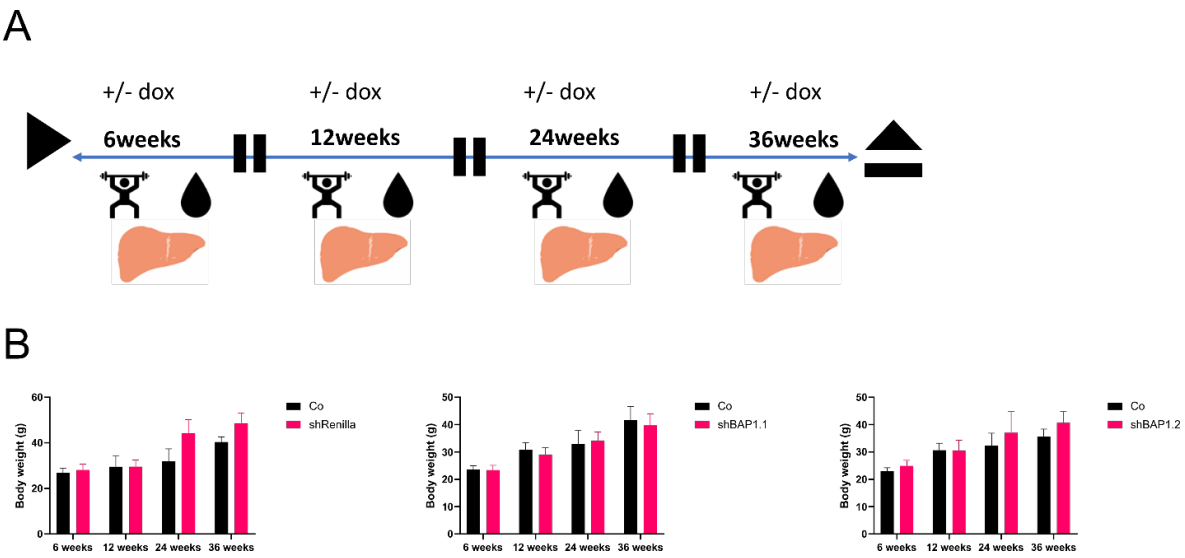

Figure 4.1.3: Long term suppression of *Bap1* has no effect on weight in mice. **(A)** Schematic depiction of the regimented experimental plan of BAP1 long term suppression. **(B)** Body weight analysis of mouse strains (panels from left to right: shRenilla, shBAP1.1 and shBAP1.2) showing stable body weight across all cohorts

In order to verify whether *Bap1* is persistently suppressed over time in the experimental setup, I performed Western blot (WB) analysis on lysates obtained from harvested livers from animals from selected timepoints (6 and 24 weeks). Importantly, WB analyses of BAP1 in the BAP1 mouse strains (shBAP1.1 and shBAP1.2) showed sustained suppression of BAP1 protein levels after 6 weeks and 24 weeks in the experimental cohort, albeit with slightly reduced efficiency in the latter **(Figure 4.1.4A&B)**. As expected, shRenilla animals showed no difference in BAP1 levels across the experimental groups **(Figure 4.1.4C)**. Immunoblot for GFP on the other hand showed strong expression in shBAP1.1 and shRenilla, while it was noticeably weakly expressed in shBAP1.2 **(Figure 4.1.4A-C)**. To complement the WB analysis and confirm the sustained expression of the BAP1 shRNAs over 36 weeks, I analyzed immunohistochemical (IHC) staining for GFP. Results indicated strong expression of GFP over 24 weeks in the experimental cohorts of shBAP1.1. The 36 weeks cohort however, showed very weak GFP staining **(Figure 4.1.4D)**. On the other hand, shBAP1.2 mouse strain displayed reduced GFP expression, manifested in a mosaic staining pattern at week 6,12 and 24 **(Figure 4.1.4 D)**. Surprisingly, GFP was strongly expressed in the experimental cohort in this strain at 36 weeks **(Figure 4.1.4D)**.

Next, I characterized histological features of shBAP1 and shRenilla mouse strains challenged with dox over time (up to 36 weeks). Hematoxylin and eosin staining (H&E) allows for differential staining of the nucleus (Hematoxylin -blue) and cytoplasm and extracellular matrix (eosin -pink) to identify cellular components[124]. Analyses of H&E stains revealed relative normal cellular architecture in all mouse strains **(Figure 4.1.5)**. Importantly, I did not observe any evidence of malignant transformation in the analyzed cohort. However, there were visible fat deposits in some of the cohorts **(Figure 4.1.5)**.

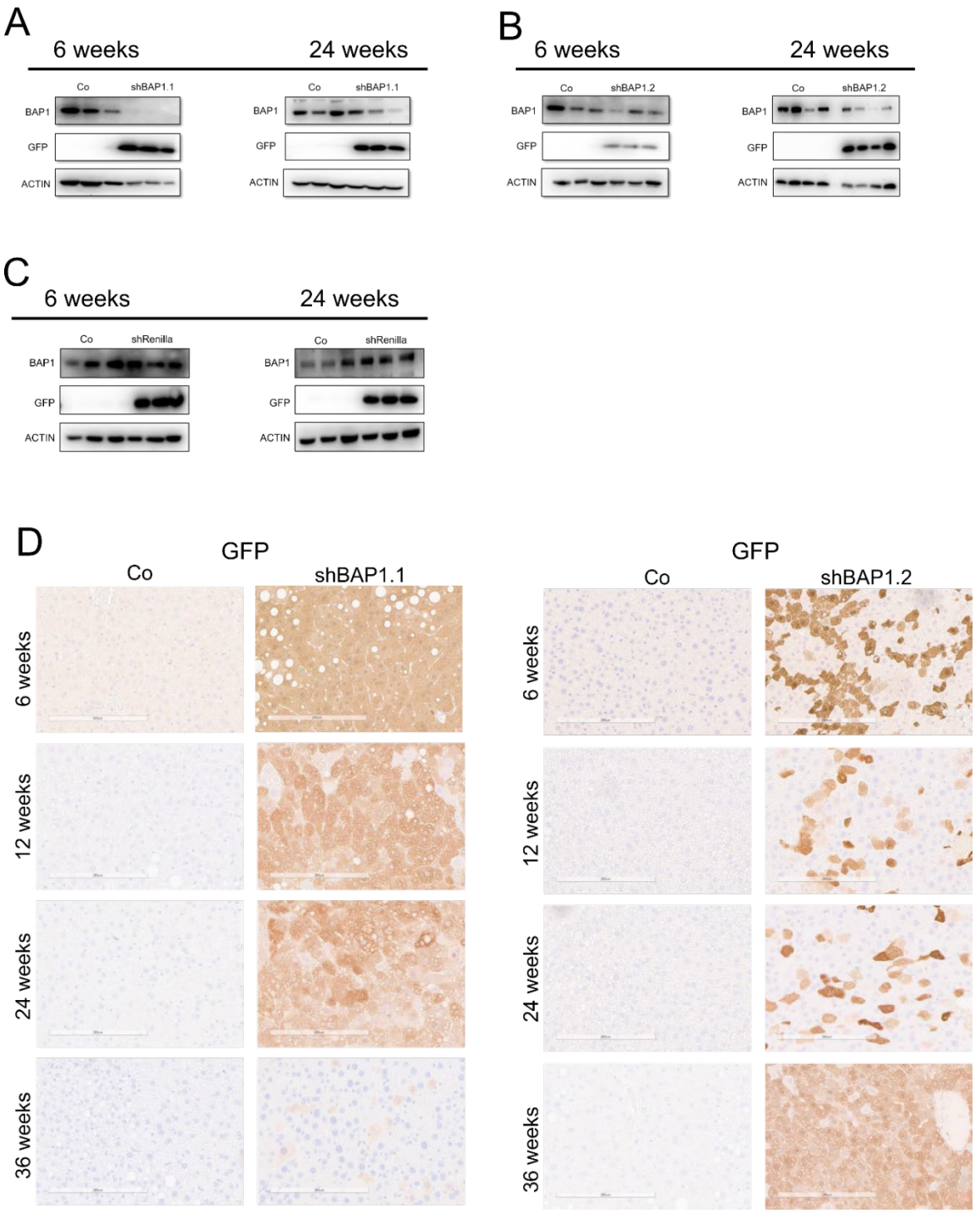

Figure 4.1.4: Sustained repression of *Bap1 in-vivo*. **(A-C)** Western blot image of experimental mouse strain showing BAP1 and GFP protein levels after sustained dox administration**.** **(D**) Representative IHC image for GFP over 36 weeks in shBAP1 mouse strains (scale bar, 200μm)

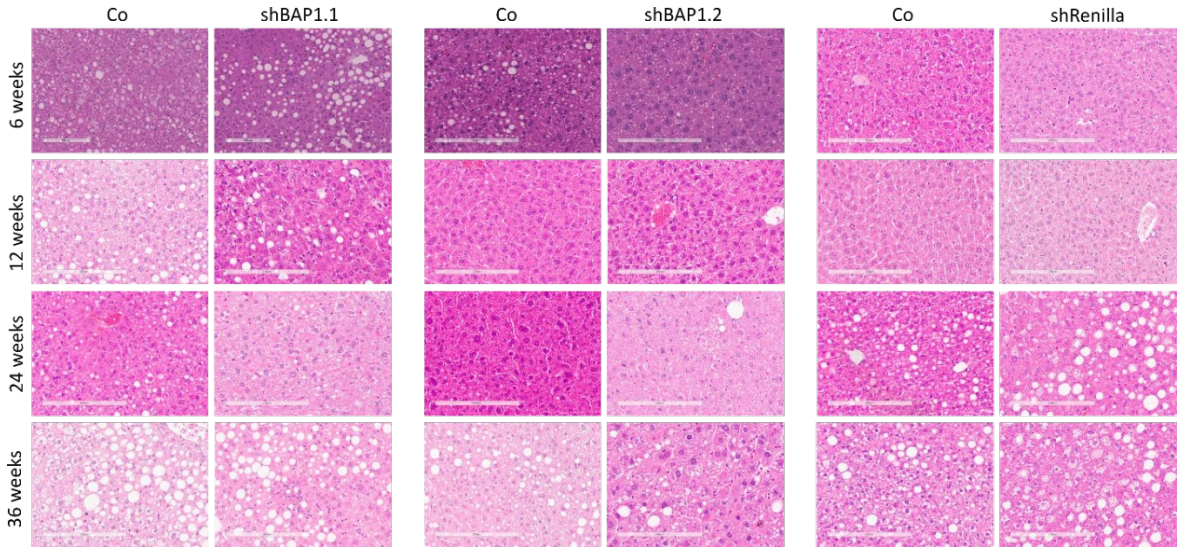

Figure 4.1.5: H&E staining of BAP1 and renilla mouse strains. From Left to right; H&E stainings for shBAP1.1, shBAP1.2 and shRenilla mouse strains (scale bar: 200µm). Co depicts control cohort (off Dox) while reference to a specific shRNA depicts expression of that shRNA (On Dox, experimental cohort).

To probe whether long term *Bap1* loss has any effect on liver function and injury, I employed a battery of assays geared towards interrogating liver function. Alanine transaminase (ALT) and Aspartate transaminase (AST), surrogates of liver function become elevated in the serum upon liver injury [125], as does Bilirubin, a product of hemoglobin catabolism, which is excreted by the liver in physiological states [126]. Thus, measurement of all three markers allows for the prediction of liver function in the mice strains upon dox challenge over 36 weeks. For shBAP1.1 strain, I observed a significant increase in ALT serum level at week 6,12 and 24, albeit within physiological levels, while no significant increase was observed in shBAP1.2 and shRenilla across all time points **(Figure 4.1.6A)**. Similarly, AST serum level was also significantly elevated in shBAP1.1 (also within physiological range) at week 6,12 and 24, while shBAP1.2 and shRenilla mouse strains showed no such changes over the evaluated time period. **(Figure 4.1.6B)**. Bilirubin on the other hand, remained fairly stable and comparable across all experimental cohorts and time points for all experimental strains **(Figure 4.1.6C)**. These results imply that the pathophysiological changes described herein are relatively mild and liver function remains intact over time upon *Bap1* depletion.

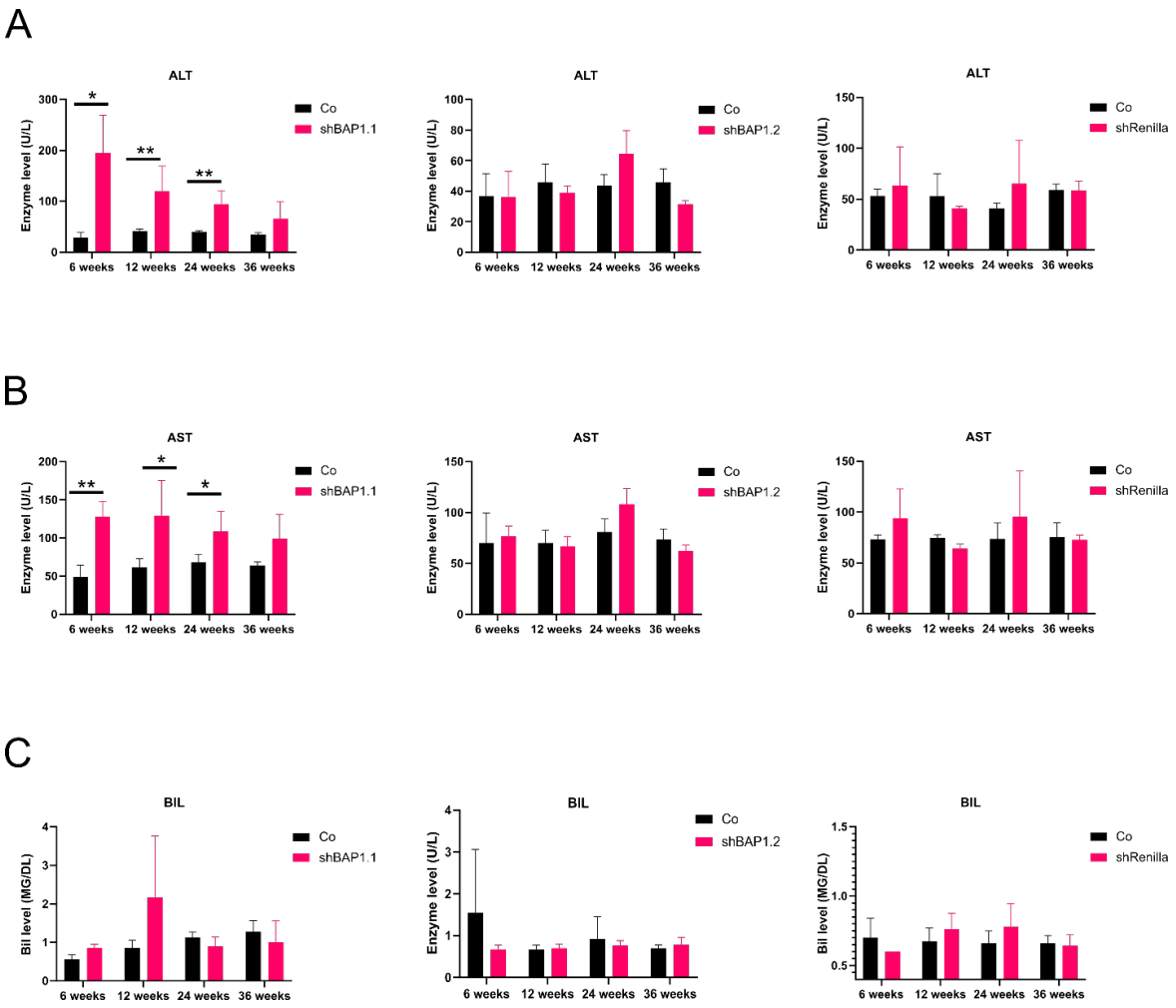

Figure 4.1.6: Sustained repression of *Bap1* in the liver does not affect organ function and health. **(A)** ALT measurement for all mouse strains across 36 weeks (panels from left to right; shBAP1.1, shBAP1.2 and shRenilla). **(B)** AST measurement for all mouse strains across 36 weeks (panels from left to right; shBAP1.1, shBAP1.2 and shRenilla). **(C)** BIL measurement for all mouse strains across 36 weeks (panels from left to right; shBAP1.1, shBAP1.2 and shRenilla). Statistical test: Student's t- test.). Co depicts control cohort (off Dox) while reference to a specific shRNA depicts expression of that shRNA (On Dox, experimental cohort).

4.1.4 *Bap1* suppression coupled with calorific overload is deleterious in mice

Long term suppression of BAP1 (up to 36 weeks) had no effect fatal outcomes in the mouse models employed in this study. However, there was relative elevated transaminases level (shBAP1.1) and steatosis (shBAP1.1). This observation, thus, informed the hypothesis that strong BAP1 physiological effect in the liver might be connected to fatty acid metabolism. Specifically, I hypothesized that combining *Bap1* loss with dietary models of liver cancer may accelerate tumorigenesis. To test this hypothesis, I placed the mouse strains (shBAP1.1, shBAP1.2 and shRenilla) on CD-HFD coupled with oral administration of doxycycline via drinking water. The control cohorts remained on ordinary drinking water (off

Dox). Surprisingly, after 3 weeks on the experimental regimen, I observed that a sizeable number of shBAP1.1 and shBAP1.2 animals became immobile with crouched back and general poor health and had to be sacrificed. At 6 weeks over 70% (shBAP1.1) and 60% (shBAP1.2) of animals had to be sacrificed **(Figure 4.1.7A)**. Of note, shRenilla animals on the same experimental regimen experienced no mortality **(Figure 4.1.7A)**. I performed analyses of H&E stainings of the livers and it revealed hyper-eosinophilic cells, a histomorphological stigmata of necrosis, and increased intercellular spaces in the moribund animals **(Figure 4.1.7B)**. IHC staining for GFP confirmed the expression of shRNA transgene in all strains **(Figure 4.1.7B)**. Importantly, IHC staining for BAP1 revealed loss of nuclear expression in Dox challenged shBAP1.1 and shBAP1.2 animals. As expected, shRenilla animals retained strong nuclear expression of BAP1 regardless of Dox status **(Figure 4.1.7B).** To strengthen this observation, I performed WB analysis for shBAP1.1 strain from the same cohort. Results corroborated loss of BAP1 protein expression and strong GFP expression in Dox administered animals while shRenilla samples displayed stable expression of BAP1 protein as well as strong GFP expression in the experimental (Dox challenged) cohort **(Figure 4.1.7C)**.

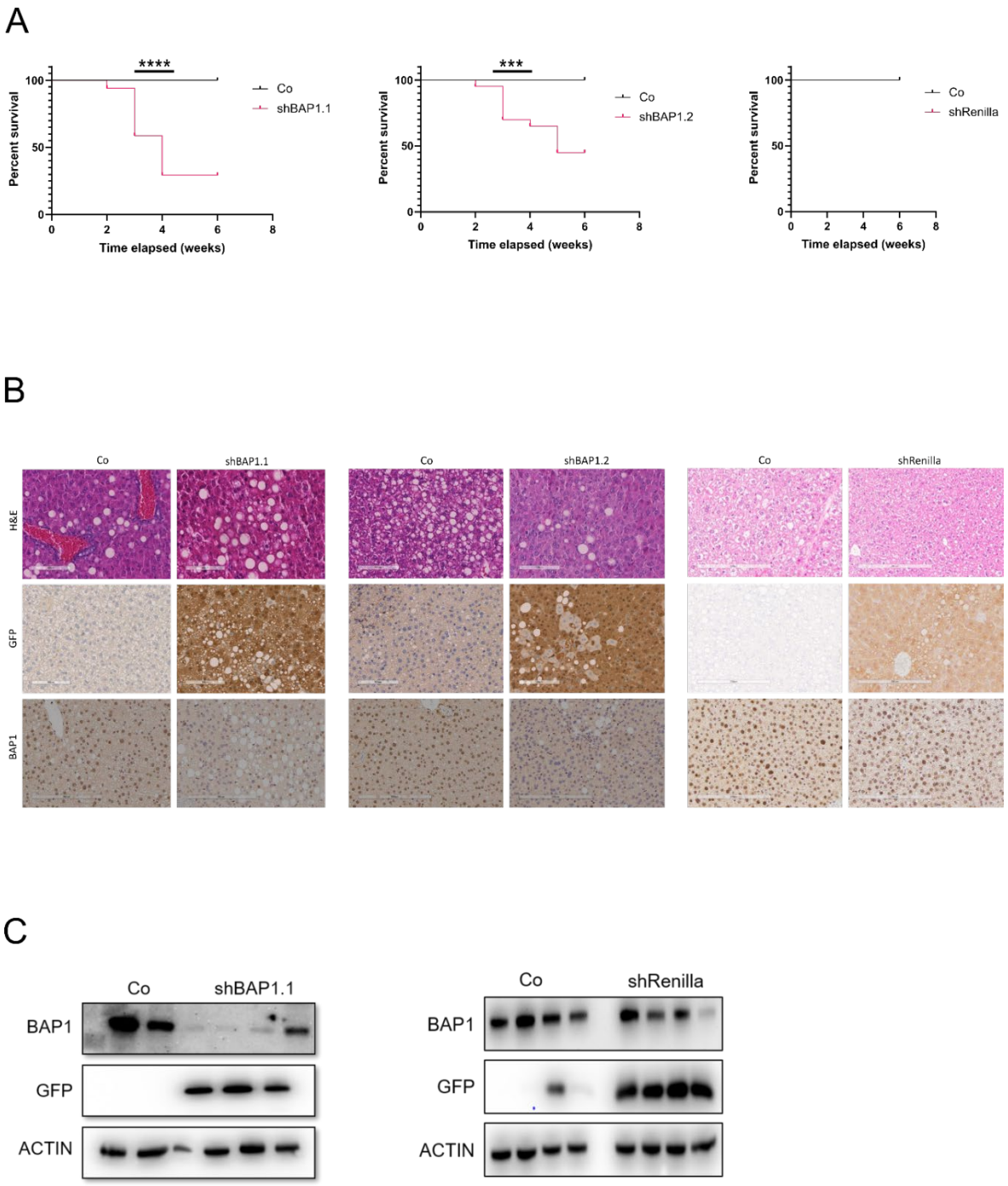

Figure 4.1.7: *Bap1* loss coupled with CD-HFD is fatal in mouse. (A) Survival curves showing significant more fatality in Dox fed shBAP1 mice. **(B)** Representative IHC panel to validate the experimental cohort (C) WB image of BAP1 and GFP.). Co depicts control cohort (off Dox) while reference to a specific shRNA depicts expression of that shRNA (On Dox, experimental cohort). (Scale bar, 200μm). Statistical tests: log-rank (Mantel-Cox) test

Furthermore, serum transaminases and bilirubin measurement revealed significantly higher levels than physiological ranges, indicating liver injury and potential liver failure in shBAP1 strains **(Figure 4.1.8A-C)**. In contrast, shRenilla mice had enzyme levels within physiological ranges and no significant difference between experimental (on Dox) and control (off Dox) cohorts **(Figure 4.1.8A-C)**.

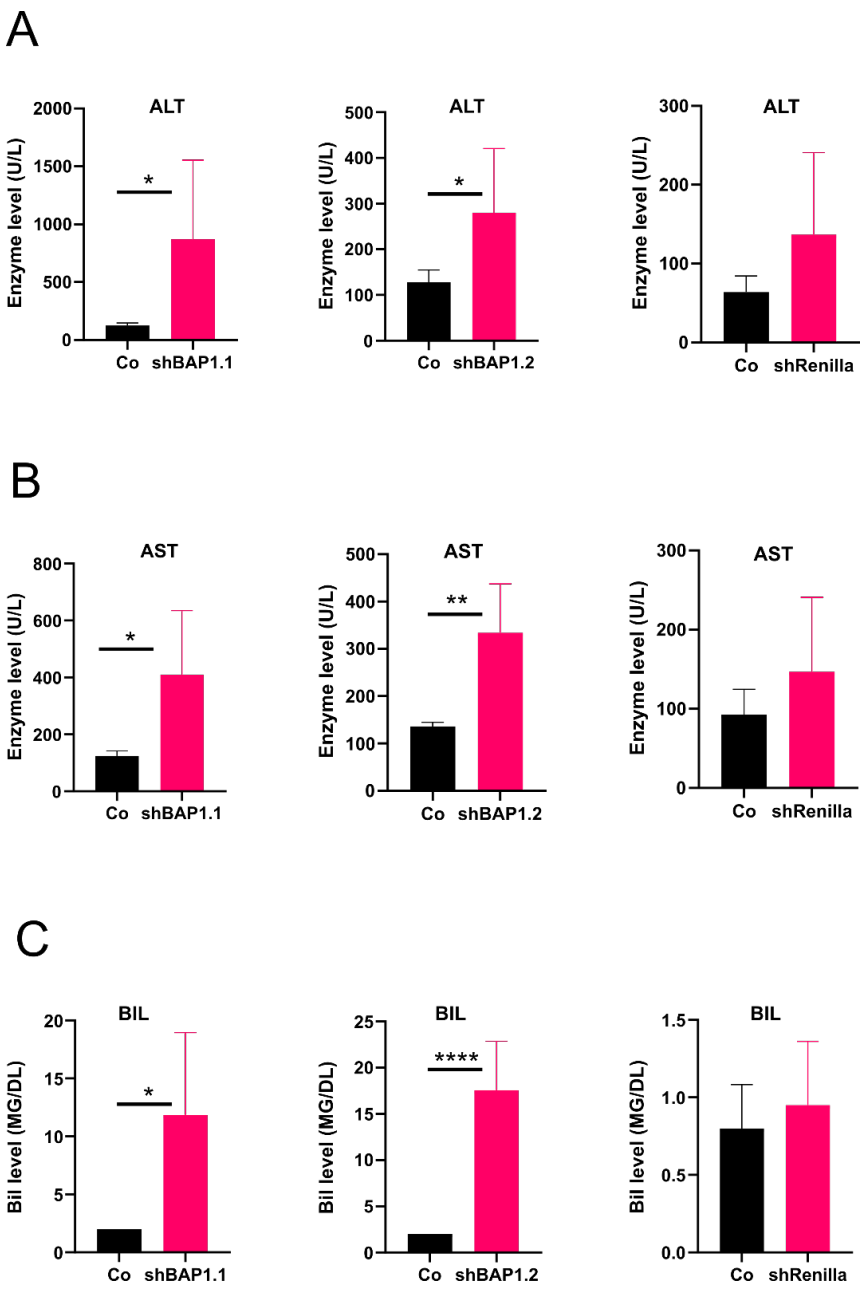

Figure 4.1.8: Serum transaminases and bilirubin measurement presents evidence of liver damage in CD-HFD fed *Bap1* repressed mice. **(A&B)** ALT measurement shows significantly elevated levels in shBAP1 strains. (C) BIL measurement is dramatically elevated in shBAP1 mice. Statistical test: Student's t- test

In order to better understand the molecular mechanism behind the surprising fatality that I observed, I analyzed IHC stainings for immune cells (macrophages (F4/80) and T cells (CD3)). There was no significant difference in the immune cell populations between the experimental and control cohort, thereby excluding the investigated immune cell populations as important players in the observed phenotype **(Figure 4.1.9A)**.

Next, I investigated cell death pathways that may be involved in the observed phenomenon. Apoptosis and necroptosis are two of the most common cell death pathways[127]. Thus, IHC staining was performed to evaluate the levels of the cleaved form of caspase 3, an executioner caspase in apoptosis and RIPK3, a necroptosis effector. Surprisingly, no significant difference was observed between the experimental and control strains across the two BAP1 strains **(Figure 4.1.9B).** This implied that the cell death observed herein may be regulated by a different pathway. In order to validate if programmed cell death and DNA damage is present in the experimental cohorts, Terminal deoxynucleotidyl transferase (TdT) dUTP Nick-End Labeling (TUNEL) assay was performed. Analyses of TUNEL assay revealed substantially more TUNEL positive cells in the shBAP1.1 and shBAP1.2 experimental cohort, whereas shRenilla animals showed no difference in TUNEL positive cells **(Figure 4.1.9C).**

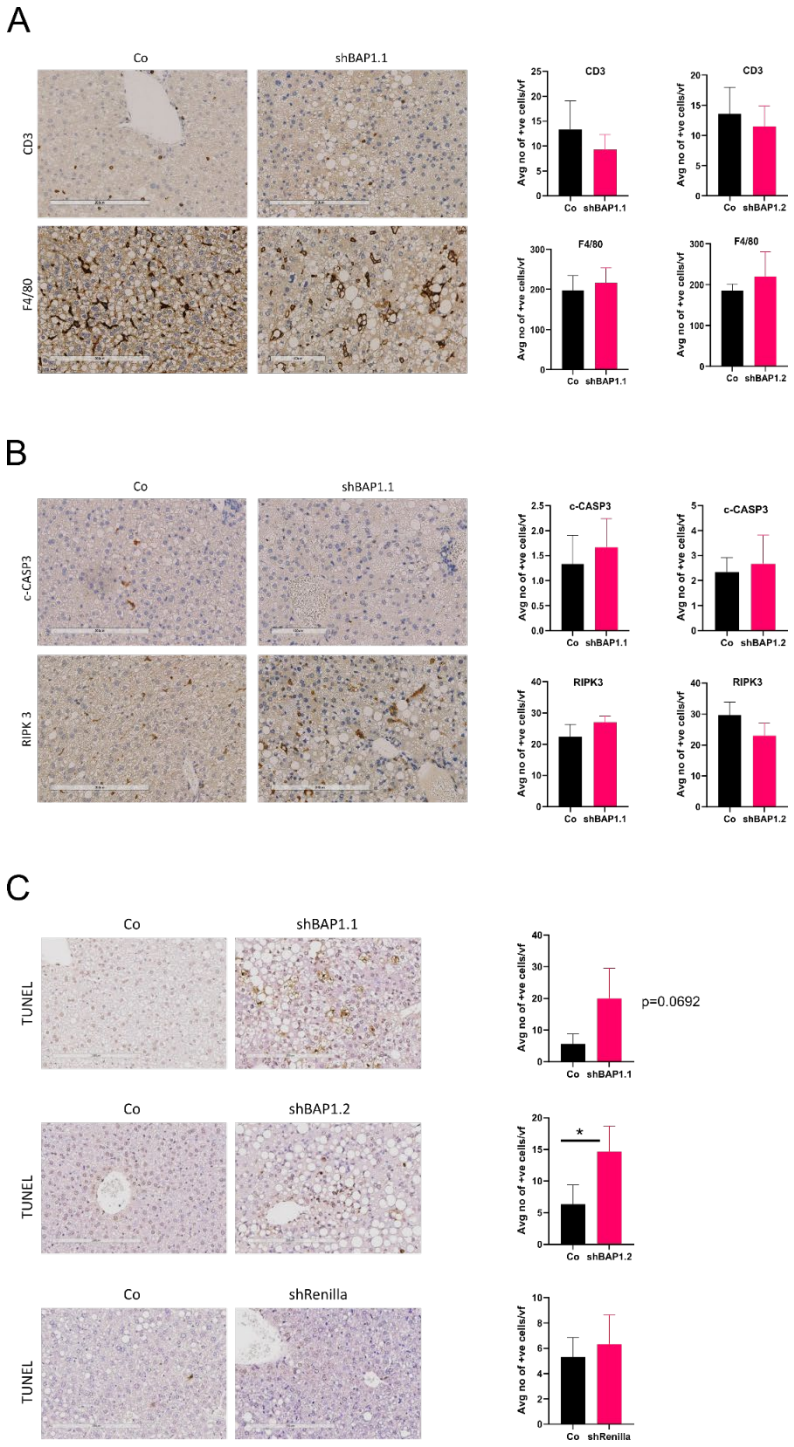

Figure 4.1.9: Dissecting potential molecular mechanism of fatality. (A) Representative image of IHC staining and its quantification for immune cells (Macrophages and T cells) in BAP1 mouse strains. **(B)** Representative image of IHC staining and its quantification for well characterized effectors of cell death pathways (Apoptosis and necroptosis) in BAP1 mouse strains**. (C)** Representative image for TUNEL assay and its quantification in BAP1 and Renilla mouse strains. Statistical test: Student's t- test.). Co depicts control cohort (off Dox) while reference to a specific shRNA depicts expression of that shRNA (On Dox, experimental cohort). (Scale bar, 200µm)

To broaden the understanding of the relationship between *Bap1* loss and CD-HFD, I wondered if the fatal outcome is due to *Bap*1 loss in itself or choline deficiency in the dietary model. To answer this question, I utilized HFD dietary model (without choline deficiency). This allows for the mirroring of the initial CD-HFD experimental plan by coupling Dox water to the diet. Remarkably, over 70% of animals challenged with dox water in the shBAP1.2 became moribund in less than 6 weeks **(Figure 4.1.10A)**. I observed the same trend in the shBAP1.1 mouse cohort where over 30% of the animals dropped out **(Figure 4.1.10A)**. Conversely, all shRenilla mice in the experimental cohort survived the dietary regimen **(Figure 4.1.10)**.

I observed elevated transaminase measurement indicative of liver injury and very high bilirubin levels symptomatic of liver failure in shBAP1.2 animals, whereas shBAP1.1 animals exhibited relatively lower transaminases and bilirubin levels in serum **(Figure 4.1.10B)**. Importantly, shRenilla animals showed no significant elevation of the assessed enzymes, although Dox challenged mice in this cohort had comparatively higher AST levels **(Figure 4.1.10B-D)**. Together, these results implicate *Bap1* loss as an important determinant of survival in metabolically challenged mice.

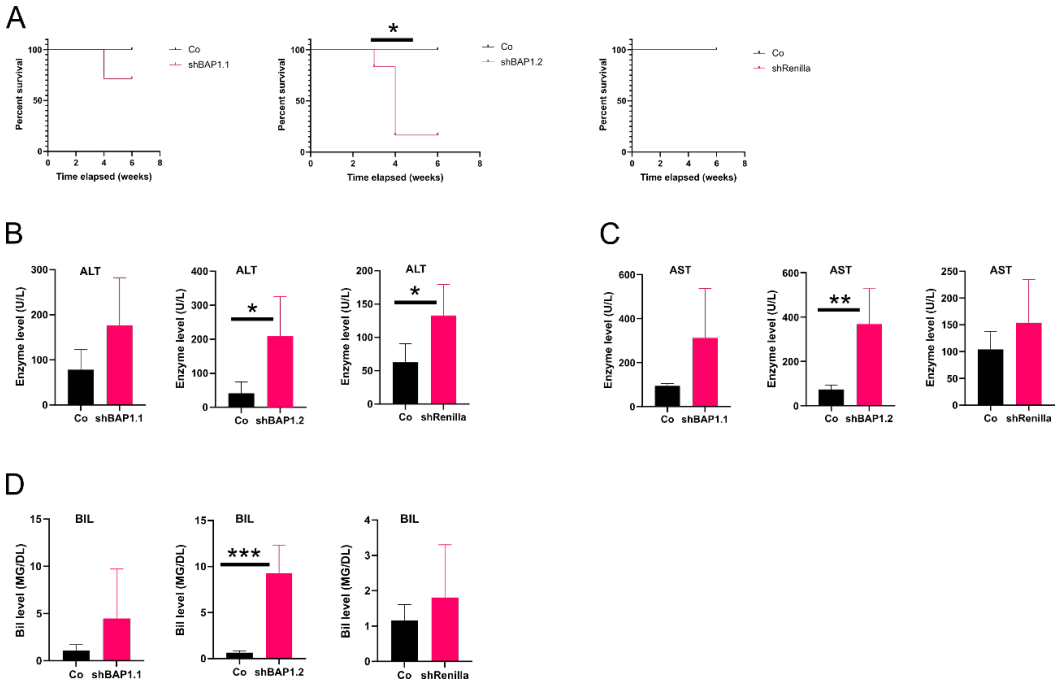

Figure 4.1.10: High fat diet mirrors CD-HFD fatality in mice. (A) Survival curve of HFD fed shRNAs mouse strains showing fatality in the shBAP1 mouse strains (**B-D)** ALT, AST and Bilirubin measurement for shBAP1.1, shBAP1.2 and shRenilla from serum. ShBAP1 mouse strains generally have higher enzyme levels. Co depicts off dox control while shBAP1.1, shBAP1.2 and shRenilla refers to the expression of the respective shRNA transgene (achieved via administration of Dox). Statistical test: Student's t- test and log-rank (Mantel-Cox) test. Co depicts control cohort (off Dox) while reference to a specific shRNA depicts expression of that shRNA (On Dox, experimental cohort).

4.1.5 Multi-omics analysis reveals dysregulated lipid metabolism and ER stress in CD-HFD fed *Bap1* repressed mice

In order to better understand the fatality phenotype observed in shBAP1.1 and shBAP1.2 mice fed with CD-HFD, I reasoned to perform complementary multi-omics experiments, designed to fully decipher the mechanism at play on multiple levels. Transcriptomics analyses allowed for detection of gene transcripts that are changed between the experimental (Dox challenged) and control cohorts (off Dox). For transcriptomics analysis, I isolated and processed RNAs from shBAP1.1 mice (Control and experimental groups), and sent them for sequencing (DKFZ core facility). Ingenuity analysis of RNA sequencing (RNAseq) data revealed tendency of downregulation of fatty metabolism related pathways and simultaneous upregulation of elements of the unfolded protein response pathway. **(Figure 4.1.11A)**. Of note, Gene Set Enrichment Analysis (GSEA) of the RNAseq data set also confirmed negative enrichment (downregulation) of hallmark fatty acid metabolism genes and positive enrichment (upregulation) of hallmark unfolded protein response genes **(Figure 4.1.11B)**. Heat map readout of selected fatty acid metabolism and unfolded protein response (UPR) genes further confirmed this trend. Briefly, fatty acid metabolism related genes were downregulated in BAP1 deficient CD-HFD fed mice. Conversely, UPR (ER stress) related genes were upregulated **(Figure 4.1.11C)**.

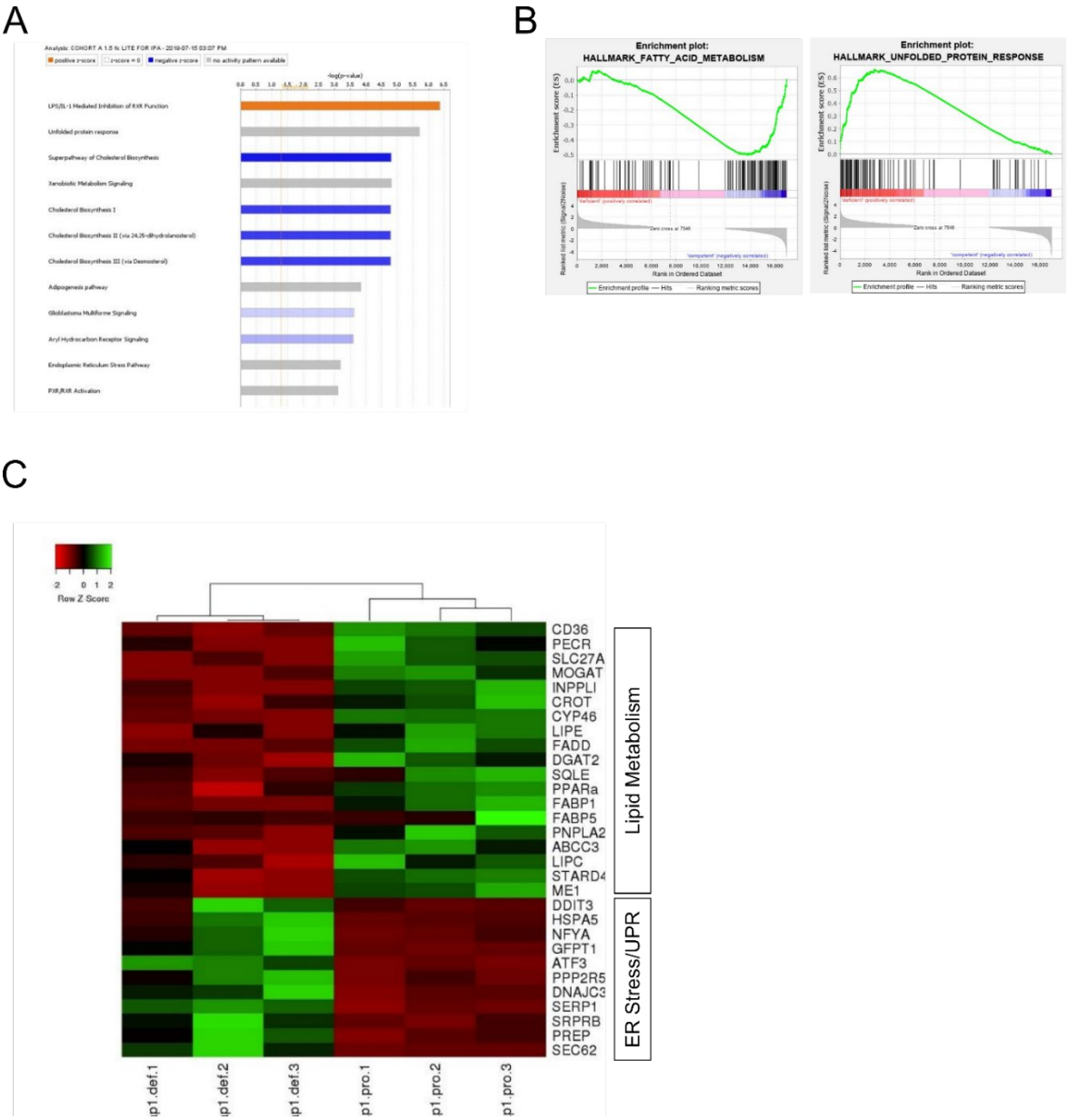

Figure 4.1.11: Transcriptomics analysis reveals dysregulated metabolism and unfolded protein response. (A) Ingenuity pathway analysis (1.5 fc cut off) showing negative enrichment of lipid metabolism genes and positive enrichment of the unfolded protein response pathway **(B)**GSEA analysis showing enriched pathways (Hallmark fatty acid metabolism and unfolded protein response)**. (C)**Heatmap showing a pictorial depiction of UPR upregulation and lipid metabolism pathway downregulation.p1.def (1-3) depicts experimental animals with *Bap1* depletion (on Dox). p1.pro (1-3) depicts control animals with intact *Bap1* (off Dox).

RNAseq results highlighted the unfolded protein response as one of the most upregulated pathways in the experimental cohort and elements of fatty acid metabolism were strongly downregulated. I observed that the ER stress sensors CHOP (gene name *Ddit3,* DNA damage inducible transcript 3) and Activating transcription factor 3 (*Atf3)* were particularly strongly enriched while lipid metabolism genes, Diacylglycerol O-Acyltransferase 2(*Dgat2*) and Fatty acid binding protein (*Fabp1*) were remarkably downregulated in the experimental cohort. To validate these findings, I performed qRT-PCR using primers targeting the aforementioned genes. Results obtained showed component of the ER stress pathway (Ddit3 and Atf3) were significantly upregulated while fatty acid metabolism pathway components were massively downregulated (*Dgat2* and *Fabp1*), thereby validating the RNAseq result (data not shown). To further strengthen the RNAseq result and interrogate the molecular mechanisms involved here, I performed analysis of IHC staining for CHOP as well as WB blot analysis for CHOP in liver protein lysates from the experimental cohorts. IHC and WB results revealed comparable levels of CHOP in shBAP1.1 mice under normal dietary conditions at 6 week's timepoint, regardless of BAP1 status **(Figure 4.1.12A-B)**. The same was observed for shRenilla mice **(Figure 4.1.12A-B)**. Remarkably, CD-HFD fed mice with BAP1 deficiency (shBAP1.1 and shBAP1.2) revealed very strong expression of CHOP both in IHC and WB **(Figure 4.1.12C-D)**. Importantly, CHOP levels remained low in the shRenilla strain **(Figure 4.1.12C-D)**. Notably, these results indicate an inverse relationship between BAP1 status and CHOP expression in CD-HFD fed mice.

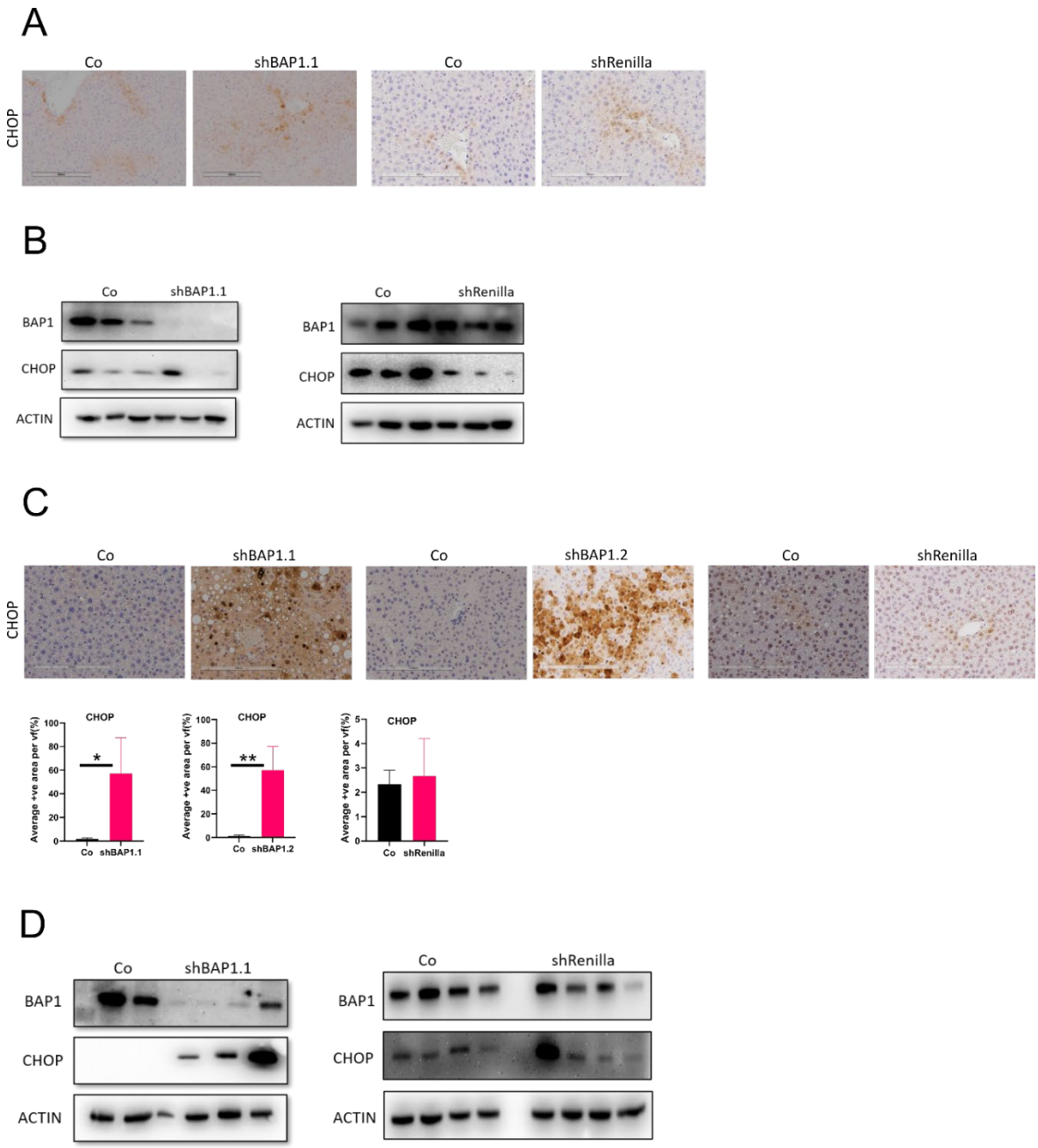

Figure 4.1.12: CHOP expression is inversely correlated with BAP1 status in CD-HFD fed mice. (A) Representative IHC image for CHOP in mouse strains under normal diet chow. Co depicts off dox control while shBAP1.1 and shRenilla refers to the expression of the respective shRNA transgene (achieved via administration of dox) (**B)** WB showing CHOP levels in normal diet fed mice **(C)** Representative CHOP IHC and quantification in CD-HFD fed shBAP1.1, shBAP1.2 and shRenilla animals. vf refers to the view field visible at 200µm magnification, 7 vf/liver were used for the quantification (**D)** WB depicting CHOP expression in CD-HFD fed BAP1 and renilla transgenic mice. Statistical test: Student's t- test. Co depicts off dox control while shBAP1.1 and shRenilla refers to the expression of the respective shRNA transgene (achieved via administration of dox). Statistical test: Student's t- test

Of note, mice were fed with exogenous lipids. Thus, lipidomics analyses allows for obtaining a global overview of changes in the lipidome (between control and experimental groups). I carefully weighted (50 g) liver samples taken from experimental animals and subjected to the lipidomic workflow (collaboration with Prof. Britta Bruegger).

Lipidomics analyses of CD-HFD fed mice revealed generally perturbed lipid homeostasis in the experimental cohort (administered dox, thus *Bap1* repressed) of shBAP1.1 and shBAP1.2 strains. Firstly, I observed that major lipid classes such as triacylglycerol (TAG) and diacylglycerol (DAG) greatly changed when compared to control **(Figure 4.1.13 A&B)**. Specifically, DAG share of the lipidome was much higher in shBAP1.1 and shBAP1.2 samples compared to their respective controls **(Figure 4.1.13B)**. shRenilla samples had comparable levels between the control and experimental samples **(Figure 4.1.13B)**. Conversely TAG levels were lower in the experimental cohort of shBAP 1.1 and shBAP1.2 mice while shRenilla mice had similar levels across experimental cohorts **(Figure 4.1.13A)**. Secondly, cholesterol (CHOL) and cholesterol esters (CE), the storage form of cholesterol, were also much higher in the experimental cohort of shBAP1.1 and shBAP1.2 mice **(Figure 4.1.13 C&D)**. While shRenilla mice had higher cholesterol levels in the experimental cohort, cholesterol ester levels were comparable to control **(Figure 4.1.13C&D)**. Moreover, specific free fatty acids (selected based on natural abundance) were examined. Here, the free fatty acids Palmitic acid (16:0), Oleic acid (18:1) and Palmitoleic acid (16:1**)** measurements were much higher in Dox challenged, CD-HFD fed shBAP1.1 and shBAP1.2 mice **(Figure 4.1.13E-H)**. Importantly, I did not observe this general increase in the shRenilla strain **(Figure 4.1.13E-H)**. Next, I examined the lipidome based on functional categorization. The analysis revealed that Dox administration and CD-HFD feeding perturbed most significantly “Sphingolipids, sterols and storage” category in shBAP1.2 strain, and “sterols” in shBAP1.1 and shRenilla strains **(Figure 4.1.13I)**. Together, these results indicate dysregulated lipidome in BAP1 deficient mice subject to metabolic distress (CD-HFD) **(Figure 4.13)**.

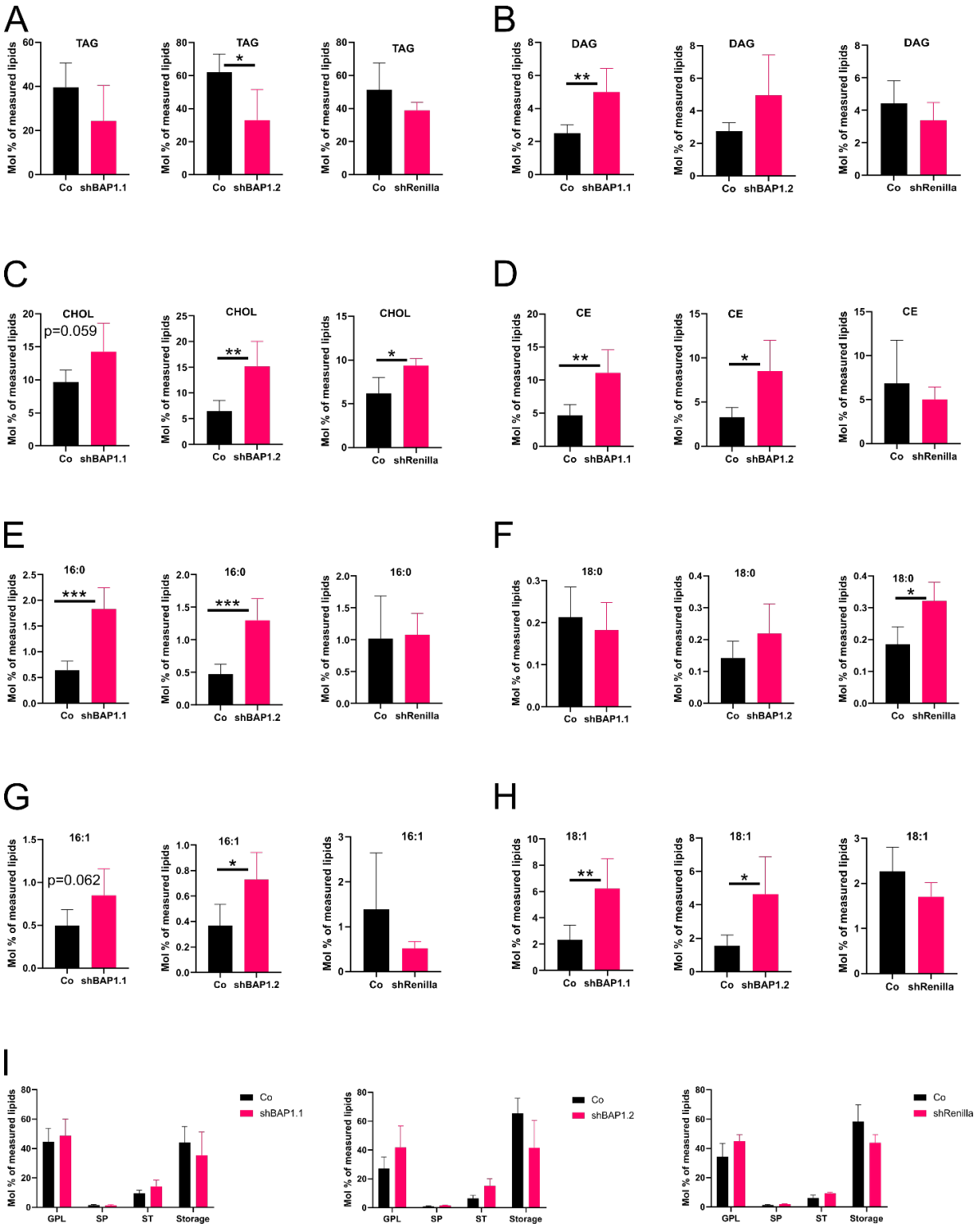

Figure 4.1.13: Dysregulated lipidomics is a hallmark of *Bap1* repression in CD-HFD fed mice. (A&B) TAG analysis and DAG analysis (left to right shBAP1.1, shBAP1.2 and shRenilla**). (C&D)** Lipidomics analysis of CHOL and CE. **(E&F)** Analysis of selected saturated fatty acid, Stearic acid (18:0) and Palmitic acid (16:0) (Left to right shBAP1.1, shBAP1.2 and shRenilla**). (G&H)** Analysis of selected unsaturated fatty acid Oleic (18:1) and Palmitoleic acid (16:1**). (I**) Graphical depiction of lipidomics analysis based on functional classification. Statistical test: Student's t- test.

Next, I wondered whether the perturbed lipidomics I observed in BAP1 deficient, CD-HFD fed mice also holds true in the steady state. Thus, lipidomics analysis was performed on shBAP1.1 mice under homeostatic conditions i.e., without metabolic distress. Control groups received normal chow while the experimental group received Dox chow. Results show vastly different situations when compared to the CD-HFD cohort. Here, I observed significantly increased TAG levels in the experimental cohort **(Fig 4.1.14A**). whereas DAG level remained stable. Cholesterol levels were reduced and in contrast Cholesterol esters levels were dramatically increased **(Figure 4.1.14 A)**. Furthermore, analysis of free fatty acid showed relative stability in the unsaturated fatty acids (stearic and palmitic acid), while the unsaturated free fatty acid tended to be increased, particularly for palmitoleic acid **(Figure 4.1.14B)**. Functional category analysis revealed significant differences in all categories. While “storage” was significantly increased, categories such as “sterol” and “glycophospholipids” were decreased in the experimental cohort relative to control **(Figure 4.1.14C)**. To further strengthen and validate the lipidomics results of shBAP1.1 mice fed with normal diet, I measured hepatic Triacylglycerols in shBAP1.1, shBAP1.2 and shRenilla mice using commercially available kits (sigma). Results showed slight increase in Triacylglycerols in Dox fed shBAP1.1 mice, however shBAP1.2 and shRenilla cohorts showed no difference **(Figure 4.1.14D)**. Taken together, these results indicate context dependent lipidomics perturbation in BAP1 deficient mice.

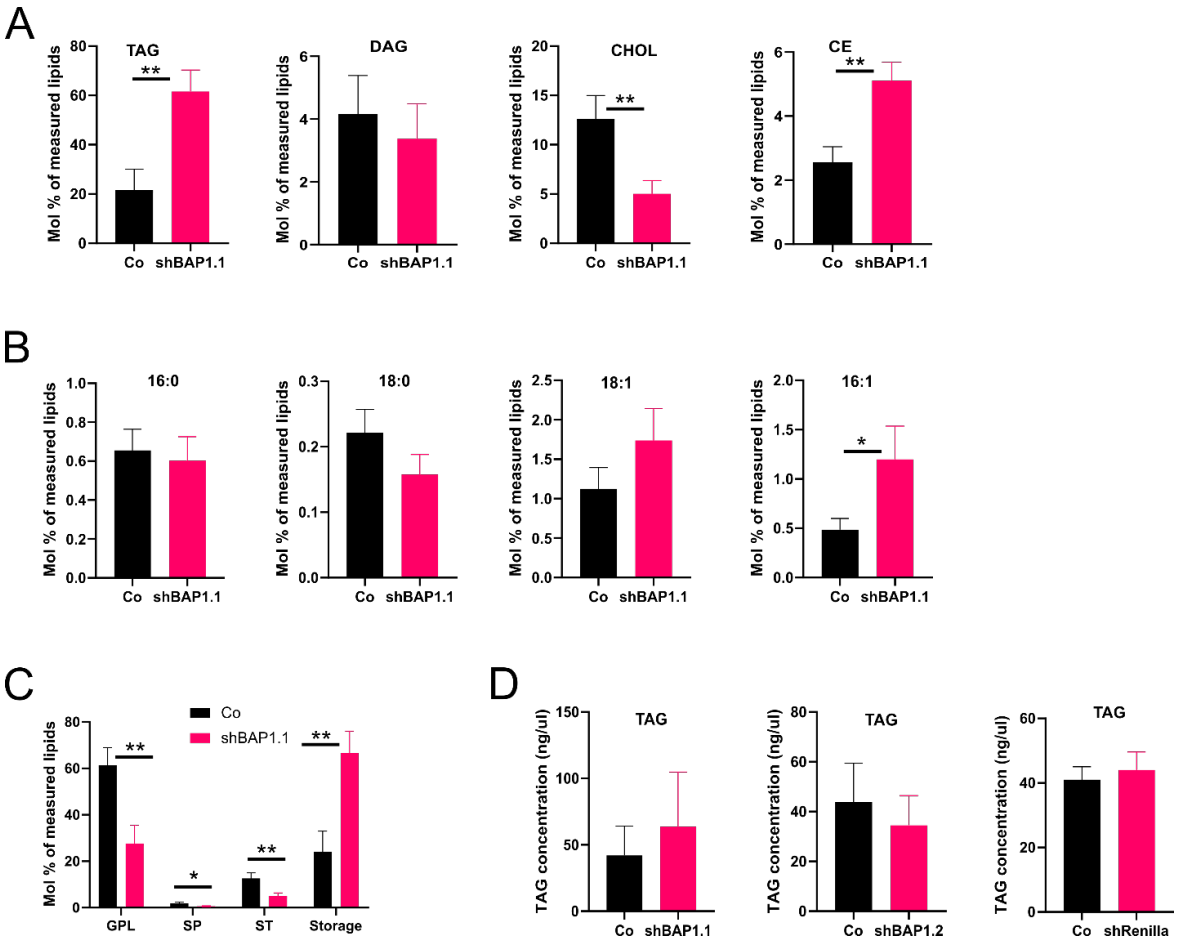

Figure 4.1.14: Lipidomics analysis in steady state. (A) Lipid class analysis in shBAP1.1 mouse strain (B) Analysis of free fatty acids in BAP1 deficient normal chow fed mice. **(C)** Lipid functional category analysis **(D)** Triacylglycerols measurement in all mouse strains (Steady state). Statistical test: Student's t- test. Co depicts off dox control while shBAP1.1 and shRenilla refers to the expression of the respective shRNA transgene (achieved via administration of dox).

4.1.6 BAP1 is indispensable for survival in metabolically distressed mice

So far, results obtained in this study have demonstrated a surprisingly fatal outcome upon *Bap1* suppression in CD-HFD receiving mice. Therefore, I hypothesized that *Bap1* is critical for cell and organ survival under metabolic distress such as high calorie diets. To test this hypothesis, I designed and implemented a *Bap1* intervention experiment. The shRNA mice strains enable temporally manipulation of target gene expression by the simple administration or withdrawal of Dox. Briefly shBAP1.1, shBAP1.2 and shRenilla mice were placed on dox water and CD-HFD. After two weeks, the animals were divided into two cohorts; one that remained on Dox water and CD-HFD (unrestored) and the intervention or restoration group where dox water is replaced with saccharose water. **(Figure 4.1.15A)** Conceptually, this should enable the restoration of *Bap1* gene *in-vivo*. Survival analysis

showed faithful recapitulation of the CD-HFD fatality phenotype in the unrestored group manifested by >60% (shBAP1.2) and >70% (shBAP1.1) mortality. Strikingly, the intervention group (BAP1 restored) survived the dietary regimen and remained healthy after 6 weeks **(Figure 4.1.15B)**. Notably, restored and unrestored groups of shRenilla mouse strain survived the experimental regimen and remained healthy after 6 weeks **(Figure 4.1.15B)**. Liver weight measurements were recorded upon sacrifice of the animals. Liver weight analysis revealed drastic reduction in liver weight in the unrestored group of shBAP1.1 and shBAP1.2 mouse strains **(Figure 4.1.15C)**. I referred to this phenomenon as liver wastage. Importantly, liver wastage was notably absent in shRenilla mouse strain (**Figure 4.1.15C)**. Furthermore, serum transaminases and bilirubin measurements revealed attenuation of liver injury and damage in the intervention group (*Bap1* restored) of shBAP1.1 and shBAP1.2 strains. **(Figure 4.1.15D)**. As expected, shRenilla restoration had no effect on transaminases and bilirubin levels **(Figure 4.1.15D)**.

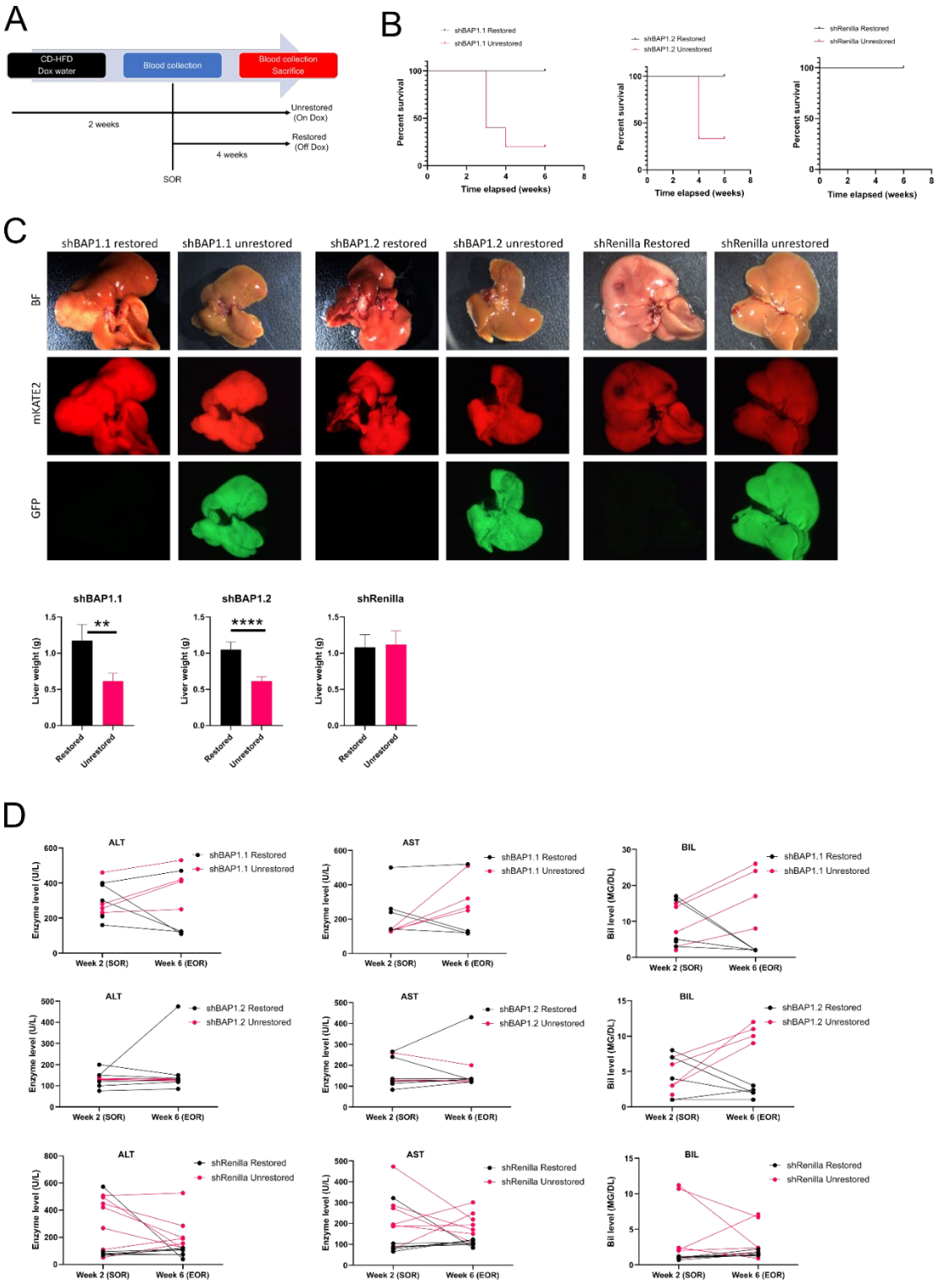

Figure 4.1.15*: Bap1* restoration attenuates liver damage. (A) Experimental schematic for investigating the effect of *Bap1* restoration in CD-HFD fed mice **(B)** Survival curve of experimental animals showing rescue of CD-HFD fed shBAP1 mice upon *Bap1* restoration **(C)** Pictorial depiction and quantification of organ wastage in CD-HFD fed shBAP1 without *Bap1* restoration (**D)** Transaminases and bilirubin measurements of in serum of mice upon BAP1 restoration throughout the course of the intervention. SOR =start of restoration, EOR=end of restoration. Statistical test: Student's t- test and log-rank (Mantel-Cox) test.

Next, I questioned if increased CHOP expression in livers from animals in the restoration cohort could be observed and whether BAP1 restoration would have a direct negative effect on CHOP levels. To answer this question, I performed analysis of IHC stainings as well as WB. IHC and Western blot analyses of BAP1 shRNA strains revealed a strong correlation between BAP1 status and CHOP expression, wherein BAP1 deficient mice presented with strong CHOP expression **(Figure 4.1.16 A&B)**. Accordingly, in samples from mice with *Bap1* restoration, very low CHOP expression was observed **(Figure 4.1.16 A&B)**. In contrast, WB analysis of shRenilla mice in the experimental cohort revealed weak to low CHOP expression **(Figure 4.1.16B).** Taken together, these results strongly indicate that BAP1 is important for survival in metabolically distressed mice and that the expression of the ER stress sensor CHOP in this context depends on BAP1 status.

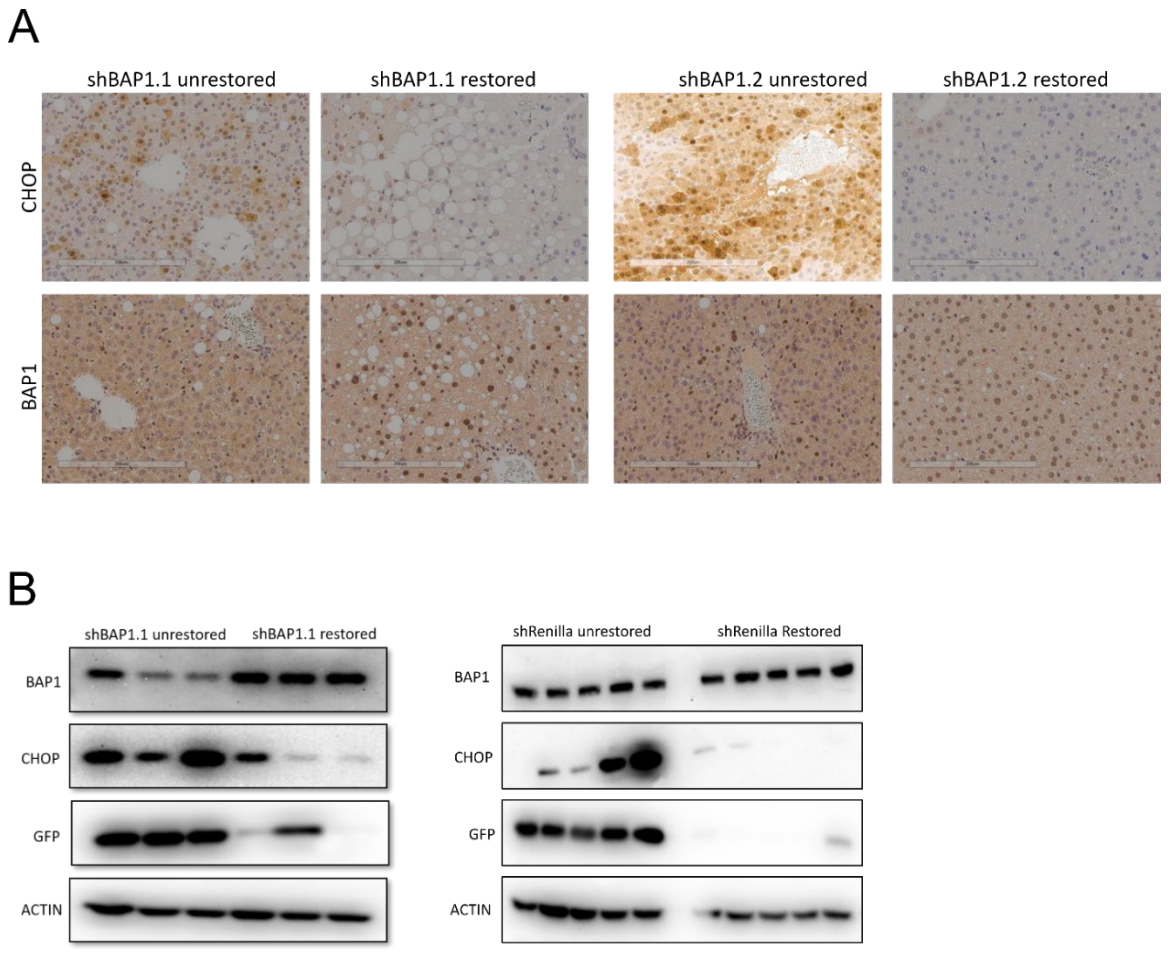

Figure 4.1.16: CHOP expression inversely correlates with BAP1. (A) Representative IHC staining for CHOP and BAP1 showing reduction in CHOP protein expression after endogenous restoration of *Bap1* **(B)** WB image panel of CHOP, BAP1 and GFP upon restoration of BAP1 (n=3 for shBAP1, n=4 for shRen)

4.2 Elucidating the functional significance of BAP1 in hepatocarcinogenesis

4.2.1 *Bap1* loss co-operates with specific oncogenic events to initiate malignant transformation

BAP1 loss of function is a recurrent tumor promoting event in many tissues including the liver[128]. Taking insights from the revelatory data I obtained from CD-HFD experiments described in this study, I hypothesized that BAP1 is a context dependent tumor suppressor in hepatic tissues. In one context it is essential for organ survival (e.g., organ wide loss and metabolic distress) and in another, it might promote carcinogenesis (e.g., loss in a subset of hepatocytes and co-operation with compatible oncogenic events). Accordingly, loss of *Bap1* in a subset of hepatocytes in the liver would be compatible with malignant transformation.

To test this hypothesis and model partial loss of BAP1 in the liver, hydrodynamic tail vein injection (HDTVI) delivering *Bap1* targeting clustered regularly interspaced short palindromic repeats (CRISPR) short guide RNAs (sgRNAs), in combination with sgRNAs targeting other hepatic tumor suppressors or vectors enabling expression of oncogenic drivers into the liver was employed. A sgRNA targeting GFP served as control. The results I obtained from combining sgBap1 with sgTrp53 (transformation related protein 53) or enforced expression of c-myc or mutant K-RAS^{G12D} indicated *Bap1* loss does not co-operate with these genetic events in liver carcinogenesis **(Figure 4.2.1A).**

Strikingly, I observed that mice injected with sgBap1 and sgPten (thus BAP1 deficient, referred to as sgPB) combination yielded hepatomegaly and became moribund and immobile within 4 to 7 months **(Figure 4.2.1A).** Crucially, the control cohort (sgPten and sgGFP, thus *Bap1* proficient, referred to as sgPG) showed no such changes **(Figure 4.2.1A)**. Total body weight remained similar across experimental and control cohorts **(Figure 4.2.1B)**. In line with the hepatomegaly phenotype, liver weight in sgPB mice was considerably higher than sgGP mice. **(Figure 4.2.1B)**. Importantly, T7 endonuclease assay confirmed Bap1 and Pten CRISPR/Cas9 mediated editing **(Figure 4.2.1C)**. Histological and immunohistological analyses of the experimental cohort showed more aggressive steatosis (comprising microvesicular and macrovesicular steatosis) and visibly higher expression of the proliferation marker Ki67 in sgPB mice when compared to sgPG mice **(Figure 4.2.1B)**. Further, analyses of IHC stainings confirmed the loss of BAP1 in sgPB while sgPG retained nuclear expression of BAP1 **(Figure 4.2.1C).**

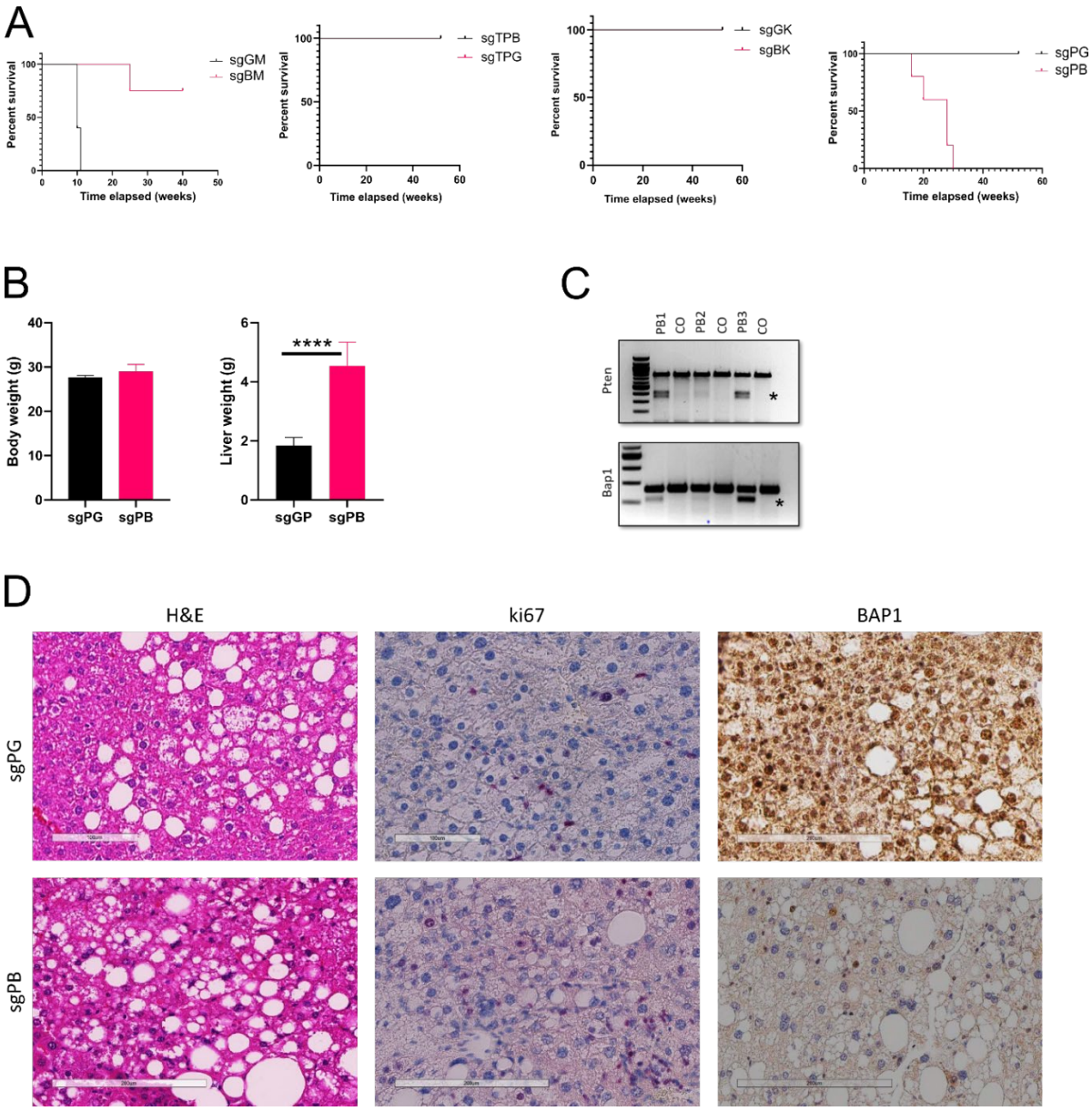

Figure 4.2.1 *Bap1* loss co-operates with *Pten* loss in mice to drive hepatic malignant transformation. (A) Survival curves of different genetic events in co-operation with *Bap1* loss. Bap1 combination with Pten loss shows tumor promoting potential **(B)** Body and liver weight measurement of sgGP and sgPB mice **(C)**T7 assay depicting editing of Pten and Bap1 at the desired loci. * Indicate the cleaved product. (**D)**Representative histological and immunohistological image showing H&E staining as well as ki67 and BAP1 staining in sgPG and sgPB mice. Scale bar; 200μm.

Next, I performed transcriptomics analyses to better understand the gene expression landscape in sgPB and sgPG samples (BAP1 deficient and proficient respectively**) (Figure 4.2.2)**. With a p-value threshold of <0.05 and log2 fold change threshold value set at < +/- 1.5, 858 genes were identified as downregulated, while 1005 genes were upregulated after *Bap1* depletion, as depicted in the volcano **(Figure 4.2.2A)**. Moreover, a blind heatmap analysis showed intra-group clustering in the samples, thus laying credence to the fidelity of the RNA samples used here **(Figure 4.2.2B)**. Furthermore, analysis of the differentially regulated genes using ingenuity pathway analysis revealed changes and enrichment in diverse pathways consistent with liver cancer initiation. Specifically, *Bap1* depletion in the context of *Pten* loss leads to activation of Aryl hydrocarbon receptor signaling, Interleukin 8 (IL-8) signaling and glutathione redox reactions pathways, among others. Downregulated pathways include super pathway of melatonin degradation and RhoGDI signaling **(Figure 4.2.2C)**. Thus, *Bap1* loss co-operate with *Pten* loss to initiate malignant transformation in the liver.

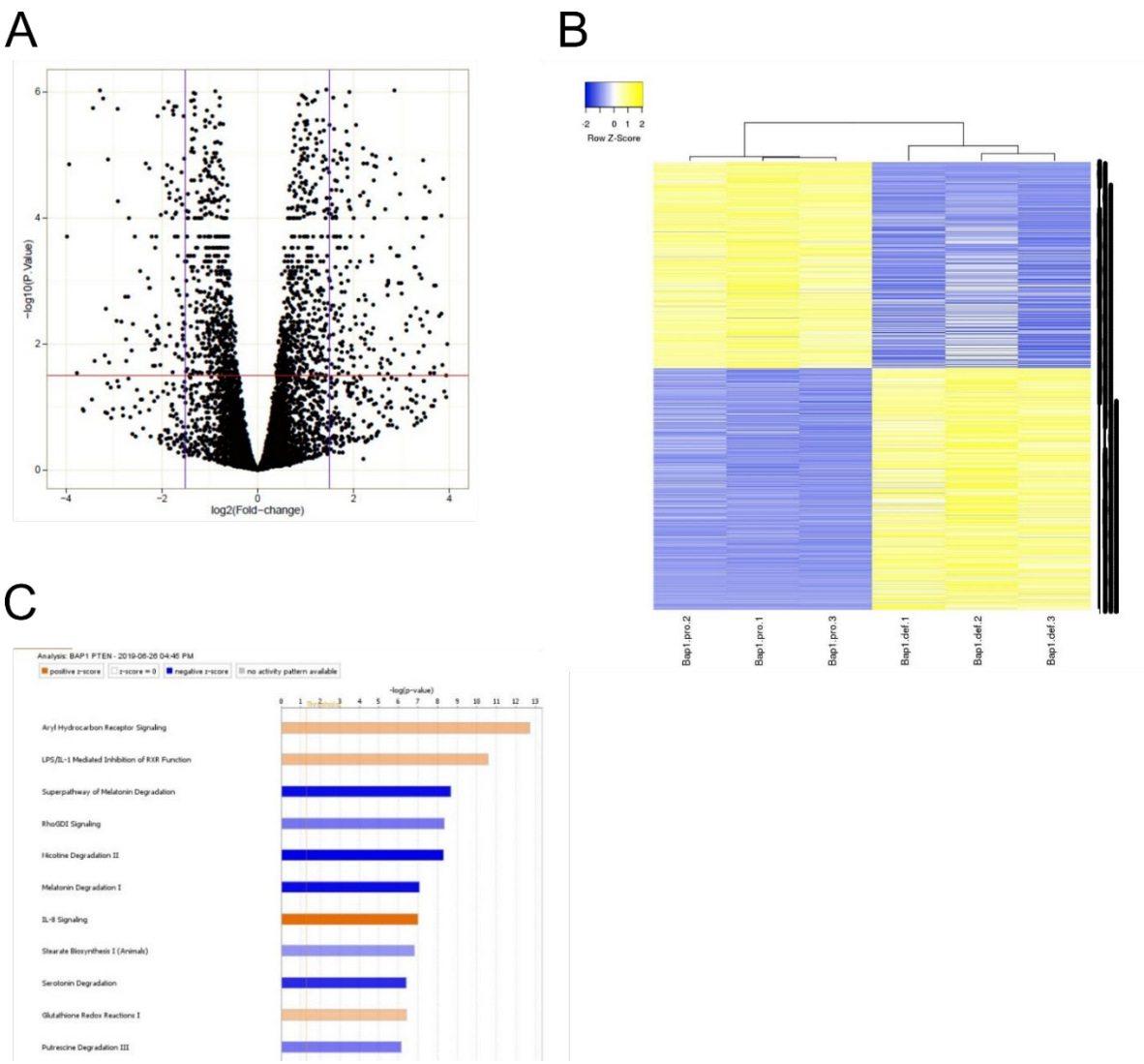

Fig 4.2.2: Transcriptomics analysis of sgPB and sgPG samples :(A) Volcano plot of the RNAseq data from sgPB and sgGP samples with threshold p-value and log2 fold change threshold set at <0.05 and <+/- 1.5 respectively. **(B)** Heatmap analysis showing clustering within their respective groups. **(C)**Ingenuity analysis shows pathway enrichment consistent with liver tumorigenesis. sgPB and sgPG samples referred to as BAP1 deficient (Bap1.def) and proficient (Bap1.pro) respectively. Bap1-deficient (Bap1-def)

Considering that the malignant transformation phenomena described here evolved over a long time (up to 7months), I hypothesized that a third independent oncogenic hit will likely accelerate (as compared to two in sgPB) *Bap1* loss driven tumorigenesis. *Pten* loss in the liver has been shown to induce yes associated protein (YAP) activation[129]. To test whether addition of *Bap1* loss to the reported synergism between *Pten* loss and YAP activation would promote liver tumorigenesis, a combination of YAP^{S127A} (a constitutively active form of YAP which ensures its enforced nuclear expression), with sgPten and sgBap1 (referred to as sgBPY) was injected into mice via HDTVI. A combination comprising of

YAP^{S127A}, sgPten and empty px330 plasmid (referred to as sgPY) served as control. Strikingly, tumor onset was significantly faster in sgBPY cohort (5 weeks) as compared to sgPY (13 weeks) **(Figure 4.2.3A)**. Analyses of the tumors themselves revealed significantly larger liver size with small tumor nodules dotted all over the liver in sgBPY cohort **(Figure 4.2.3B)**. In contrast sgPY mice had larger nodules but overall smaller liver size (**Figure 4.2.3B**). Total body weight remained the same across both experimental cohorts (**Figure 4.2.3B**). IHC analysis confirmed loss of BAP1 expression in BPY mice **(Figure 4.2.3C)**. Conversely, sgPY mice maintained strong BAP1 expression **(Figure 4.2.3C)**. To further corroborate the result, WB analysis was performed using lysates derived from sgPY and sgBPY tumors. Expectedly, results show reduction in expression of BAP1 protein in sgBPY samples compared to sgPY **(Figure 4.2.3C)**. Together these results suggest that *Bap1* loss accelerates YAP; *Pten* driven tumorigenesis in murine livers.

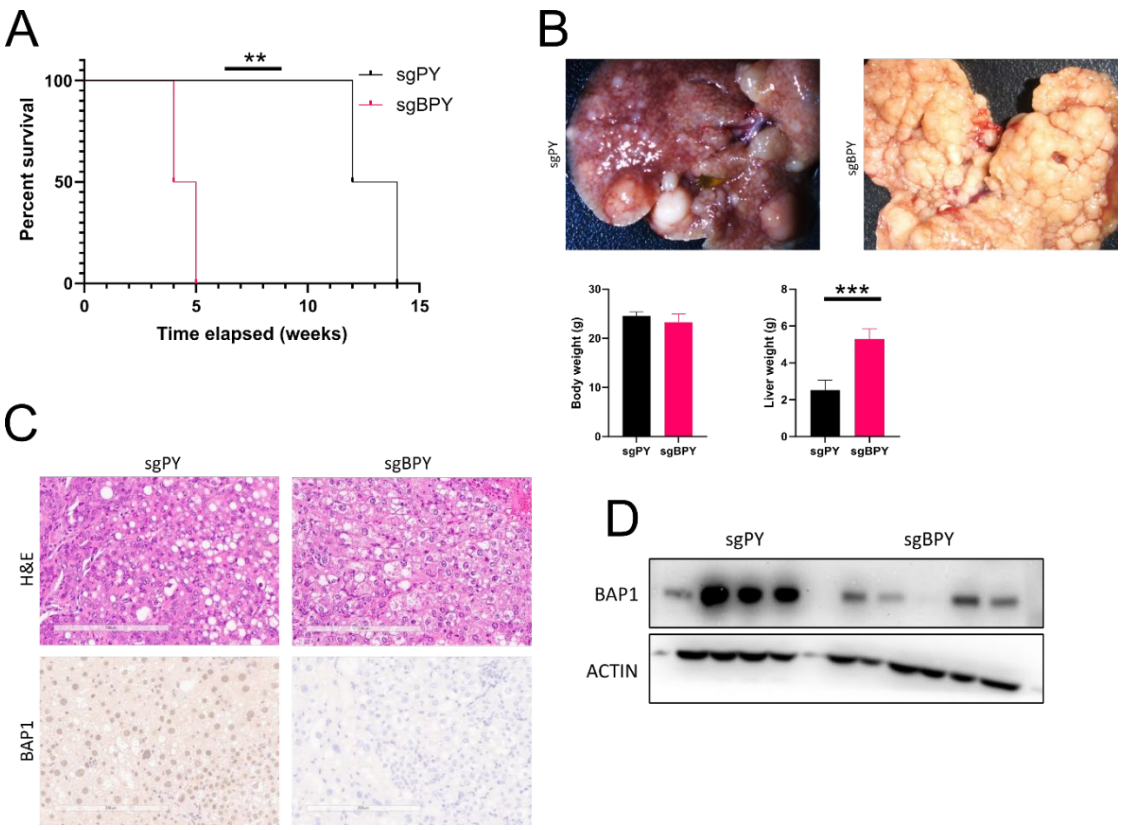

Figure 4.2.3: *Bap1* loss accelerates *Pten* loss and YAP activation driven tumorigenesis. **(A)** Survival analysis of sgPY and sgBPY unveils reduced survival with *Bap1* loss (sgBPY) **(B)** Representative photograph of sgPY and sgBPY tumors showing significantly larger liver in sgBPY mice when compared to sgPY **(C)** Representative IHC image confirms the absence of BAP1 expression in the nucleus of sgBPY mice; Scale bar; 200µm **(D)** WB analysis shows reduced BAP1 protein levels in sgBPY tumors. Statistical tests: student's t-test and log-rank (mantel-cox) test

Next, I questioned whether *Bap1* loss can co-operate with YAP^{S127A} to drive *in-vivo* hepatocarcinogenesis, independent of *Pten* loss. sgBAP1 was combined with a plasmid expressing YAP^{S127A} (referred to as sgBY) and injected into mouse livers via HDTVI. YAP^{S127A} alone with pX330 plasmid was used as control (referred to as YAP). Remarkably, most of the mice in the sgBY developed tumors at week 16 (4 out of 5) post HDTVI **(Figure 4.2.4A&B)**. Notably, at the end of the experiment, one of YAP^{S127A} developed tumors at 12 months post HDTVI. H&E analysis confirmed sgBY tumors as HCC like **(Figure 4.2.4C)**. Further, IHC analysis confirmed loss of BAP1 expression in the nucleus in the sgBY cohort **(Figure 4.2.4C)**. As expected, YAP^{s127a} retained strong expression of BAP1 protein **(Figure 4.2.4C)**. Together, these results suggest *Bap1* loss co-operates with YAP and *Pten* independently as well as co-operatively in liver tumorigenesis.

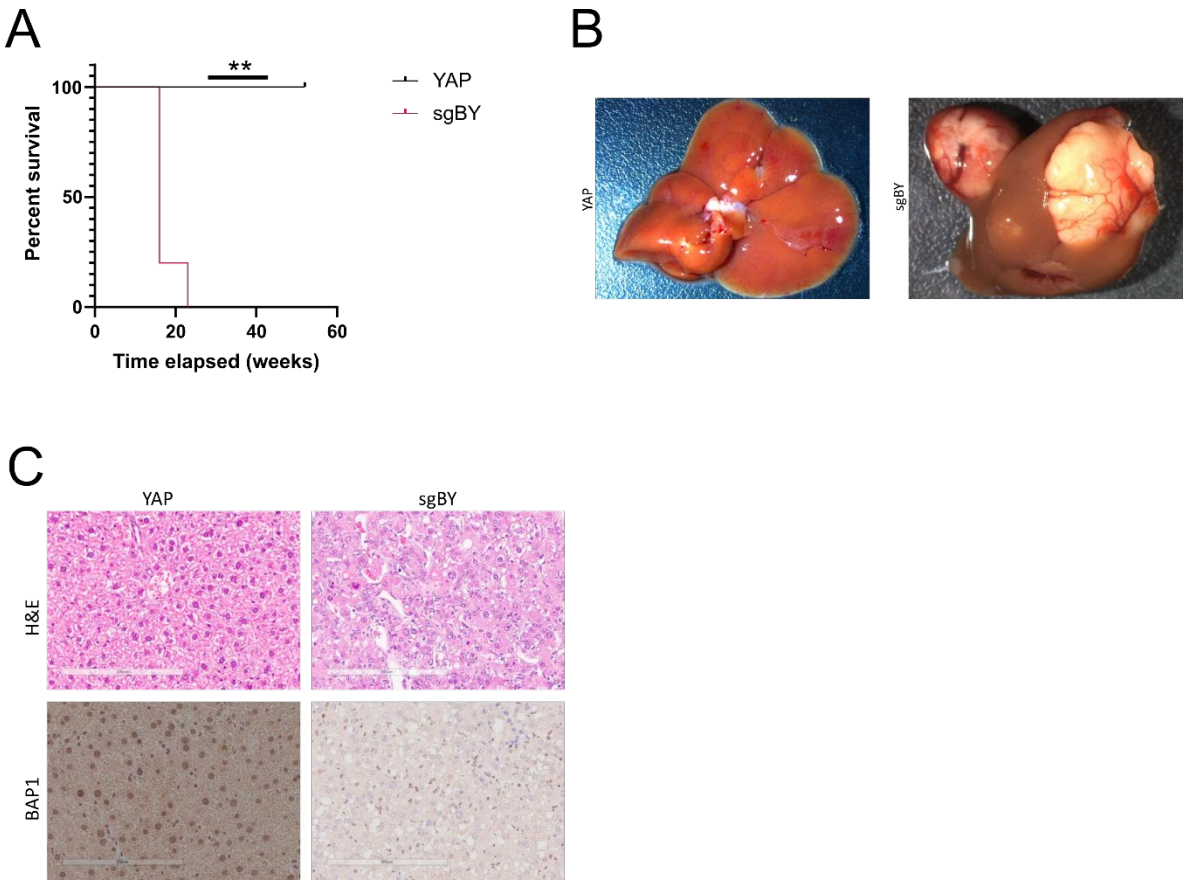

Figure 4.2.4: BAP1 co-operates with YAP to drive hepatocarcinogenesis. **(A)** Survival analysis of YAP and sgBPY mice unveils reduced survival with *Bap1* loss (sgBY) **(B)** Representative photograph of YAP and sgBY mice highlighting the presence of tumor nodules in sgBY mice **(C)** Representative IHC image confirming the absence of BAP1 expression in the nucleus of sgBY mice and HCC like appearance. Scale bar; 200µm. Statistical tests: log-rank (Mantel-Cox) test.

4.2.2 BAP1 deficient tumors and cell lines expresses the ER stress sensor CHOP

Hitherto in this study, I observed strong CHOP overexpression in BAP1 deficient models of metabolic distress (e.g., CD-HFD). However, it is unclear if this phenomenon is restricted to only a metabolic stress context or if it also applies to BAP1 deficient tumors. To test whether CHOP is strongly expressed in BAP1 deficient tumors, I performed analyses of IHC staining for CHOP and BAP1 in the *Bap1* loss driven tumor models described. Strikingly, IHC analyses revealed strong expression of CHOP in all BAP1 deficient mouse tumor model (sgPB, sgBPY and sgBY) **(Figure 4.2.5A-C)**. Importantly, CHOP expression was significantly lower in the respective control cohorts (without *Bap1* loss) **(Figure 4.2.5A-C)**. As expected BAP1 expression was low in BAP1 deficient tumor samples (sgPB, sgBPY and sgBY). Conversely strong BAP1 nuclear expression was observed in the BAP1 proficient samples (controls) **(Figure 4.2.5A-C)**. Thus, these results indicate CHOP expression is a hallmark of *Bap1* loss in the liver, at least in metabolic distress and tumorigenesis contexts.

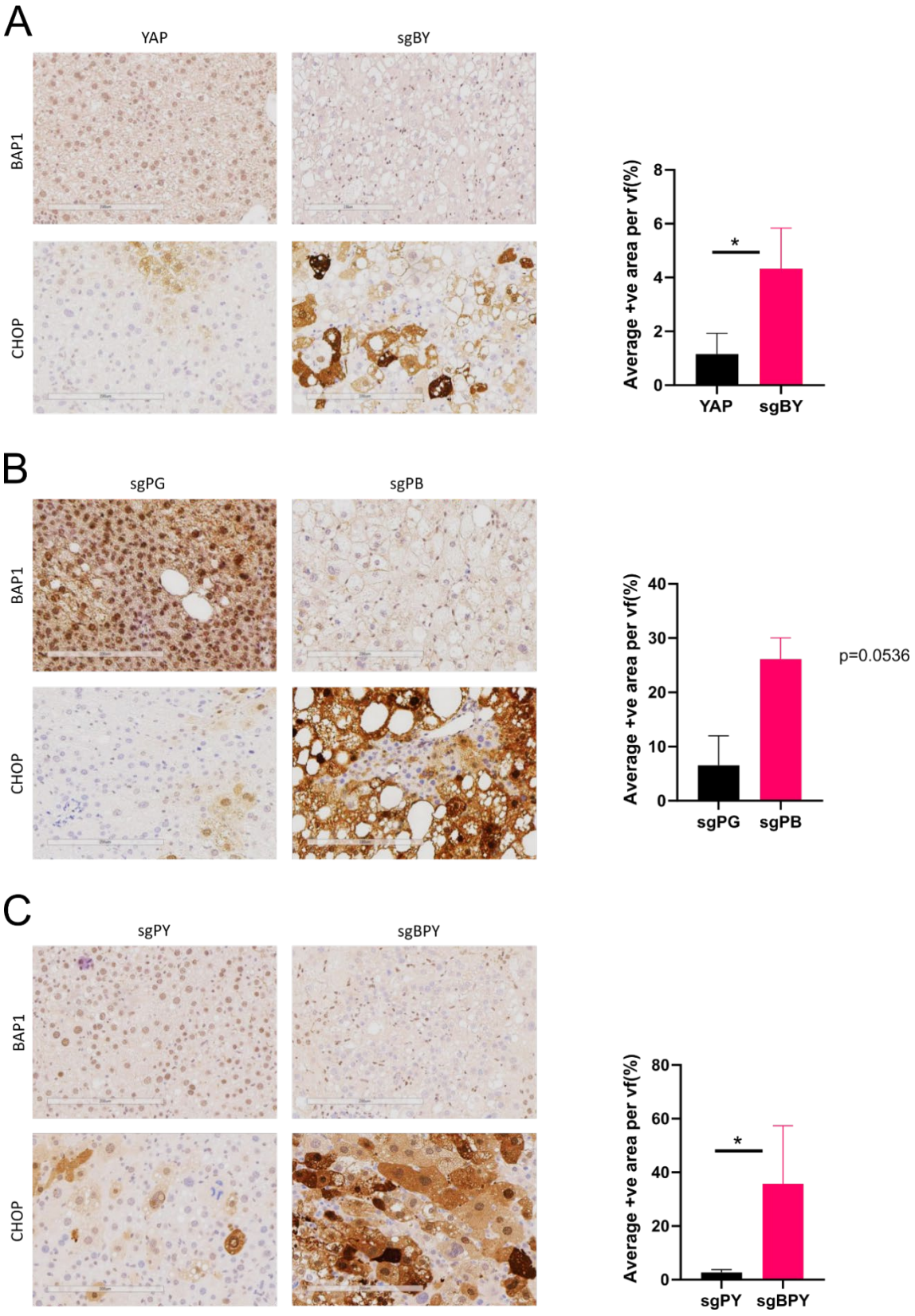

Figure 4.2.5: BAP1 deficient tumors strongly expresses CHOP. **(A-C)** Representative IHC image showing that CHOP expression is dependent on BAP1 status in *Bap1* knockout tumor models (sgPY, sgPB and sgBY) (Right). Quantification of CHOP expression in the BAP1 knockout tumor models (Left). Scale bar; 200µm Statistical test: Student's t-test.

To further probe the relationship between BAP1 and CHOP, I established cell lines from sgBPY and sgPY tumors. For sgPY tumor models, two cell lines were established (sgPY1 and sgPY2). To test whether *Bap1* loss will induce CHOP overexpression in sgPY cell lines, I transformed the cells with sgBAP1 to achieve *Bap1* knockout (KO). In parallel, I also utilized two independent shRNAs (exactly the same as the one used in the shRNA mouse model) to achieve *Bap1* knockdown (KD). Here, result showed potent upregulation of CHOP in the *Bap1* KO and KD samples as compared to empty vector control **(Figure 4.2.6A)**. Encouraged by the results, I performed the converse experiment utilizing sgBPY cell lines. To this end, I performed lentiviral transduction of these cells with human BAP1 cDNA as well as with lentiviral vectors encoding two catalytically dead BAP1 mutants (BAP1C91A and BAP1H169Q). CHOP western blot analysis using protein lysates obtained from the afore-described cell lines revealed very interesting results. Firstly, BAP1 cDNA reduced CHOP expression levels in sgBPY cell lines **(Figure 4.2.6A)**. Conversely, cell lines containing enzymatically dead version of BAP1 had no reductive effect on CHOP levels, similar to empty vector control **(Figure 4.2.6A).** These results indicate that BAP1 regulation of CHOP requires its enzymatic activity.

To answer the question if this observed BAP1 regulation of CHOP has any functional consequence, I constituted an exploratory experiment utilizing sgPY cell lines with *Bap1* KD (referred to as sgPY shBAP1). Next, I performed proliferation assay to investigate the role of *Bap1* KD (and as a consequence, CHOP protein expression) on cell proliferation. Results obtained revealed no difference in proliferation in sgPY cell lines, regardless of *Bap1* status **(Figure 4.2.6B)**. Additionally, I assessed cell reproductive fitness by performing Colony forming assay (CFA) utilizing sgPY and sgBPY cell lines. Once again, I observed no difference in colony forming capacity in sgPY and sgBPY cell lines regardless of BAP1 status and BAP1 enzymatic activity (results not shown). This observed lack of functional significance for CHOP overexpression raises the question if it is because tumors were already established. To address this, I generated a px330 plasmid simultaneously expressing sgBap1 and sgDdit3. I combined this with a px330 plasmid expressing sgPten and a vector expressing YAP^{S127A} (sgC-BPY). The cocktail was subsequently injected into murine livers via HDTVI. sgBPY was used as control. Conceptually, if CHOP overexpression plays a role in *Bap1* loss driven tumorigenesis, simultaneous knockout of *Bap1* and *Ddit3* (CHOP) should delay or abrogate tumor evolution. Results revealed no difference in tumor evolution in sgBPY and sgC-BPY cohort with both developing tumors at the same time **(Figure 4.2.6C)**. Liver weight analysis also revealed no difference in liver weight between the two cohorts **(Figure 4.2.6D)**. Additionally, WB analysis of sgBPY and

sgC-BPY lysates revealed strong expression of CHOP in both groups, raising the question if CHOP was in fact edited *in-vivo* **(Figure 4.2.6E)**. BAP1 levels was uncharacteristically high in both groups **(Figure 4.2.6E)**. H&E analyses revealed highly steatotic HCC like appearance in the tumors of both cohorts. (sgBPY and sgC-BPY) **(Figure 4.2.6F)**. The results I obtained here indicate that the functional relevance of CHOP in the context of *Bap1* loss driven tumorigenesis is inconclusive.

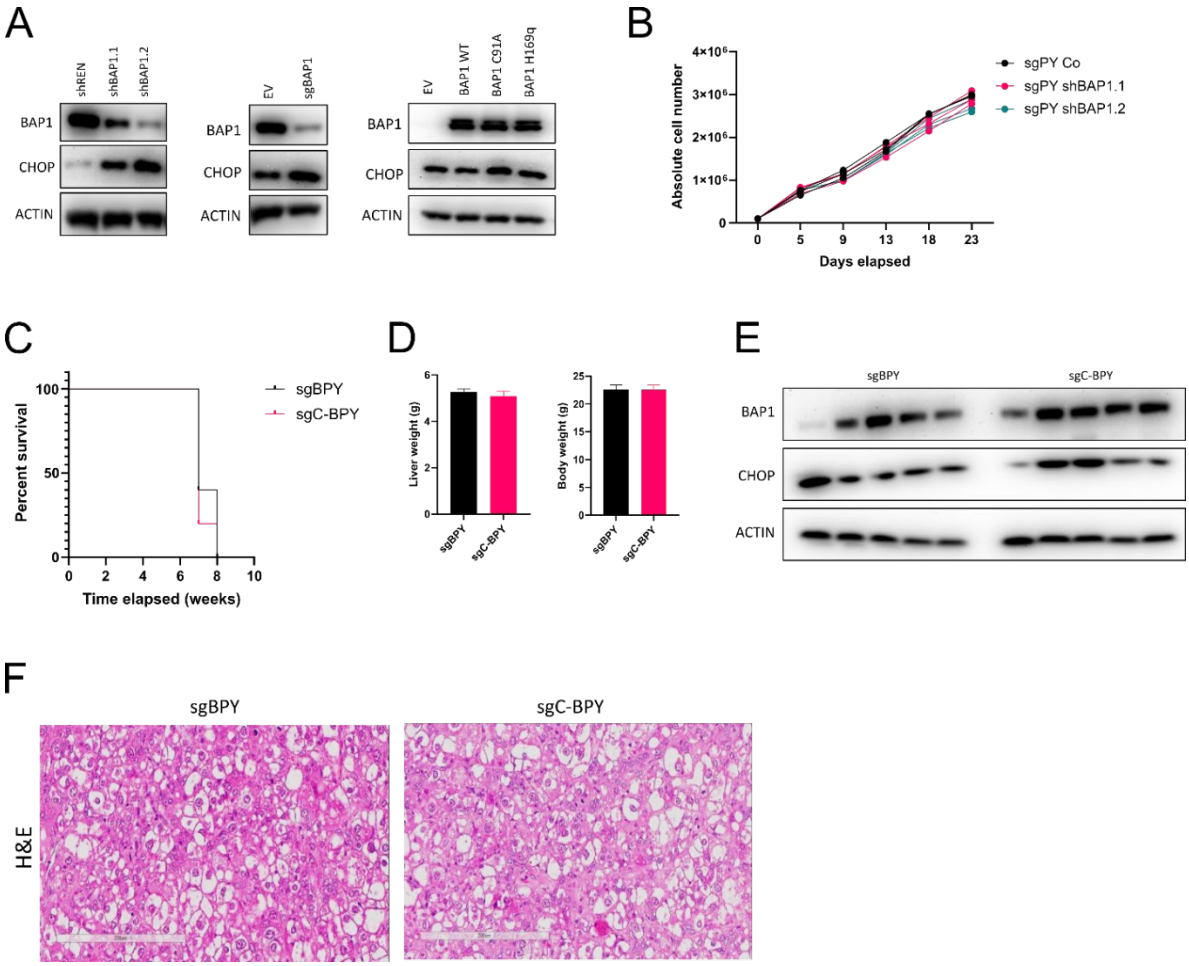

Figure 4.2.6: BAP1 status dynamically regulates CHOP levels in murine cell lines. (A) (From left to right) WB analysis showing *Bap1* KD in sgPY cell lines reveals upregulation of CHOP in the BAP1 deficient cell lines (N=3); WB analysis reveals knockout of *Bap1* in sgPY cell line triggers increased CHOP protein levels (N=2); Overexpression of BAP1 in sgBPY cell line reduces CHOP protein expression. Overexpression of catalytically dead BAP1 has no reductive effect on CHOP protein levels (N=3). **(B)**Proliferation assay analysis shows no difference in sgPY cell line proliferation regardless of BAP1 status (N=2)**. (C)** Survival curve showing no difference in survival between sgBPY and sgC-BPY cohorts. **(D)** Liver and body weight analysis in sgBPY and sgC-BPY cohort. **(E)** Western blot analysis of lysates from sgBPY and sgC-BPY tumors revealed near intact CHOP and BAP1 expression levels**. (F)** Representative H&E image showing similar histological phenotype in sgBPY and sgC-BPY tumors. Scale bar; 200µm

4.2.3 *Bap1* loss co-operates with *Arid1a* loss and YAP^{S127A} to trigger hepatic lineage switch

Hepatic lineage switch and plasticity have been previously described. From transdifferentiation[87, 88] to dedifferentiation[86], hepatocytes can transform into tumors bearing phenotypic resemblance of those from the cholangiocytic lineage. This phenotypic switch during tumorigenesis has been described to arise from oncogenic combination of myrAKT (myristolated AKT) coupled with Notch intracellular domain overexpression(NICD)[87], as well as a combination of YAP^{S127A}, P53 loss and NICD[86]. These distinct combinations gave rise to hepatocytes derived iCCA (intrahepatic cholangiocarcinoma). The commonality of NICD in the two studies suggest that it may play a central role in the process.

Considering *BAP1* mutational prevalence in iCCA and a lower prevalence in HCC, I hypothesized that *BAP1* loss may play a similar role to NICD in liver cell plasticity. In order to test this hypothesis, I designed an investigational concept. Briefly, three experimental combinations (each comprising constructs targeting Bap1) were established. The first combination comprised of sgBap1 coupled with myrAKT (referenced as sgBAKT), with control group being administration either sgBap1 alone or myrAKT alone, thus mirroring the first study and directly testing the potential of two combinations in liver cell plasticity. The remaining combinations utilizes three different genetic combination, thus mirroring the second study with three oncogenic events. The second group comprised of sgPten, sgArid1a and sgBap1 (referenced as sgPAB). The third combination comprised of sgBAP1, sgArid1a and YAP^{S127A} (sgBAY). The control cohorts have the respective constructs except sgBap1. All combinations were delivered into the liver of C57BL6/N mice via HDTVI. Afterwards, tumor evolution and survival were evaluated post HDTVI.

For the first combination (sgBAKT), I observed that animals became immobile and manifested evidence of hepatomegaly (with protruded belly) within the first 9 to 12 weeks. **(Figure 4.2.7A)**. This observation is also true for the control myrAKT (referred to as AKT) alone, with hepatomegaly noticeable within 6 to 10 weeks. **(Figure 4.2.7A)**. Of note, the sgBAP1 control survived up until the end of the experiment (12 months). Histological analysis of sgBAKT and AKT showed steatosis but no evidence of a phenotypic switch while sgBAP1 samples look relatively normal **(Figure 4.2.7A)**.

Next, I evaluated the second combination (sgPAB). Here most of the animals survived up until 20 weeks post HDTVI at which point they had to be sacrificed due to palpable liver

hardness and increased liver size. In contrast, the bulk of the control cohort (sgPA) survived until the end of the experiment (12 months) **(Figure 4.27B)**. Histological evaluation revealed a steatotic phenotype reminiscent of the previously described sgPB model for both cohorts. Importantly there was no visible phenotypic switch **(Figure 4.2.7B)**.

Furthermore, I evaluated the third combination (sgBAY). Here, 4 out of 5 animals developed tumors within 15 weeks and the last developed tumors at 18 weeks. Of note, one animal in the control combination (sgAY) developed a tumor at approximatively 10 months post HDTVI. For the others, I observed no palpable tumors until they were sacrificed at the end of the experiment (12 months) **(Figure 4.2.7C)**. WB analysis of lysates obtained from sgBAY tumors confirmed lack of BAP1 protein expression. Remarkably, the ER stress sensor, CHOP, was strongly expressed in the sgBAY sample, further strengthening the association between BAP1 and CHOP **(Figure 4.2.7C)**. Surprisingly, the solitary sgAY tumor had no BAP1 expression and strong CHOP expression as observed via WB **(Figure 4.2.7C)**. The remaining sgAY samples had stable BAP1 protein expression and no CHOP expression **(Figure 4.2.7C)**. Histological analysis of the sgBAY tumors unearthed some startling observations. I analyzed H&E stainings of the tumors and this revealed a distinct iCCA like phenotype with visible desmoplastic stroma deposition and a mass forming appearance reminiscent of iCCA **(Figure 4.2.7C)**. Importantly, control samples (sgAY) displayed no such phenotypic switch **(Figure 4.2.7C)**. As expected, analyses of IHC staining for BAP1 revealed loss of nuclear expression in sgBAY tumor samples **(Figure 4.2.7D)**. Further, analyses of IHC staining for the proliferation marker Ki67 on the tumor samples revealed very strong, liver wide expression. As is now typical for BAP1 deficient tumors, IHC staining revealed CHOP was strongly expressed in sgBAY tumor samples **(Figure 4.2.7D)**. To validate whether there is indeed a lineage switch and stroma deposition in the sgBAY samples, I analyzed IHC staining for CK19 and HNF4α, markers for cholangiocytes and hepatocytes respectively. These analyses showed strong CK19 staining in the tumor area, thus suggesting a possible phenotypic switch **(Figure 4.2.7E)**. HNF4α was mildly positive in sgBAY tumors. Remarkably, Gomori methenamine silver staining (referred to as GS), which selectively stains collagen revealed collagen deposition in sgBAY tumor samples **(Figure 4.2.7E).** Importantly, CK19 and GS staining for sgPBY tumor samples revealed weak (CK19) to no signal (GS) in the evaluated samples **(Figure 4.2.7E)**. sgBPY livers were positive for HNF4α. Taken together, these results suggest *Bap1* loss co-operates with *Arid1a* loss and YAP enforced expression to mediate cell plasticity in liver tumorigenesis.

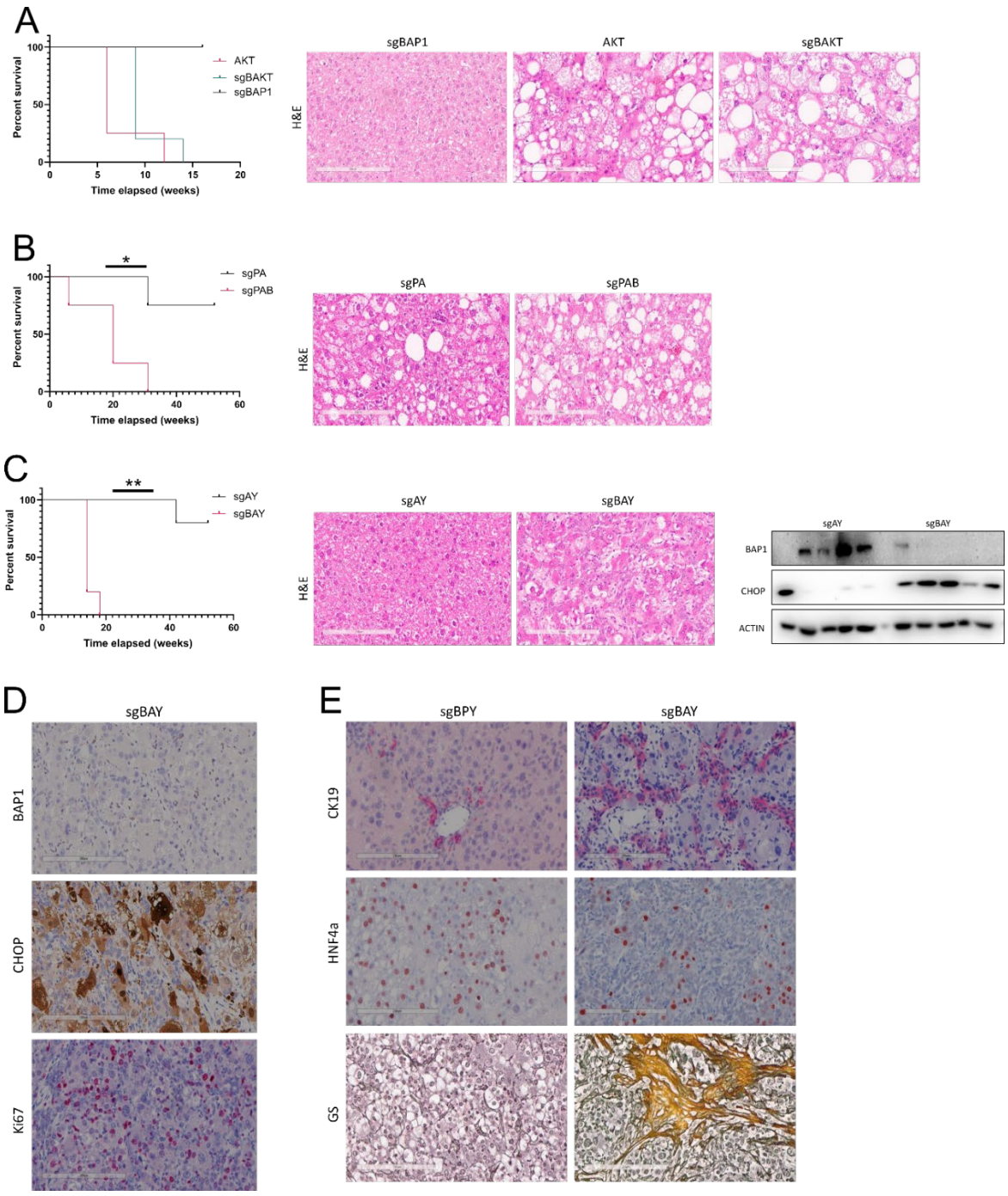

Figure 4.2.7: *Bap1* loss co-operates with *Arid1a* loss and YAP enforced expression to trigger hepatic lineage switch. **(A) (**Left to right) Survival curve for tumor bearing mice AKT, sgBAP1 and sgBAKT combinations. Representative H&E images showing relatively normal liver (sgBAP1) and steatotic livers without any visible lineage switch (AKT and BAKT). **(B)** (left to right) Survival analysis and representative H&E image for sgPA and sgPAB. **(C)** (Left to right) Survival analysis of sgAY and sgBAY cohorts showing fast tumor evolution in sgBAY cohort. Representative H&E image confirming a possible lineage change in sgBAY samples. WB analysis showing loss of BAP1 and increased CHOP expression in sgBAY lysates**. (D)** Representative IHC panel for BAP1, ki67 and CHOP in sgBAY tumors**. (E)** CK19, HNF4α and Gomori silver staining confirms a possible lineage switch in sgBAY tumors. Statistical tests: log-rank (Mantel-Cox) test.

4.3 Exploiting BAP1 deficiency as a therapeutic target in tumors

4.3.1 BAP1 deficient tumors are not vulnerable to fatty acid overload

Results obtained thus far in this study indicated *Bap1* contextually safeguards hepatic cell survival as well as tumorigenesis. *Bap1* loss is lethal in CD-HFD fed mice in a metabolic distress dependent context. In another context, *Bap1* loss co-operates with selected oncogenic events (such as Pten loss and YAP overexpression) to drive hepatocarcinogenesis. This raises the question whether one could exploit these two distinct phenomena by converging their attributes. Briefly, I hypothesized that fatty acid overload would represent a vulnerability in BAP1 deficient tumors. To test this hypothesis, I utilized the previously described sgPY cell lines with *Bap1* knockdown. I challenged the cell lines with the fatty acids, palmitic acid (16:0) and oleic acid (18:1) at equimolar ratios (1:1), and at a non-toxic concentration (500μM). Next, I performed Colony forming assay (CFA) to interrogate the proliferative and reproductive fitness of the cell lines. Results showed a slight increase in colony forming capacity in sgPY shBAP1.1 and sgPY shBAP1.2 cell lines when compared to sgPY shRenilla cell line **(Figure 4.3.1A&B)**. In the fatty acid challenged group intervention, I observed no difference in colony forming capacity in sgPY cell lines irrespective of Bap1 status **(Figure 4.3.1A&B)**. Of note, the fatty acid intervention here does not fully recapitulate CD-HFD intervention (since many more fatty acid species are available in CD-HFD compared to the fatty acid intervention described herein). Thus, it stands to reason that challenging BAP1 deficient tumors with CD-HFD would represent a better intervention. C57BL6/N were injected with the genetic cocktail that yields sgBPY tumors. In the next step, I challenged mice with CD-HFD, ten days after HDTVI (just before tumor formation). Survival analysis revealed no difference in tumor burden between the interventional group (CD-HFD challenge) and control group (normal diet, ND) **(Figure 4.3.1 C)**. Furthermore, liver weight analysis showed no significant difference in liver weight **(Figure 4.3.1C)**. Taken together, the results described here suggest BAP1 deficient tumors are not vulnerable to fatty acid overload *in-vitro* and *in-vivo*.

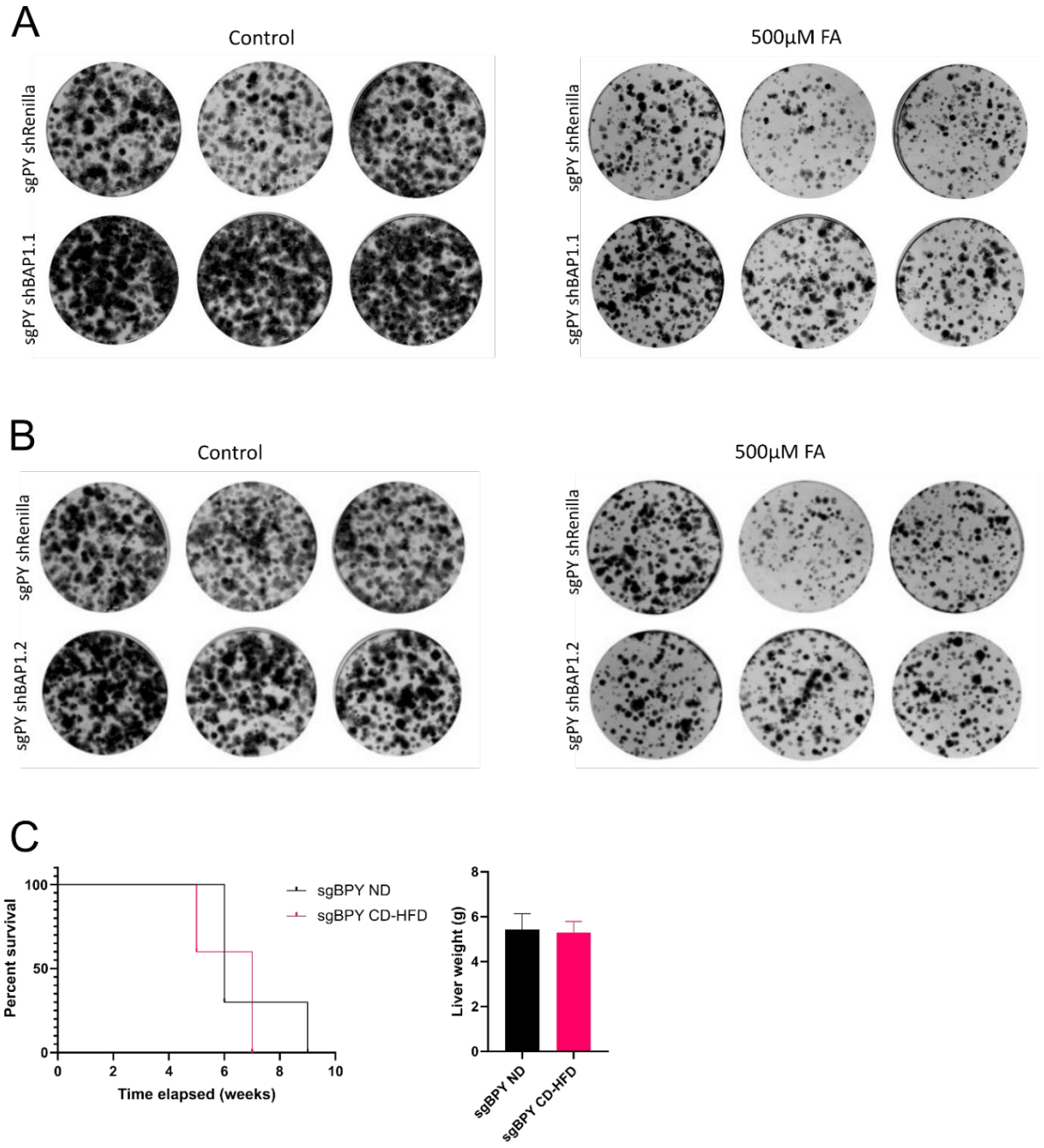

Figure 4.3.1: BAP1 deficient tumors are not vulnerable to fatty acid overload. (A&B) Colony forming assay showing no significant difference in sgPY cell lines after fatty acid challenge (Palmitic acid and oleic acid) regardless of Bap1 status. n=3 **(C)** Survival) Survival analysis shows no difference in survival after challenging sgBPY mice with CD-HFD (left). Liver weight analysis in sgBPY mice show no difference between CD-HFD challenged and normal chow fed animals(right).

4.3.2 *Bap1* repression is a genetic vulnerability in Myc; *Trp53*$^{-/-}$ tumors.

Upon the realization that BAP1 deficient tumors harbor no vulnerability related to dietary overload, I reasoned that the genetic vulnerabilities, conferred by mutations, might exist instead. Mining publicly available tumor sequencing data, I made a very interesting observation. Briefly, *BAP1* and Tumor protein 53 (*TP53*) mutations are significantly mutually exclusive in pan-cancer sequencing data (MSK IMPACT) as accessed on cBioPortal (**Supplementary Figure 1**). Hepatocellular carcinoma sequencing data (TCGA) also confirmed the same trend.

Armed with this information, I hypothesized that *BAP1* loss is incompatible with *TP53* loss in the course of tumor evolution. Accordingly**,** BAP1 deficiency would represent a genetic vulnerability in *TP53* loss driven tumors. In order to test this hypothesis, I utilized the previously described C-myc;Trp53$^{-/-}$ tumor model (referred to as MP)[130], modified to sufficiently address the question at hand. Briefly, I constituted a three-plasmid system (referred to as MP shBAP1 or MP shRenilla). For the first plasmid, I cloned shBAP1.1 (or shRenilla) into a Sleeping Beauty (SB) transposon vector harboring the TRE promoter (thus Dox-inducible) and t-RFP for fluorescent reporting of shRNA expression. The second plasmid, a SB transposon vector containing EF1α-driven c-MYC and rtTA3, allows for constitutive expression of rtTA3. The basic px330 vector harboring sgP53 (third plasmid) completes the set up **(Figure 4.3.2A)**. This configuration enables doxycycline-dependent expression of the target shRNAs only in the presence of plasmid number 1 and 2. Since the third plasmid harbors sgP53, tumors can arise when plasmid number 2 and 3 are present in the same cell. To circumvent this, a disproportionately more amount of plasmid 1 (4x more than both plasmids 2 and 3) was injected. This essentially guarantees that all 3 plasmids will be present in a cell in the event of a tumor.

Seven days post HTVI, mice were divided into two groups. I placed the interventional group on doxycycline diet to enable expression of shBAP1 or shRenilla, while the control group remained on normal chow. Strikingly, survival analysis suggests abrogation of tumor-forming capacity in MP shBAP1.1 mice challenged with Dox. Here, only a solitary mouse out of five developed tumors, with delayed tumor initiation (12 weeks post HTVI) **(Figure 4.3.2B)**. Conversely, three out of five MP shBAP1.1 mice without Dox challenge (thus no *Bap1* repression) developed tumors with faster initiation (4 to 6 weeks) **(Figure 4.3.2B)**. Importantly, MP shRenilla mice developed tumors at a comparable penetrance and speed, thus implying shRenilla has no effect on tumor development. Here, four out of 5 mice and 5

out of 5 mice developed tumors within four to 6 weeks, in the on Dox and off Dox groups respectively **(Figure 4.3.2B)**.

To interrogate whether all three plasmids were present in the derived tumors, I inspected MP shBAP1/shRenilla tumors obtained from animals challenged with Dox under the dissectoscope. Surprisingly, the solitary MP shBAP1.1 tumor had very weak fluorescence of tRFP, suggesting an endogenous silencing of the short hairpin **(Figure 4.3.2C)** Of note, all MP shRenilla tumors exhibited strong fluorescence in the dissectoscope red channel **(Figure 4.3.2C)**. In the next step, I analyzed IHC stainings for tRFP and BAP1 in the MP samples. As expected, MP shRenilla samples expressed BAP1 and tRFP in on Dox tumors, while off Dox tumors expressed BAP1 but were negative for tRFP) **(Figure 4.3.2D)**. MP shBAP1 off Dox tumors were negative for tRFP and had strong nuclear expression for BAP1. The only MP shBAP1 on dox tumor weakly stained for tRFP (in a mosaic fashion), thereby consolidating the initial observation from the dissectoscope imaging **(Figure 4.3.2B)**. Accordingly, the tumor also had strong nuclear BAP1 expression, thus confirming the hypothesis that the short hairpin was indeed silenced *in-vivo* **(Figure 4.3.2B)**. Taken together, this set of data implies that *in-vivo* loss of *Bap1* abrogates tumor formation in MP mouse tumor model.

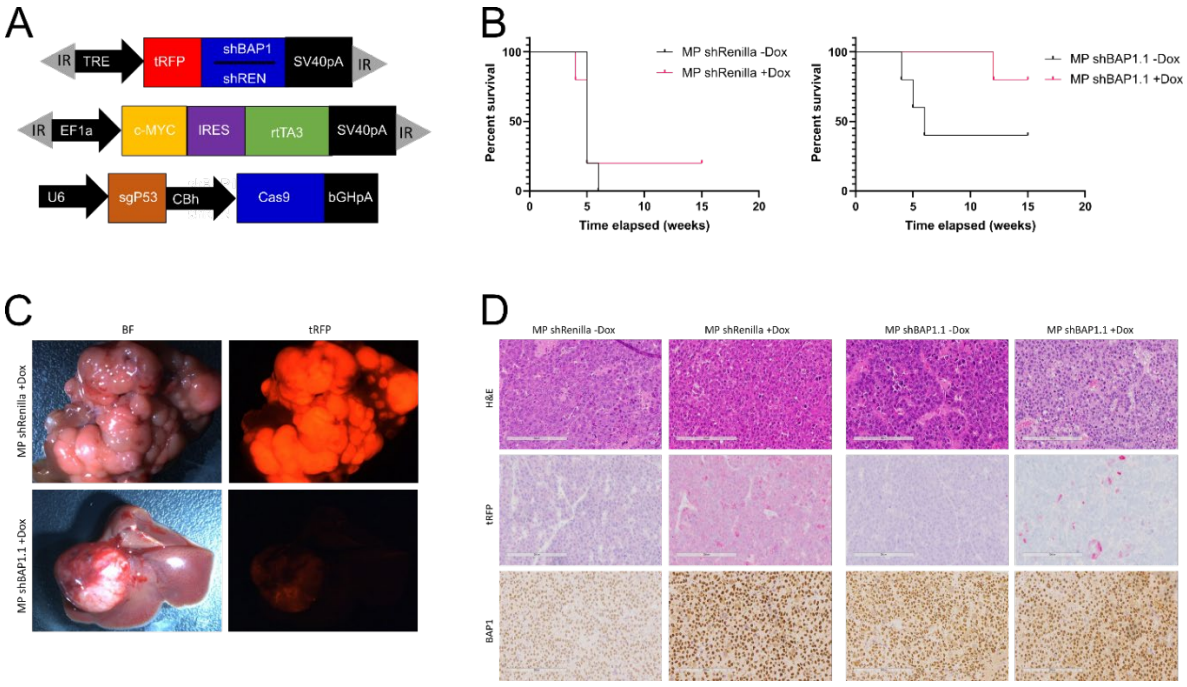

Figure 4.3.2: *Bap1* repression abrogates MP loss driven tumor formation *in-vivo*. (A) Illustration of the 3-pronged plasmid system designed to investigate the therapeutic utility of *Bap1* repression in murine tumors **(B)** Survival curve showing reduced tumor penetrance in Bap1 repressed MP tumor model **(C)** Dissectoscope image showing weak tRFP expression in MP shBAP1 on Dox tumor. **(D)** Representative IHC image panel showing very weak RFP expression and BAP1 nuclear expression in MP shBAP1.1 on Dox tumor. Scale bar: 200µm.

4.3.3 BAP1 deficiency is a therapeutic vulnerability in TP53$^{-/-}$ tumors *in-vitro*

To elucidate the tumor formation abrogation phenomenon in C-myc;Trp53$^{-/-}$ tumors with additional *Bap1* repression, I established cell lines from MP shBAP1 and MP shRenilla tumors. To investigate the fidelity of the dox inducible system, I subjected MP shBAP1 and MP shRenilla tumors cell lines to doxycycline treatment for 7 days. Afterwards I obtained cell lysates for WB. Western blot analyses revealed tRFP expression in Dox treated group across all cell lines **(Figure 4.3.3A)**. Importantly MP shBAP1.1 cell line treated with Dox had significantly reduced BAP1 protein levels when compared to off Dox control **(Figure 4.3.3A)**. MP shRenilla cell lines had comparable BAP1 protein levels across both groups (off and On Dox) **(Figure 4.3.3A).**

To delineate the functional consequence of *Bap1* repression in MP cell lines *in-vitro*, I performed colony forming assay and proliferation assays. Briefly, I utilized two MP shBAP1.1 cell lines from two different mice (Referred to as MP BAP2B and MP BAP2C respectively) and two MP shRenilla cell lines (Referred to as MP REN1 and MP REN2). I further divided the cell lines into a group with Dox treatment and another without.

Proliferation assay for MP REN1 showed no significant difference in proliferation between on Dox and off Dox cell lines **(Figure 4.3.3B)**. Remarkably, MP BAP2B and MP BAP2C cell lines showed significant reduction in cell proliferation in the Dox treated cell lines compared to the off Dox control **(Figure 4.3.3B)**. Next, colony forming assay was performed to validate the proliferation assay finding. In agreement with the proliferation data, MP REN1 and REN2 cell line showed no difference in colony forming capacity between Dox treated and Dox naive cell lines **(Figure 4.3.3C)**. I observed significantly lower colony numbers in Dox treated MP BAP2B and MP BAP2C cell lines relative to Dox naive control **(Figure 4.3.3D)**. In summary, *Bap1* repression represent an unexpected Achilles hill and leads to growth retardation of MP cell lines *in-vitro*.

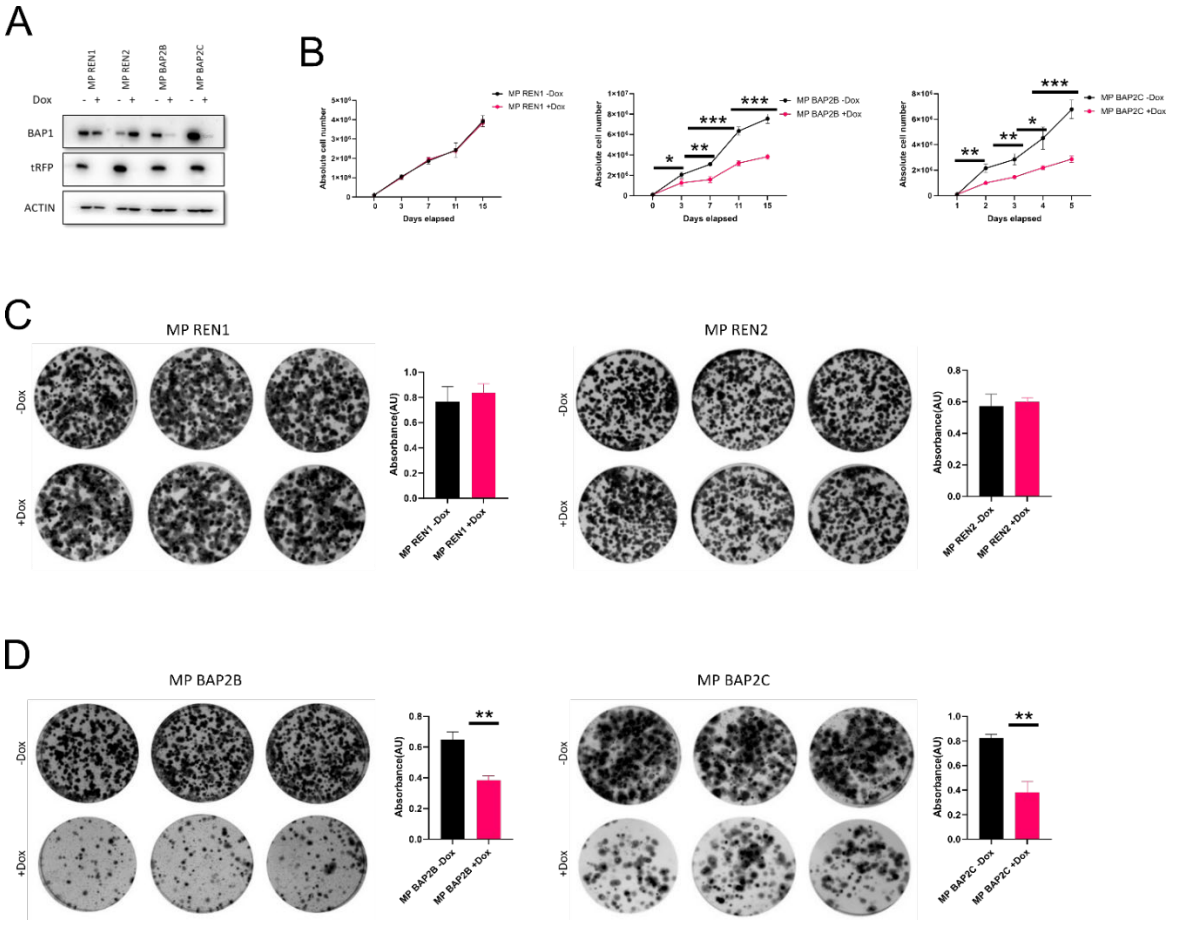

Figure 4.3.3: *Bap1* repression retards MP cell lines proliferation and colony forming potential. (A) Western blot analysis showing reduction in BAP1 protein in MP BAP2B and MP BAP2C upon Dox treatment. MP REN1 and MP REN2 BAP1 protein levels remains stable after Dox challenge. **(B)** Proliferation assay showing retardation of proliferation in MP BAP2B and MP BAP2C cell lines after dox treatment N=3 **(C)** Colony forming assay in MP REN1 and MP REN2 cell line, N=2. **(D)** Colony forming assay showing reduction in colonies in MP BAP2B and MP BAP2C cell lines after dox treatment; N=3. Column graphs represent colony quantification. Statistical test: Student's t-test.

To test for the applicability of this finding in the human setting, I designed an experimental approach utilizing human liver cancer cell lines with *TP53* mutations. Firstly, I transfected Hep3B (possessing *TP53* null mutation), HuH7 (with have *TP53* mutation resulting in overexpression) and HepG2 (with wild-type (WT) p53) cell lines with virus containing human sgBAP1 to generate *BAP1* KO variants of these cell lines **(Figure 4.3.4A)**. Next, I performed proliferation assay, and results obtained revealed significant growth retardation in Hep3B cell lines with *BAP1* KO but not in HuH7 and HePG2 cell lines, relative to their respective control **(Figure 4.3.4B)**. Encouraged by this observation, I performed colony forming assay (CFA) to further corroborate the finding. Here, CFA analysis revealed reduced colony forming capacity in Hep3B *BAP1* KO cell lines. HuH7 and HePG2 cell lines had similar colony forming capacity regardless of *BAP1* status **(Figure 4.3.4C)**. In agreement with the *in-vivo* and *in-vitro* murine tumor data, these results imply that *BAP1* loss constituted an unexpected vulnerability in *TP53*$^{-/-}$ setting.

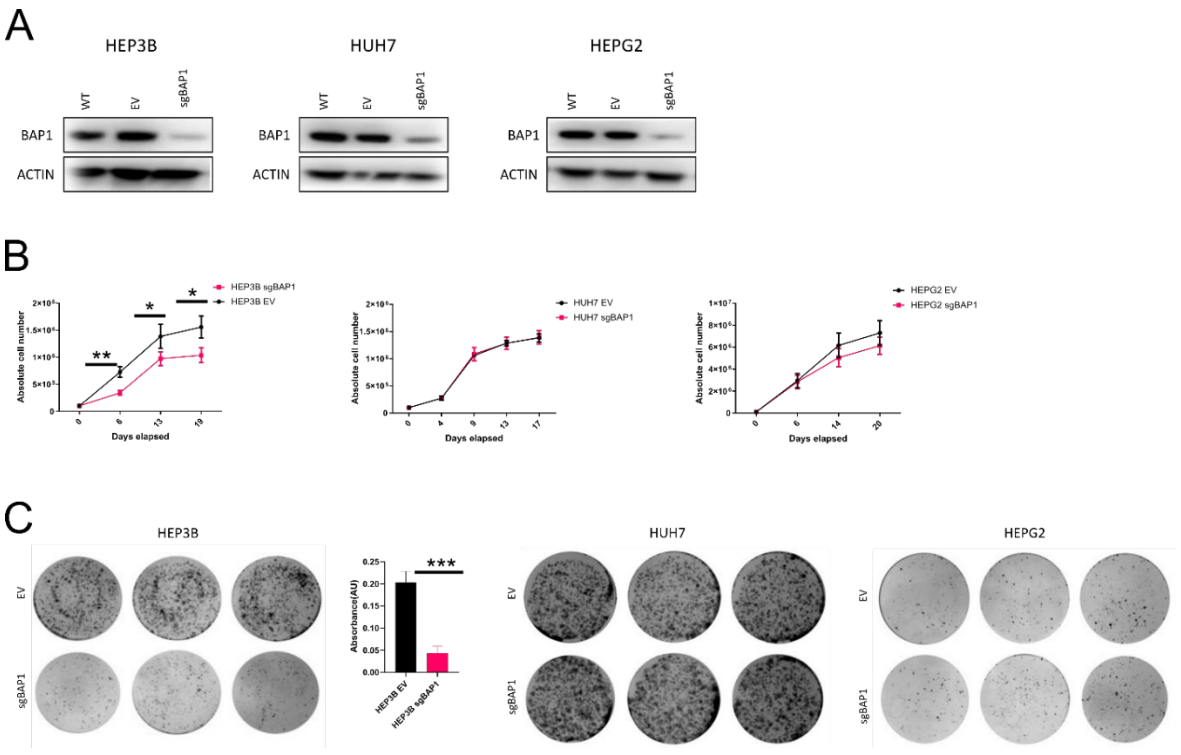

Figure 4.3.4: BAP1 deficiency leads to growth retardation in p53 null human liver cancer cell line. (A) WB analysis confirming knockout of *BAP1* in human liver cancer cell lines. **(B)** Proliferation assays showing reduced proliferation in *BAP1* KO Hep3B cell line, with concomitant lack of effect on proliferation in HuH7 and HepG2 cell lines with *BAP1* KO, n=3 **(C)** Reduced colony forming capacity only in *TP53* null (Hep3B) BAP1 deficient cell line, with P53 proficient cell lines not exhibiting any changes in colony formation in the context of BAP1 deficiency, n=2. Statistical test: Student's t-test.

4.3.4 BAP1 catalytic function attenuates growth retardation in MP mouse model with *Bap1* repression

To gain further insight into the molecular principles of *Bap1* repression driven growth retardation and reduced cellular fitness in C-myc;Trp53$^{-/-}$ cell line, I designed and executed a powerful *BAP1* rescue experiment. I employed BAP1 human cDNA overexpression plasmid (BAP1 WT) as well as two catalytically deficient *BAP1* cDNAs (BAP1^{C91A} and BAP1^{H169Q}) to generate MP BAP2B cell lines with BAP1 overexpression. Of note, these cell lines harbor Dox regulatable shBAP1.1. Conceptually, treating the cell lines with Dox allows for Dox dependent *Bap1* repression and subsequent growth retardation, while the exogenous cDNA should rescue and mitigate *Bap1* repression dependent growth retardation. To test whether the system work as expected, I performed Western blot analyses on lysates obtained from the cell lines. BAP1 protein expression was markedly reduced in on Dox conditions with empty vector control (EV) (i.e., no BAP1 overexpression). Dox treated MP BAP2B BAP1 WT cell line had slightly lower BAP1 protein level when compared to off Dox control, implying rescue of *Bap1*. The same observation holds true for the two *Bap1* overexpression mutants (C91A and H91Q). Together the results validate the robustness of the *Bap1* rescue setup **(Figure 4.3.5A)**.

Next, I performed colony forming assay on MP BAP2B cell lines. EV cell line treated with Dox had significantly lower number of colonies when compared to its off Dox counterpart **(Figure 4.3.5B)**. Notably, MP BAP2B with overexpression of BAP1 WT rescued the reduced colony forming capacity phenotype after Dox challenge, with colonies being of roughly the same density as the off Dox counterpart **(Figure 4.3.5A)**. Importantly, BAP1 mutant cDNAs could not rescue the phenotype, with considerably lesser colony density observed in Dox-challenged samples as compared to off Dox control **(Figure 4.3.5B)**. To control for Dox-dependent and off-target shRNA-induced effects, the same experiments were carried out on MP shREN1 cells. Notably, I observed no difference in colony forming capacity regardless of Dox and BAP1 status in MP shREN1 cell lines **(Figure 4.3.5C)**. In summary, these results implicate the enzymatic activity of BAP1 in the growth retardation phenotype described here.

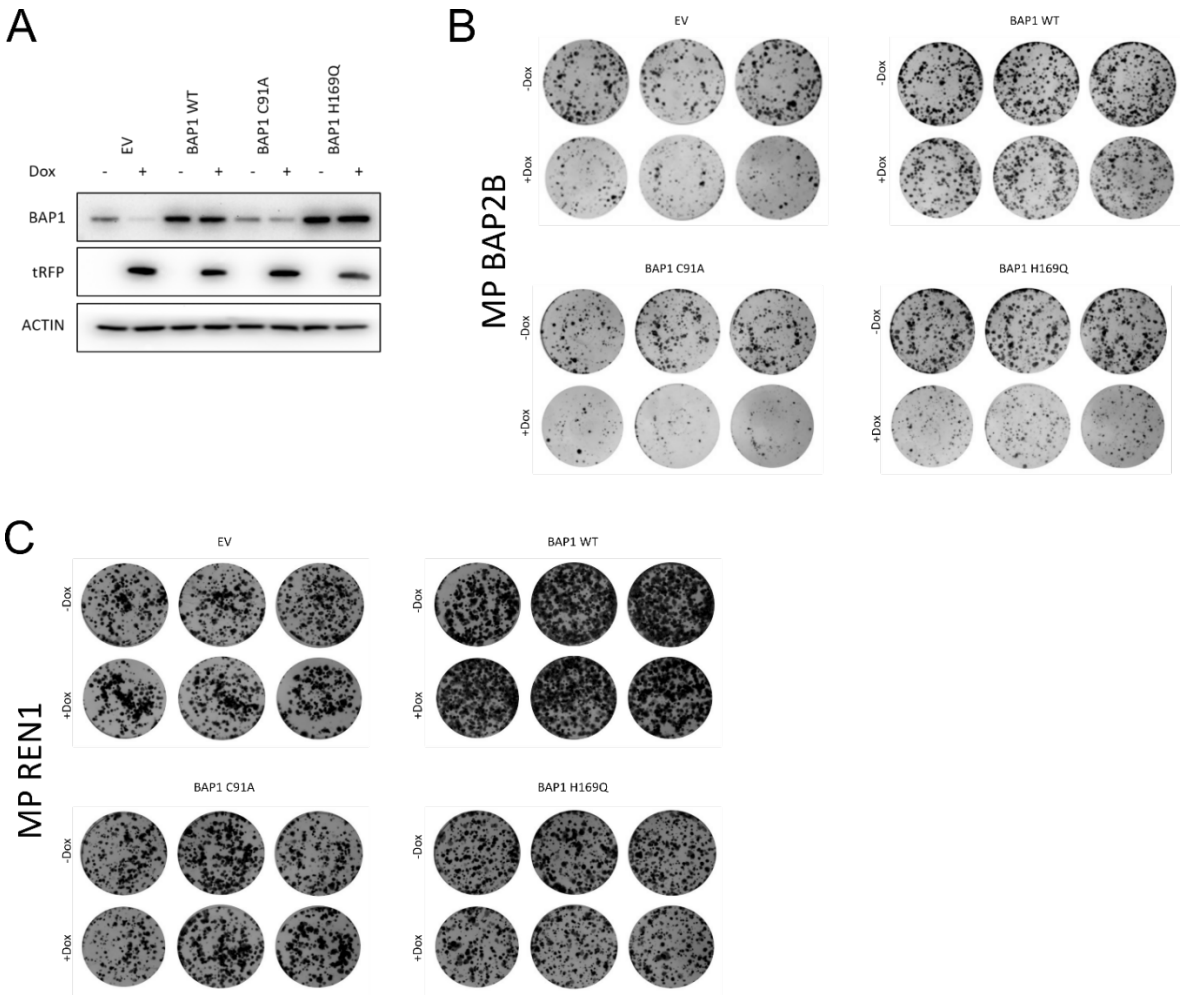

Figure 4.3.5: BAP1 overexpression rescues growth retardation in MP cell lines. (A) Western blot analysis confirming the robustness of the rescue setup. BAP1 overexpression cell lines rescues Dox dependent repression of *Bap1* **(B)** Colony forming assay showing rescue of growth retardation in MP cell lines after Dox dependent *Bap1* repression. WT BAP1 but not enzymatically deficient ($BAP1^{C91A}$ and $BAP1^{H169Q}$) BAP1 rescues growth retardation n=2. **(C)** Colony forming assay showing Dox dependent renilla repression has no effect on colony forming capacity regardless of BAP1 enzymatic status. n=2.

4.3.5 *Bap1* suppression as a therapeutic modality in MP tumors *in-vivo*

To investigate whether *Bap1* suppression can be utilized as a targeted therapy in *Trp53* null liver cancers, I designed an interventional experiment. Here, I utilized the previously described shBAP1 transgenic murine strain. Briefly, a constitutively expressed C-Myc vector was co-injected with a px330 vector expressing sgTrp53 via HDTVI **(Figure 4.3.6A)**. Tumor formation was monitored by palpation and by small animal MRI **(Figure 4.3.6A)**. Upon tumor detection, tumor bearing animals were divided into two groups, namely off Dox and on Dox groups and their survival was monitored over time **(Figure 4.3.6A)**. Out of 9 injected animals, only 2 developed tumors **(Figure 4.3.6B)**. I detected tumors in the first tumor bearing animal (referred to as Exhibit A) at 4 weeks post HDTVI. Exhibit A was

immediately placed on Dox. Dox challenge could not truncate the tumor growth trajectory and the animal succumbed to the tumor burden at 6 weeks (2 weeks of Dox intervention) **(Figure 4.3.6C)**. The second tumor bearing mice (Exhibit B) developed tumors at 6 weeks post HDTVI and was also placed on Dox instantaneously. Strikingly, Dox challenge truncated tumor growth trajectory with the tumor size remaining the same up until the end of the experiment **(Figure 4.3.6D)**. Together, the result from the experiment I performed here highlight the utility of *Bap1* repression as a novel therapeutic strategy in *TP53* null tumors.

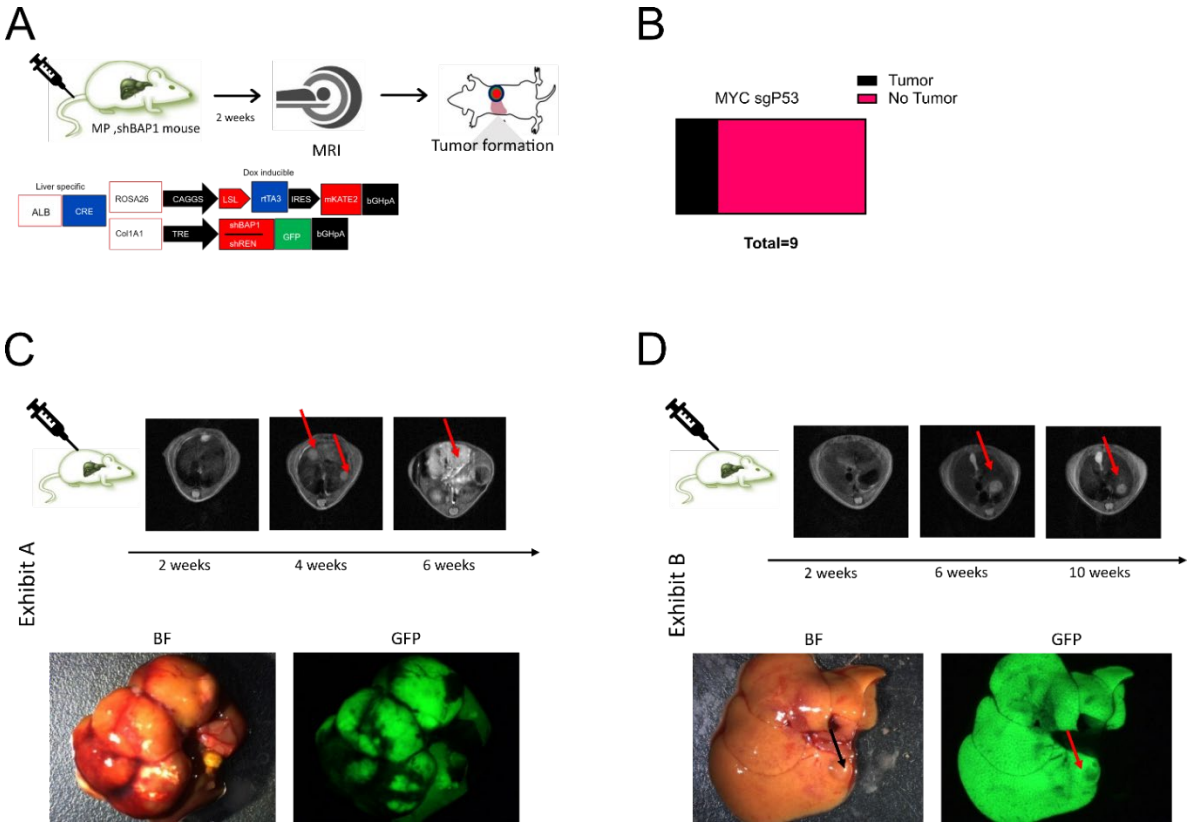

Figure 4.3.6: *Bap1* suppression as a novel therapy in MP tumors. (A) Experimental schematic of the *Bap1* repression-based intervention in MP tumors. **(B)** Horizontal slice graph depicting the tumor penetrance after MP HTVI in shBAP1 mice. **(C)** Exhibit A denoting tumor bearing MP shBAP1 mice with Dox challenge without tumor growth retardation. **(D)** Exhibit B denoting tumor bearing Dox challenged MP shBAP1 mice with successful arrest of tumor growth.

5.0 Discussion

Primary liver cancer remains one of leading causes of cancer related deaths worldwide with prevalence almost equaling mortality [65]. However, despite the deadly consequence of the disease, effective therapeutic options remain limited[61]. Recent genetic sequencing efforts have highlighted the genetic heterogeneity of primary liver cancer and its mutational landscape[91, 131, 132]. However, there remains a lack of comprehensive studies investigating the functional consequence of these genetic mutations in liver homeostasis, tumorigenesis and the development of tailored genotype specific therapies. To bridge this knowledge gap, I set out to investigate the role of the histone deubiquitinase BAP1, which is frequently altered in liver cancer.

Using Dox regulatable shRNA mouse strains and in vivo CRISPR-Cas9 technology, I unveiled the context dependent role of *Bap1* loss in the liver along the lines of hepatic cell survival, tumor suppression and initiation, as well as a poisoned chalice for liver tumors harboring certain mutations.

5.1 Liver specific *Bap1* suppression leads to mild hepatic pathological changes

In order to evaluate the role of *Bap1* in liver homeostasis, I suppressed *Bap1* expression over 36 weeks by challenging shBAP1 mice with doxycycline. The mosaic expression of GFP (surrogate for shBAP1 expression) I observed in shBAP1.2 mice may be cellular adaptation to the stress of *Bap1* loss or part silencing of the short hairpin RNAs. Overall, the data suggests mild-pathological but tolerable changes upon *Bap1* repression in the liver. Importantly, no tumor related changes were detected.

In stark contrast to this finding, Baughman *et al.* showed that liver-specific *Bap1* loss is fatal in mice, with neonates expiring 48 hours after birth[133]. The lack of consensus in the reported findings may stem from the differences in the mouse models. The mouse models employed in this study is tetracycline-regulatable, thus *Bap1* knockdown is temporally controlled and triggered only in adult mice (8 weeks and above). Whereas, in the liver-specific model utilized by Baughman *et al., Bap1* deletion (as against suppression) is acquired at birth[133]. This implies that *Bap1* loss may be critical in embryonic survival and development[119]. While systemic deletion of *Bap1* in adult mice coupled with reconstitution of the hematopoietic system is tolerable with mice surviving beyond 12 weeks post KO ,and effects including mild liver and pancreatic injury [133], it may also lead to acute fatality (4 weeks post KO) with accompanying liver damage presumably due to intrinsic

apoptosis[134], suggesting that the reported findings in these studies may be influenced by contributions from multiple tissues and cell types.

Clearly, developmental context matters when interpreting results from *Bap1* mouse models. It will be interesting to test if whole body repression of *Bap1* will be tolerable using the shRNA transgenic mouse model employed in the current study.

5.2 *Bap1* is essential for survival in metabolically distressed mice

In order to evaluate the role of BAP1 in metabolic distress, I coupled *Bap1* repression with metabolic stress inducing diets such as CD-HFD and HFD. I observed acute liver damage and fatality in both settings, albeit with CD-HFD being more fatal. Further, transcriptomics analysis revealed downregulation of lipid metabolism genes and upregulation of the unfolded protein response pathway including the ER stress sensor CHOP. Lipidomics analysis revealed general perturbation of the lipidome with cholesterol, fatty acids and diglycerides generally being elevated in the *Bap1* depleted samples. Accordingly, *Bap1* restoration attenuated liver damage and fatality.

CD-HFD has been shown to be a more potent driver of NASH than HFD [135], thus that may explain the higher fatality (as derived from serum liver transaminases measurements) I observed. In fact, HFD is unable to drive NASH related phenotypes in mouse[136], making it a weaker model of metabolic distress when compared to CD-HFD. While *Bap1* repression alone is generally tolerable in adult mice in the model employed in this study, other studies utilizing tamoxifen inducible whole-body knockout of *Bap1* reported fatality in adult mice[134].

As reported by He and colleagues, this *Bap1* loss dependent fatality is driven by intrinsic apoptosis, with additional knockout of the proapoptotic genes Bax and Bak rescued fatality[134]. However, I did not observe activation of the intrinsic apoptosis pathway as mice livers were generally negative for cleaved caspase 3. Instead, the livers were positive for TUNEL, suggesting both regulated and unregulated cell death processes may be involved. This could be because BAP1 deficient cells are unable to properly execute regulated cell death pathways.

Supporting the aforementioned notion, BAP1 has been implicated in promoting diverse regulated cell death pathways including apoptosis and ferroptosis. In a study by Bononi *et al,* BAP1 was implicated in promoting apoptosis through deubiquitylation mediated

stabilization of type-3 inositol-1,4,5-trisphosphate-receptor (IP3R3)[117]. Accordingly, BAP1 deficient cells were unable to properly execute apoptosis[117] . In a similar study, BAP1 was reported, via its deubiquitylating activity to promote ferroptosis, an iron-dependent regulated cell death pathway, by blocking cysteine uptake through the repression of the cysteine transporter, SLC7A11[137]. This way, BAP1 deficient cell lines are unable to repress cysteine and promote ferroptosis. This stands to reason that perhaps, *Bap1* repression in the liver of adult mice already primed the liver for damage. Further damage potentiated by CD-HFD likely pushed hepatocytes to a point of no return, with fatality occurring in a mostly unregulated manner.

Transcriptomics analysis of CD-HFD fed *Bap1* repressed mice revealed downregulation of lipid metabolism related genes including the rate limiting enzyme in triacylglycerol synthesis, *Dgat2*, the lipid transporter CD36 and the lipid chaperones *Fabp1* and *Fabp5*. Interestingly, transcriptomics analysis of human organoids with *BAP1* loss reported downregulation of *FABP1* gene[138]. In corroboration of the stated facts, a proteomic analysis of *Bap1* KO mice also highlighted downregulation of lipid processes related genes including the lipid chaperones *Fabp1* and *Fabp5*[133]. Altogether, these finding suggest deregulation of fatty acid related processes in a BAP1 deficient settings.

Furthermore, in relation to the transcriptomics data, I observed upregulation of the unfolded protein response pathway, including the ER stress associated transcription factors *Atf3* and *Ddit3* (encoding CHOP), suggesting pervasive ER stress in *Bap1* repressed CD-HFD fed mice. Utilizing a glucose starvation model of metabolic stress in UMRC6 cell lines, Dai *et al* demonstrated that BAP1 inhibits glucose deprivation induced apoptosis by restricting the transcription of CHOP and ATF3, a process controlled by its catalytic activity. Here, BAP1 deficiency in the context of glucose deprivation promotes CHOP and ATF3 mediated apoptosis [118]. The pro-survival role of BAP1 reported here is in line with what was observed in the current study. However, despite CHOP and ATF3 upregulation, no apoptosis was detected.

A critical mechanism of ER stress dependent apoptosis is the upregulation of CHOP[139].Accordingly, CHOP has been shown to regulate ER stress intrinsic induced apoptosis in murine neuronal cells[140] as well as in pancreatic islets of lactating rats[141]. CHOP has also been implicated in the extrinsic apoptosis pathway in ovarian carcinoma[142] and also in TRAIL mediated apoptosis in carnosic acid treated human cancer cell lines[143]. However, CHOP overexpression might not always have an apoptotic effect, even in the presence of ER stress. Using a CCLx4 model of hepatotoxicity, Campos

and colleagues found evidence of ER stress, CHOP overexpression as well as cell death. However, genetic depletion of *Ddit3* (CHOP) did not protect against CCL4 induced cell death[144]. This implies that CHOP upregulation may have other significance aside apoptosis, especially in the liver.

Results from the lipidomics analysis may in part, explain the *Bap1* suppression dependent hepatic fatality I observed in CD-HFD fed mice. Diacylglycerol's accumulation is considered toxic[145] . The increase in diacylglycerols and concomitant decrease in triacyclglycerols may be due to downregulation of *Dgat2* (which catalyzes the formation of triacyclglycerols), as reported in the transcriptomic analysis. In agreement with this hypothesis, *Dgat2* inhibition utilizing antisense oligonucleotides led to a 45% decrease in hepatic diglycerides level in mice[146]. In another study , cardiac tissue restricted *Dgat2* knockout led to reduction of cardiac triacylglycerol levels[147].

These studies, as well as the current study imply TAG levels may be affected by *Dgat2* status in mice. Reduction in TAGs likely means more free fatty acid in the lipidome. Accordingly, fatty acid levels, including Palmitic acid were generally elevated upon *Bap1* repression and CD-HFD treatment. Several studies have implicated palmitic acid accumulation in pulmonary ER stress[148], lipotoxicity and apoptosis[149]. In agreement, using human hepatic cell lines, Ricchi et al also found a lipotoxic role for palmitic acid[150].

It is difficult to delineate if the ER stress and deregulated lipidomics I observed here is a cause or consequence of one another. It would be tempting to disrupt the ER stress pathway and access if it has a direct role on the observed effect. However, such studies are difficult to carry out *in-vivo*. The fatal outcome associated with coupling *Bap1* repression with metabolic distress (CD-HFD or HFD) was attenuated upon *Bap1* restoration. Reduced CHOP levels in the restored cohort imply attenuation of ER stress and UPR and implicate BAP1 as a critical controller of this effect.

The damage attenuation effect upon *Bap1* restoration is visible not only in survival analysis but also in reduced bilirubin and transaminases measurements. Bilirubin measurements were particularly high (up to 10-fold higher) in *Bap1* repressed samples. High Bilirubin levels are an indication of liver disease and may be deleterious to hepatocytes[126]. The restoration of bilirubin measurements to homeostatic levels upon *Bap1* restoration suggests the fatal outcome observed here might involve bilirubin. BAP1 deficiency has been implicated in metabolism related processes from hepatic glucose and cholesterol metabolism[133] to a Warburg effect related metabolism disruption[151]. Thus, it is

instructive to wonder if BAP1 deficiency have a similar effect on bilirubin metabolism. Studies designed to elucidate the relationship between BAP1 deficiency and bilirubin metabolism in a metabolic distress context would help to shed light on the issue.

5.3 Loss of *Bap1* is essential for YAP driven tumorigenesis

Results from this study shed light on the tumor suppressive and tumor promoting function of *Bap1* loss in the context of YAP driven tumorigenesis. *Bap1* loss co-operates with oncogenic YAP activation to initiate liver tumorigenesis. Further, *Bap1* loss accelerates *Pten* loss and YAP activation driven tumorigenesis. While the results I obtained in this study support the notion that *Bap1* is a tumor suppressor or at least the possibility that *Bap1* loss is a tumor initiating event, a few studies have ascribed pro-oncogenic functions to BAP1. In a recent study by Park et al , *BAP1* was implicated to possess tumor promoting properties through its regulation of epithelial mesenchymal transition in prostate cancer cell lines[152]. Other studies have attributed similar oncogenic properties to *BAP1* in uveal melanoma[153] and breast cancer[154].

That foregoing notwithstanding, the bulk of evidence from literature supports the notion that *BAP1* is a tumor suppressor in many tissues. Sequencing efforts have highlighted the prevalence of *BAP1* inactivating mutations in diverse tumor entities such as melanoma, mesothelioma, renal clear cell carcinoma and intrahepatic cholangiocarcinoma[89, 128, 131, 155]. The tumor suppressive functions of BAP1 have been widely studied in different tissues and different contexts. For instance, in iCCA cell lines, BAP1 was implicated in tumor suppression by modulating the ERK 1/ 2 and JNK/c-Jun pathways[156]. Using a constitutively active oncogenic BRAF ($BRAF^{V600E}$) and ultra-violet (UV), Webster and colleagues were able to demonstrate the tumor suppressive role of *Bap1* in melanoma albeit with a low penetrance[157]. *Bap1* loss driven melanomas are characterized by increased DNA damage and hyper-ubiquitination of H2A, highlighting these events as molecular hallmarks of *Bap1* null tumors[157].

Using fibroblast derived from carriers of *BAP1* heterozygous germline mutations, Bononi *et al* highlighted impaired apoptosis occasioned by reduced IP3R3 levels and Ca^{2+} flux as responsible for subsequent cellular transformation upon exposure to environmental stress such as ionizing radiation and asbestos. Together, these studies demonstrate that BAP1 functions (either as tumor suppressive or pro-oncogenic ones) may be entirely context dependent and should be interpreted as such.

Mouse studies in agreement with the current study demonstrating the co-operation between *Bap1* loss and YAP activation (a proxy for deregulated hippo signaling) have been reported. Interestingly, *Bap1* genetic depletion has been demonstrated to co-operate with oncogenic $KRAS^{G12D}$ to drive pancreatic adenocarcinoma with tumors exhibiting deregulated hippo signaling[158]. There are fewer studies demonstrating the tumor suppressive or tumor initiation function of *Bap1* in the liver. Human liver organoids transformed with a cocktail comprising of *BAP1* loss as well as *TP53*, *PTEN*, *SMAD4*, and *NF1* mutations led to the acquisition of malignant features after xenotransplantation in immunocompromised mice[138]. The number of cells transforming events utilized in the above cited study makes it difficult to pinpoint which of the mutations actually co-operates with *BAP1* loss. The relevance and novelty of the current study is thus highlighted by the discovery of minimum number of decipherable oncogenic events that co-operates with *Bap1* loss. In the current study, I demonstrated the co-operation of *Bap1* loss with *Pten* loss in malignant transformation of hepatocyte and in oncogenic YAP driven liver tumorigenesis. Supporting the results I obtained in this study, BAP1 has been reported to have a stabilizing effect on PTEN. In prostate cancer cell lines, PTEN degradation was demonstrably inhibited through the deubiquitinase activity of BAP1 [159]. Repression of BAP1 in this setting leads to decrease of PTEN protein and activation of the Akt signaling axis and promoting malignant transformation and metastasis, thereby highlighting the tumor suppression role of the BAP1-PTEN axis. Mechanistic studies designed to shed more light on the tumor suppressive co-operation between BAP1 and PTEN deficiency as well as the molecular interaction between *Bap1* loss and YAP oncogenic activation will help push this field forward.

5.4 Role of BAP1 in liver cancer plasticity

Utilizing CRISPR-Cas9 mediated transformation of hepatocytes, I demonstrated lineage switch of transformed hepatocytes into iCCA like tumors. The switching or plasticity inducing combination includes *Bap1* loss, *Arid1a* loss and oncogenic YAP activation. Current literature points to the fact that the liver is a plastic organ. In certain contexts such as organoid culture system containing insulin and epidermal growth factors[160], as well as during bile duct ligation and toxic biliary injury[161] mature hepatocytes can transdifferentiate into cholangiocytes[160]. These discoveries probably begged the question whether hepatocytes contribute to what is thought to be cholangiocytes derived iCCA. Using mouse models several studies reported that transdifferentiated hepatocytes can give rise to iCCA by relying on NICD as a cell fate switch [86-88].However, hepatocyte to cholangiocyte conversion during liver tumorigenesis has also been described

independent of NICD. Hill *et al* reported iCCA derived from hepatocytes by employing a mouse model of liver injury coupled with *Trp53* loss and oncogenic KRAS activation[162]. Together these studies highlight the plasticity of the liver in liver cancer development.

It is currently unclear why *Bap1* loss and *Arid1a* loss co-operate with oncogenic YAP to trigger iCCA like liver cancer. ARID1A containing SWF/SNF complex has been suggested to have inhibitory properties on YAP[163], thus inactivated ARID1A should enable the release oncogenic of YAP. On the other hand, deregulation of the hippo pathway, through persistent activation of YAP has been demonstrated to sufficiently initiate de-differentiation of hepatocytes into a progenitor like state[86, 164].

Thus, it is instructive to speculate here that *Arid1a* loss and YAP^{S127a} prime hepatocyte towards a progenitor-like state, while additional loss of *Bap1*, with mutational prevalence in iCCA[131] then pushes the de-differentiated hepatocytes into a cholangiocytic like state which is then manifested as iCCA like tumors. Testing this hypothesis using novel mouse models would help illuminate the problem. For example, utilizing a dox inducible model of *Bap1* repression in an *Arid1a* loss and oncogenic YAP setting would help provide proof as to whether *Bap1* loss is responsible for the phenotypic switch by simple withdrawal of dox. Further, utilizing cell lines derived from this temporally regulated hypothetical mouse model would help provide a further mechanistic proof of the molecular interaction between BAP1 deficiency, *Arid1a* loss and oncogenic YAP.

5.5 BAP1 status is dynamically inversely correlated with CHOP expression

One of the seminal findings I demonstrated in this study is the inverse correlation between BAP1 status and CHOP expression in all contexts investigated. From metabolic distress (CD-HFD) to tumorigenesis and lineage switch contexts, BAP1 deficiency leads to CHOP induction. Accordingly, restoration of *Bap1 in-vitro* and *in-vivo* antagonizes CHOP induction. Supporting this observation, a direct inhibitory relationship between BAP1 and CHOP has been reported in kidney cell lines utilizing glucose starvation to induce ER stress[118]. Of note, this relationship was established *in-vitro.*

Considering the strong correlation between CHOP and BAP1 in all the context investigated in this study, it is tempting to speculate that perhaps CHOP overexpression after *Bap1* loss might fuel BAP1 deficiency dependent tumorigenesis. Although testing this hypothesis utilizing *in-vivo* CRISPR-Cas9 mediated simultaneous disruption of *Ddit3* (gene encoding

CHOP) and *Bap1* was inconclusive in the current study, utilizing a tighter system may yet shed more light on the issue.

Moreso, the preferential overexpression of CHOP in BAP1 deficient liver tumors may present a rare therapeutic opportunity. Developing therapeutic antibodies against CHOP (or potentially its induced downstream targets, if any) may represent a useful personalized treatment option for BAP1 deficient liver tumors. I propose that CHOP overexpression be considered a hallmark of BAP1 deficient tumors and utilized clinically as a biomarker for *BAP1* loss driven tumors. Further experiments testing the BAP1-CHOP inverse relationship in human liver tumor samples are required to validate this proposal.

5.6 BAP1 deficiency opens up a therapeutic opportunity in *TP53* null tumors

Investigating the striking lack of co-occurrence of *BAP1* and *TP53* mutations, despite their respective high prevalence in liver, I made a novel discovery. Utilizing *in-vivo* and *in-vitro* system respectively, BAP1 deficiency was uncovered as an unexpected therapeutic vulnerability in TP53 null tumors. Further, mechanistic studies utilizing a powerful genetic rescue strategy provided novel evidence implicating BAP1 catalytic activity in this genetic vulnerability.

Easily the most mutated gene in human cancers, *TP53*, the so-called guardian of the genome functions in diverse processes such as Apoptosis, Cell cycle signaling and DNA damage response[165]. Due to its role in DNA damage response and repair, it can be assumed that TP53 deficient cells inefficiently repair DNA damage[165]. Accordingly, *Trp53* null cells rely on alternative DNA repair pathways mediated by Ataxia-telangiectasia mutated (ATM) to ensure survival after DNA damage[166]. In the same vein, BAP1 is important in the DNA repair machinery. BAP1 mediates the accumulation of DNA repair factors such as BRCA1 and RAD51 at sites of DNA damage[167, 168].

BAP1 itself has been demonstrated to be recruited to DNA damage foci where it deubiquitylates Ub-H2AK119 in a poly (ADP ribose) polymerase 1 and 2 (PARP) dependent manner[168]. In agreement, BAP1 deficiency has been shown to negatively impact Homologous combination (HR) DNA repair[167, 168]. Yu and colleagues as well as Ismail *et al* independently demonstrated that BAP1 is phosphorylated at DNA damage sites by ATM in a PARP dependent manner[167, 168]. Together, the studies suggests that BAP1 role in DNA damage repair may be dependent on its catalytic function and its

phosphorylation[167, 168], however, its recruitment to site of DNA damage may depend solely on its catalytic function[168].

In view of the foregoing, it is then tempting to speculate that *TP53* null mutations may shift DNA repair protein recruitment on ATM. With an additional BAP1 deficiency, ATM phosphorylation of BAP1 and its recruitment to DNA damage sites is impaired. BAP1 dependent recruitment of DNA repair factors such as BRCA1 and RAD51 is then made impossible, leaving the cells with this double DNA damage response deficiency particularly vulnerable to cell death occasioned by lack of a DNA repair machinery.

BAP1 deficiency has been directly and indirectly utilized as novel tumor vulnerabilities in certain tissues. Probably due to its analogous role to BRCA1 in DNA damage repair and its relationship with PARP 1 and 2, BAP1 deficient tumors respond favorably to PARP inhibition. In a seminal finding, BAP1 deficiency sensitizes renal cell carcinoma cell line to the PARP inhibitor Olaparib[169]. Recently Sabbatino *et al* reported a case of a patient with *BAP1* mutated iCCA who responded positively to PARP inhibition[170]. Despite the foregoing, mesothelioma sensitivity to PARP inhibition is not dependent on BAP1 status[171], thereby raising the possibility that the described vulnerability is tissue dependent.

Another therapeutic avenue in BAP1 deficiency is utilizing the molecular signatures that accompany its mutations. BAP1 deficiency leads to suppression of Polycomb repressive complex 2 (PRC2) targets and accumulation of methylated histone H3 lysine 27 (H3K27)[172, 173]. Accordingly, inhibition of enhancer of zeste homolog 2 (EZH2), a protein component of PRC2 and a catalytic enzyme for H3K27 trimethylation, triggered apoptosis in BAP1 deficient mesothelioma cell lines[172]. A similar study utilizing uveal melanoma cells found no accumulation of methylated upon *BAP1* loss and reported general resistance to EZH2 inhibition regardless of BAP1 status[174]. This serves as a cautionary tale against the generalization of results in different tissues and further highlights the context dependence of BAP1 functions in diverse tumor entities.

The seminal finding, I reported in this thesis opens up new possibilities to utilize genetically conferred vulnerabilities in tumors. Similar to synthetic lethalities, I would imagine that genetically conferred vulnerabilities exist beyond the reported BAP1-TP53 relationship. As a first step, experiments geared towards better understanding the vulnerability reported in this study and its therapeutic utilization has to be carried out. Additionally, tumor suppressor

deficiency screens aimed at unveiling further genetic vulnerability partnerships will help to create a new class of personalized therapies.

5.7 Summary and outlook

Altogether, this study demonstrated the functional consequence of *Bap1* loss in different contexts. While long term suppression of *Bap1* alone resulted in mild pathophysiological changes, its combination with CD-HFD led to acutely fatal outcomes. Accordingly, *Bap1* restoration attenuated liver damage and rescued mice fatality, thereby implicating BAP1 as a guardian of hepatic cell survival in metabolic distress contexts. *Bap1* was also demonstrated as bonafide liver tumor suppressor in YAP oncogenic activation and *Pten* loss driven contexts. Another seminar discovery in this study links *Bap1* loss to liver cancer plasticity. A strong dynamically inverse relationship between *Bap1* loss and CHOP overexpression was also demonstrated. Finally, this study unveiled the unexpected vulnerability conferred by BAP1 deficiency on *TP53*$^{-/-}$ tumors. Here BAP1 deficiency is an Achilles heel of *TP53* null tumors. The novel findings presented in this study highlights BAP1 as a context dependent player in hepatic homeostatic and pathologic settings. This will lay the foundation for further revelatory studies on BAP1 in the liver and beyond.

References

1. Trefts, E., M. Gannon, and D.H. Wasserman, *The liver.* Current Biology, 2017. **27**(21): p. R1147-R1151.
2. Stanger, B.Z., *Cellular homeostasis and repair in the mammalian liver.* Annu Rev Physiol, 2015. **77**: p. 179-200.
3. Vekemans, K. and F. Braet, *Structural and functional aspects of the liver and liver sinusoidal cells in relation to colon carcinoma metastasis.* World journal of gastroenterology, 2005. **11**(33): p. 5095-5102.
4. Schulze, R.J., et al., *The cell biology of the hepatocyte: A membrane trafficking machine.* The Journal of cell biology, 2019. **218**(7): p. 2096-2112.
5. Rui, L., *Energy metabolism in the liver.* Comprehensive Physiology, 2014. **4**(1): p. 177-197.
6. Zhou, Z., M.-J. Xu, and B. Gao, *Hepatocytes: a key cell type for innate immunity.* Cellular & molecular immunology, 2016. **13**(3): p. 301-315.
7. Banales, J.M., et al., *Cholangiocyte pathobiology.* Nat Rev Gastroenterol Hepatol, 2019. **16**(5): p. 269-281.
8. Franchitto, A., et al., *Recent advances on the mechanisms regulating cholangiocyte proliferation and the significance of the neuroendocrine regulation of cholangiocyte pathophysiology.* Ann Transl Med, 2013. **1**(3): p. 27.
9. Maroni, L., et al., *Functional and structural features of cholangiocytes in health and disease.* Cellular and molecular gastroenterology and hepatology, 2015. **1**(4): p. 368-380.
10. Alvaro, D., et al., *Proliferating cholangiocytes: a neuroendocrine compartment in the diseased liver.* Gastroenterology, 2007. **132**(1): p. 415-31.
11. Dixon, L.J., et al., *Kupffer cells in the liver.* Compr Physiol, 2013. **3**(2): p. 785-97.
12. Ju, C., et al., *Protective role of Kupffer cells in acetaminophen-induced hepatic injury in mice.* Chem Res Toxicol, 2002. **15**(12): p. 1504-13.
13. Ramachandran, P. and J.P. Iredale, *Macrophages: central regulators of hepatic fibrogenesis and fibrosis resolution.* J Hepatol, 2012. **56**(6): p. 1417-9.
14. Chiang, D.J., M.T. Pritchard, and L.E. Nagy, *Obesity, diabetes mellitus, and liver fibrosis.* Am J Physiol Gastrointest Liver Physiol, 2011. **300**(5): p. G697-702.
15. Sato, M., S. Suzuki, and H. Senoo, *Hepatic stellate cells: unique characteristics in cell biology and phenotype.* Cell Struct Funct, 2003. **28**(2): p. 105-12.
16. Yin, C., et al., *Hepatic stellate cells in liver development, regeneration, and cancer.* J Clin Invest, 2013. **123**(5): p. 1902-10.

17. Wilkinson, A.L., M. Qurashi, and S. Shetty, *The Role of Sinusoidal Endothelial Cells in the Axis of Inflammation and Cancer Within the Liver.* Frontiers in Physiology, 2020. **11**(990).
18. Poisson, J., et al., *Liver sinusoidal endothelial cells: Physiology and role in liver diseases.* J Hepatol, 2017. **66**(1): p. 212-227.
19. Kimura, T., et al., *Metabolic Functions of G Protein-Coupled Receptors in Hepatocytes-Potential Applications for Diabetes and NAFLD.* Biomolecules, 2020. **10**(10).
20. Lorente, S., M. Hautefeuille, and A. Sanchez-Cedillo, *The liver, a functionalized vascular structure.* Sci Rep, 2020. **10**(1): p. 16194.
21. Kalra, A., et al., *Physiology, Liver*, in *StatPearls*. 2021, StatPearls Publishing
Copyright © 2021, StatPearls Publishing LLC.: Treasure Island (FL).
22. Kietzmann, T., *Metabolic zonation of the liver: The oxygen gradient revisited.* Redox Biol, 2017. **11**: p. 622-630.
23. Boyer, J.L., *Bile formation and secretion.* Compr Physiol, 2013. **3**(3): p. 1035-78.
24. Asrani, S.K., et al., *Burden of liver diseases in the world.* J Hepatol, 2019. **70**(1): p. 151-171.
25. Wang, F.S., et al., *The global burden of liver disease: the major impact of China.* Hepatology, 2014. **60**(6): p. 2099-108.
26. Blachier, M., et al., *The burden of liver disease in Europe: a review of available epidemiological data.* J Hepatol, 2013. **58**(3): p. 593-608.
27. Seitz, H.K., et al., *Alcoholic liver disease.* Nature Reviews Disease Primers, 2018. **4**(1): p. 16.
28. Singal, A.K., et al., *ACG Clinical Guideline: Alcoholic Liver Disease.* The American journal of gastroenterology, 2018. **113**(2): p. 175-194.
29. Osna, N.A., T.M. Donohue, Jr., and K.K. Kharbanda, *Alcoholic Liver Disease: Pathogenesis and Current Management.* Alcohol research : current reviews, 2017. **38**(2): p. 147-161.
30. Lieber, C.S., *Alcoholic fatty liver: its pathogenesis and mechanism of progression to inflammation and fibrosis.* Alcohol, 2004. **34**(1): p. 9-19.
31. Teli, M.R., et al., *Determinants of progression to cirrhosis or fibrosis in pure alcoholic fatty liver.* Lancet, 1995. **346**(8981): p. 987-90.
32. Benedict, M. and X. Zhang, *Non-alcoholic fatty liver disease: An expanded review.* World J Hepatol, 2017. **9**(16): p. 715-732.
33. Rooks, M.G. and W.S. Garrett, *Gut microbiota, metabolites and host immunity.* Nat Rev Immunol, 2016. **16**(6): p. 341-52.

34. Huang, D.Q., H.B. El-Serag, and R. Loomba, *Global epidemiology of NAFLD-related HCC: trends, predictions, risk factors and prevention.* Nat Rev Gastroenterol Hepatol, 2021. **18**(4): p. 223-238.
35. Anstee, Q.M., et al., *From NASH to HCC: current concepts and future challenges.* Nat Rev Gastroenterol Hepatol, 2019. **16**(7): p. 411-428.
36. Chalasani, N., et al., *The diagnosis and management of nonalcoholic fatty liver disease: Practice guidance from the American Association for the Study of Liver Diseases.* Hepatology, 2018. **67**(1): p. 328-357.
37. Younossi, Z., et al., *Global burden of NAFLD and NASH: trends, predictions, risk factors and prevention.* Nat Rev Gastroenterol Hepatol, 2018. **15**(1): p. 11-20.
38. Younossi, Z.M., et al., *From NAFLD to MAFLD: Implications of a Premature Change in Terminology.* Hepatology, 2021. **73**(3): p. 1194-1198.
39. Fang, Y.L., et al., *Pathogenesis of non-alcoholic fatty liver disease in children and adolescence: From "two hit theory" to "multiple hit model".* World J Gastroenterol, 2018. **24**(27): p. 2974-2983.
40. Dowman, J.K., J.W. Tomlinson, and P.N. Newsome, *Pathogenesis of non-alcoholic fatty liver disease.* Qjm, 2010. **103**(2): p. 71-83.
41. Takaki, A., D. Kawai, and K. Yamamoto, *Multiple hits, including oxidative stress, as pathogenesis and treatment target in non-alcoholic steatohepatitis (NASH).* Int J Mol Sci, 2013. **14**(10): p. 20704-28.
42. Byrne, C.D. and G. Targher, *NAFLD: a multisystem disease.* J Hepatol, 2015. **62**(1 Suppl): p. S47-64.
43. Kitade, H., et al., *Nonalcoholic Fatty Liver Disease and Insulin Resistance: New Insights and Potential New Treatments.* Nutrients, 2017. **9**(4).
44. Watt, M.J., et al., *The Liver as an Endocrine Organ-Linking NAFLD and Insulin Resistance.* Endocr Rev, 2019. **40**(5): p. 1367-1393.
45. Kaps, L., et al., *Non-alcoholic fatty liver disease increases the risk of incident chronic kidney disease.* United European Gastroenterol J, 2020. **8**(8): p. 942-948.
46. Buzzetti, E., M. Pinzani, and E.A. Tsochatzis, *The multiple-hit pathogenesis of non-alcoholic fatty liver disease (NAFLD).* Metabolism, 2016. **65**(8): p. 1038-48.
47. Cusi, K., *Role of insulin resistance and lipotoxicity in non-alcoholic steatohepatitis.* Clin Liver Dis, 2009. **13**(4): p. 545-63.
48. Kirpich, I.A., L.S. Marsano, and C.J. McClain, *Gut-liver axis, nutrition, and non-alcoholic fatty liver disease.* Clin Biochem, 2015. **48**(13-14): p. 923-30.

49. Ni, Y., et al., *Novel Action of Carotenoids on Non-Alcoholic Fatty Liver Disease: Macrophage Polarization and Liver Homeostasis.* Nutrients, 2016. **8**(7).
50. Friedman, S.L., *Liver fibrosis -- from bench to bedside.* J Hepatol, 2003. **38 Suppl 1**: p. S38-53.
51. Kisseleva, T. and D. Brenner, *Molecular and cellular mechanisms of liver fibrosis and its regression.* Nat Rev Gastroenterol Hepatol, 2021. **18**(3): p. 151-166.
52. Bataller, R. and D.A. Brenner, *Liver fibrosis.* J Clin Invest, 2005. **115**(2): p. 209-18.
53. Hernandez-Gea, V. and S.L. Friedman, *Pathogenesis of liver fibrosis.* Annu Rev Pathol, 2011. **6**: p. 425-56.
54. Xu, R., Z. Zhang, and F.S. Wang, *Liver fibrosis: mechanisms of immune-mediated liver injury.* Cell Mol Immunol, 2012. **9**(4): p. 296-301.
55. Friedman, S.L., *Mechanisms of hepatic fibrogenesis.* Gastroenterology, 2008. **134**(6): p. 1655-69.
56. Liu, Y., et al., *IL-13 induces connective tissue growth factor in rat hepatic stellate cells via TGF-β-independent Smad signaling.* J Immunol, 2011. **187**(5): p. 2814-23.
57. Meng, F., et al., *Interleukin-17 signaling in inflammatory, Kupffer cells, and hepatic stellate cells exacerbates liver fibrosis in mice.* Gastroenterology, 2012. **143**(3): p. 765-776.e3.
58. Iredale, J.P., *Models of liver fibrosis: exploring the dynamic nature of inflammation and repair in a solid organ.* J Clin Invest, 2007. **117**(3): p. 539-48.
59. Fujiwara, N., et al., *Risk factors and prevention of hepatocellular carcinoma in the era of precision medicine.* J Hepatol, 2018. **68**(3): p. 526-549.
60. Pinter, M., et al., *Cancer and liver cirrhosis: implications on prognosis and management.* ESMO open, 2016. **1**(2): p. e000042-e000042.
61. Feng, M., et al., *Therapy of Primary Liver Cancer.* Innovation (N Y), 2020. **1**(2): p. 100032.
62. Shaib, Y. and H.B. El-Serag, *The epidemiology of cholangiocarcinoma.* Semin Liver Dis, 2004. **24**(2): p. 115-25.
63. Liu, C.Y., K.F. Chen, and P.J. Chen, *Treatment of Liver Cancer.* Cold Spring Harb Perspect Med, 2015. **5**(9): p. a021535.
64. Bray, F., et al., *Global cancer statistics 2018: GLOBOCAN estimates of incidence and mortality worldwide for 36 cancers in 185 countries.* CA Cancer J Clin, 2018. **68**(6): p. 394-424.
65. Singal, A.G., P. Lampertico, and P. Nahon, *Epidemiology and surveillance for hepatocellular carcinoma: New trends.* J Hepatol, 2020. **72**(2): p. 250-261.
66. McGlynn, K.A., J.L. Petrick, and H.B. El-Serag, *Epidemiology of Hepatocellular Carcinoma.* Hepatology, 2021. **73 Suppl 1**(Suppl 1): p. 4-13.

67. Petrick, J.L., et al., *International trends in hepatocellular carcinoma incidence, 1978-2012.* Int J Cancer, 2020. **147**(2): p. 317-330.
68. Yang, J.D., et al., *A global view of hepatocellular carcinoma: trends, risk, prevention and management.* Nat Rev Gastroenterol Hepatol, 2019. **16**(10): p. 589-604.
69. Suresh, D., A.N. Srinivas, and D.P. Kumar, *Etiology of Hepatocellular Carcinoma: Special Focus on Fatty Liver Disease.* Frontiers in Oncology, 2020. **10**: p. 2673.
70. Sagnelli, E., et al., *Epidemiological and etiological variations in hepatocellular carcinoma.* Infection, 2020. **48**(1): p. 7-17.
71. Dhanasekaran, R., S. Bandoh, and L.R. Roberts, *Molecular pathogenesis of hepatocellular carcinoma and impact of therapeutic advances.* F1000Res, 2016. **5**.
72. Ho, D.W.-H., et al., *Molecular Pathogenesis of Hepatocellular Carcinoma.* Liver cancer, 2016. **5**(4): p. 290-302.
73. Ozturk, M., *p53 mutation in hepatocellular carcinoma after aflatoxin exposure.* Lancet, 1991. **338**(8779): p. 1356-9.
74. Guichard, C., et al., *Integrated analysis of somatic mutations and focal copy-number changes identifies key genes and pathways in hepatocellular carcinoma.* Nat Genet, 2012. **44**(6): p. 694-8.
75. Hernandez-Gea, V., et al., *Role of the microenvironment in the pathogenesis and treatment of hepatocellular carcinoma.* Gastroenterology, 2013. **144**(3): p. 512-27.
76. Budhu, A., et al., *Prediction of venous metastases, recurrence, and prognosis in hepatocellular carcinoma based on a unique immune response signature of the liver microenvironment.* Cancer Cell, 2006. **10**(2): p. 99-111.
77. Macek Jilkova, Z., K. Kurma, and T. Decaens, *Animal Models of Hepatocellular Carcinoma: The Role of Immune System and Tumor Microenvironment.* Cancers (Basel), 2019. **11**(10).
78. Shibata, T., Y. Arai, and Y. Totoki, *Molecular genomic landscapes of hepatobiliary cancer.* Cancer Sci, 2018. **109**(5): p. 1282-1291.
79. Maithel, S.K., et al., *Multidisciplinary approaches to intrahepatic cholangiocarcinoma.* Cancer, 2013. **119**(22): p. 3929-42.
80. Gupta, A. and E. Dixon, *Epidemiology and risk factors: intrahepatic cholangiocarcinoma.* Hepatobiliary surgery and nutrition, 2017. **6**(2): p. 101-104.
81. Dodson, R.M., et al., *Intrahepatic cholangiocarcinoma: management options and emerging therapies.* J Am Coll Surg, 2013. **217**(4): p. 736-750.e4.

82. Massarweh, N.N. and H.B. El-Serag, *Epidemiology of Hepatocellular Carcinoma and Intrahepatic Cholangiocarcinoma.* Cancer control : journal of the Moffitt Cancer Center, 2017. **24**(3): p. 1073274817729245-1073274817729245.
83. Saleh, M., et al., *Intrahepatic cholangiocarcinoma: pathogenesis, current staging, and radiological findings.* Abdom Radiol (NY), 2020. **45**(11): p. 3662-3680.
84. Sia, D., et al., *Intrahepatic cholangiocarcinoma: pathogenesis and rationale for molecular therapies.* Oncogene, 2013. **32**(41): p. 4861-70.
85. Labib, P.L., G. Goodchild, and S.P. Pereira, *Molecular Pathogenesis of Cholangiocarcinoma.* BMC Cancer, 2019. **19**(1): p. 185.
86. Tschaharganeh, D.F., et al., *p53-dependent Nestin regulation links tumor suppression to cellular plasticity in liver cancer.* Cell, 2014. **158**(3): p. 579-92.
87. Sekiya, S. and A. Suzuki, *Intrahepatic cholangiocarcinoma can arise from Notch-mediated conversion of hepatocytes.* J Clin Invest, 2012. **122**(11): p. 3914-8.
88. Fan, B., et al., *Cholangiocarcinomas can originate from hepatocytes in mice.* The Journal of clinical investigation, 2012. **122**(8): p. 2911-2915.
89. Jiao, Y., et al., *Exome sequencing identifies frequent inactivating mutations in BAP1, ARID1A and PBRM1 in intrahepatic cholangiocarcinomas.* Nat Genet, 2013. **45**(12): p. 1470-1473.
90. Simbolo, M., et al., *Multigene mutational profiling of cholangiocarcinomas identifies actionable molecular subgroups.* Oncotarget, 2014. **5**(9): p. 2839-52.
91. Ma, B., et al., *Distinct clinical and prognostic implication of IDH1/2 mutation and other most frequent mutations in large duct and small duct subtypes of intrahepatic cholangiocarcinoma.* BMC Cancer, 2020. **20**(1): p. 318.
92. Pollard, J.W., *Tumour-educated macrophages promote tumour progression and metastasis.* Nat Rev Cancer, 2004. **4**(1): p. 71-8.
93. Llovet, J.M., et al., *Molecular therapies and precision medicine for hepatocellular carcinoma.* Nat Rev Clin Oncol, 2018. **15**(10): p. 599-616.
94. Siegel, R.L., K.D. Miller, and A. Jemal, *Cancer statistics, 2018.* CA Cancer J Clin, 2018. **68**(1): p. 7-30.
95. Llovet, J.M., et al., *Hepatocellular carcinoma.* Nature Reviews Disease Primers, 2021. **7**(1): p. 6.
96. Couri, T. and A. Pillai, *Goals and targets for personalized therapy for HCC.* Hepatology International, 2019. **13**(2): p. 125-137.

97. Wong, R.J., et al., *Increased long-term survival among patients with hepatocellular carcinoma after implementation of Model for End-stage Liver Disease score.* Clin Gastroenterol Hepatol, 2014. **12**(9): p. 1534-40.e1.
98. DeOliveira, M.L., et al., *Cholangiocarcinoma: thirty-one-year experience with 564 patients at a single institution.* Ann Surg, 2007. **245**(5): p. 755-62.
99. Spolverato, G., et al., *Can hepatic resection provide a long-term cure for patients with intrahepatic cholangiocarcinoma?* Cancer, 2015. **121**(22): p. 3998-4006.
100. Daher, S., et al., *Current and Future Treatment of Hepatocellular Carcinoma: An Updated Comprehensive Review.* J Clin Transl Hepatol, 2018. **6**(1): p. 69-78.
101. Abou-Alfa, G.K., et al., *Pemigatinib for previously treated, locally advanced or metastatic cholangiocarcinoma: a multicentre, open-label, phase 2 study.* Lancet Oncol, 2020. **21**(5): p. 671-684.
102. Ikenoue, T., et al., *A novel mouse model of intrahepatic cholangiocarcinoma induced by liver-specific Kras activation and Pten deletion.* Sci Rep, 2016. **6**: p. 23899.
103. Carlessi, R., et al., *Mouse Models of Hepatocellular Carcinoma*, in *Hepatocellular Carcinoma*, J.E.E. Tirnitz-Parker, Editor. 2019, Codon Publications
Copyright: The Authors.: Brisbane (AU).
104. Freimuth, J., et al., *Application of magnetic resonance imaging in transgenic and chemical mouse models of hepatocellular carcinoma.* Molecular cancer, 2010. **9**: p. 94-94.
105. Katz, S.F., et al., *Disruption of Trp53 in livers of mice induces formation of carcinomas with bilineal differentiation.* Gastroenterology, 2012. **142**(5): p. 1229-1239.e3.
106. Brown, Z.J., B. Heinrich, and T.F. Greten, *Mouse models of hepatocellular carcinoma: an overview and highlights for immunotherapy research.* Nat Rev Gastroenterol Hepatol, 2018. **15**(9): p. 536-554.
107. Zhang, G., V. Budker, and J.A. Wolff, *High levels of foreign gene expression in hepatocytes after tail vein injections of naked plasmid DNA.* Hum Gene Ther, 1999. **10**(10): p. 1735-7.
108. Kovacsics, D. and J. Raper, *Transient expression of proteins by hydrodynamic gene delivery in mice.* J Vis Exp, 2014(87).
109. Liu, F., Y. Song, and D. Liu, *Hydrodynamics-based transfection in animals by systemic administration of plasmid DNA.* Gene Ther, 1999. **6**(7): p. 1258-66.
110. Zhang, G., et al., *Hydroporation as the mechanism of hydrodynamic delivery.* Gene Ther, 2004. **11**(8): p. 675-82.
111. Dupuy, A.J., et al., *Mammalian mutagenesis using a highly mobile somatic Sleeping Beauty transposon system.* Nature, 2005. **436**(7048): p. 221-226.

112. Louie, B.H. and R. Kurzrock, *BAP1: Not just a BRCA1-associated protein.* Cancer Treat Rev, 2020. **90**: p. 102091.
113. Masclef, L., et al., *Roles and mechanisms of BAP1 deubiquitinase in tumor suppression.* Cell Death Differ, 2021. **28**(2): p. 606-625.
114. Campagne, A., et al., *BAP1 complex promotes transcription by opposing PRC1-mediated H2A ubiquitylation.* Nat Commun, 2019. **10**(1): p. 348.
115. Wang, L., et al., *Resetting the epigenetic balance of Polycomb and COMPASS function at enhancers for cancer therapy.* Nat Med, 2018. **24**(6): p. 758-769.
116. Nishikawa, H., et al., *BRCA1-associated protein 1 interferes with BRCA1/BARD1 RING heterodimer activity.* Cancer Res, 2009. **69**(1): p. 111-9.
117. Bononi, A., et al., *BAP1 regulates IP3R3-mediated Ca(2+) flux to mitochondria suppressing cell transformation.* Nature, 2017. **546**(7659): p. 549-553.
118. Dai, F., et al., *BAP1 inhibits the ER stress gene regulatory network and modulates metabolic stress response.* Proceedings of the National Academy of Sciences of the United States of America, 2017. **114**(12): p. 3192-3197.
119. Dey, A., et al., *Loss of the tumor suppressor BAP1 causes myeloid transformation.* Science (New York, N.Y.), 2012. **337**(6101): p. 1541-1546.
120. Farzin, M., et al., *Loss of expression of BAP1 predicts longer survival in mesothelioma.* Pathology, 2015. **47**(4): p. 302-7.
121. Jin, S., et al., *Comprehensive Analysis of BAP1 Somatic Mutation in Clear Cell Renal Cell Carcinoma to Explore Potential Mechanisms in Silico.* J Cancer, 2018. **9**(22): p. 4108-4116.
122. Dow, L.E., et al., *Conditional reverse tet-transactivator mouse strains for the efficient induction of TRE-regulated transgenes in mice.* PLoS One, 2014. **9**(4): p. e95236.
123. Dow, L.E., et al., *Apc Restoration Promotes Cellular Differentiation and Reestablishes Crypt Homeostasis in Colorectal Cancer.* Cell, 2015. **161**(7): p. 1539-1552.
124. Feldman, A.T. and D. Wolfe, *Tissue processing and hematoxylin and eosin staining.* Methods Mol Biol, 2014. **1180**: p. 31-43.
125. Goorden, S.M., et al., *[Liver disorders in adults: ALT and AST].* Ned Tijdschr Geneeskd, 2013. **157**(43): p. A6443.
126. Hamoud, A.R., et al., *Bilirubin in the Liver-Gut Signaling Axis.* Trends Endocrinol Metab, 2018. **29**(3): p. 140-150.
127. Del Re, D.P., et al., *Fundamental Mechanisms of Regulated Cell Death and Implications for Heart Disease.* Physiol Rev, 2019. **99**(4): p. 1765-1817.

128. Carbone, M., et al., *Biological Mechanisms and Clinical Significance of BAP1 Mutations in Human Cancer.* Cancer Discov, 2020. **10**(8): p. 1103-1120.
129. Jeong, S.H., et al., *Hippo-mediated suppression of IRS2/AKT signaling prevents hepatic steatosis and liver cancer.* J Clin Invest, 2018. **128**(3): p. 1010-1025.
130. Revia, S., et al., *Histone H3K27 demethylase KDM6A is an epigenetic gatekeeper of mTORC1 signalling in cancer.* Gut, 2021.
131. Jiao, Y., et al., *Exome sequencing identifies frequent inactivating mutations in BAP1, ARID1A and PBRM1 in intrahepatic cholangiocarcinomas.* Nature Genetics, 2013. **45**(12): p. 1470-1473.
132. Nakagawa, H., M. Fujita, and A. Fujimoto, *Genome sequencing analysis of liver cancer for precision medicine.* Seminars in Cancer Biology, 2019. **55**: p. 120-127.
133. Baughman, J.M., et al., *NeuCode Proteomics Reveals Bap1 Regulation of Metabolism.* Cell Rep, 2016. **16**(2): p. 583-595.
134. He, M., et al., *Intrinsic apoptosis shapes the tumor spectrum linked to inactivation of the deubiquitinase BAP1.* Science, 2019. **364**(6437): p. 283-285.
135. Wolf, M.J., et al., *Metabolic activation of intrahepatic CD8+ T cells and NKT cells causes nonalcoholic steatohepatitis and liver cancer via cross-talk with hepatocytes.* Cancer Cell, 2014. **26**(4): p. 549-64.
136. Hebbard, L. and J. George, *Animal models of nonalcoholic fatty liver disease.* Nat Rev Gastroenterol Hepatol, 2011. **8**(1): p. 35-44.
137. Zhang, Y., et al., *BAP1 links metabolic regulation of ferroptosis to tumour suppression.* Nat Cell Biol, 2018. **20**(10): p. 1181-1192.
138. Artegiani, B., et al., *Probing the Tumor Suppressor Function of BAP1 in CRISPR-Engineered Human Liver Organoids.* Cell Stem Cell, 2019. **24**(6): p. 927-943.e6.
139. Tabas, I. and D. Ron, *Integrating the mechanisms of apoptosis induced by endoplasmic reticulum stress.* Nat Cell Biol, 2011. **13**(3): p. 184-90.
140. Galehdar, Z., et al., *Neuronal apoptosis induced by endoplasmic reticulum stress is regulated by ATF4-CHOP-mediated induction of the Bcl-2 homology 3-only member PUMA.* The Journal of neuroscience : the official journal of the Society for Neuroscience, 2010. **30**(50): p. 16938-16948.
141. Bromati, C.R., et al., *UPR induces transient burst of apoptosis in islets of early lactating rats through reduced AKT phosphorylation via ATF4/CHOP stimulation of TRB3 expression.* Am J Physiol Regul Integr Comp Physiol, 2011. **300**(1): p. R92-100.

142. Chang, C.C., et al., *Tanshinone IIA Facilitates TRAIL Sensitization by Up-regulating DR5 through the ROS-JNK-CHOP Signaling Axis in Human Ovarian Carcinoma Cell Lines.* Chem Res Toxicol, 2015. **28**(8): p. 1574-83.
143. Jung, K.-J., et al., *Carnosic acid sensitized TRAIL-mediated apoptosis through down-regulation of c-FLIP and Bcl-2 expression at the post translational levels and CHOP-dependent up-regulation of DR5, Bim, and PUMA expression in human carcinoma caki cells.* Oncotarget, 2015. **6**(3): p. 1556-1568.
144. Campos, G., et al., *The transcription factor CHOP, a central component of the transcriptional regulatory network induced upon CCl4 intoxication in mouse liver, is not a critical mediator of hepatotoxicity.* Archives of Toxicology, 2014. **88**(6): p. 1267-1280.
145. Wali, J.A., et al., *Cardio-Metabolic Effects of High-Fat Diets and Their Underlying Mechanisms-A Narrative Review.* Nutrients, 2020. **12**(5): p. 1505.
146. Liu, Y., et al., *Knockdown of acyl-CoA:diacylglycerol acyltransferase 2 with antisense oligonucleotide reduces VLDL TG and ApoB secretion in mice.* Biochim Biophys Acta, 2008. **1781**(3): p. 97-104.
147. Roe, N.D., et al., *The Role of Diacylglycerol Acyltransferase (DGAT) 1 and 2 in Cardiac Metabolism and Function.* Scientific Reports, 2018. **8**(1): p. 4983.
148. Chu, S.G., et al., *Palmitic Acid-Rich High-Fat Diet Exacerbates Experimental Pulmonary Fibrosis by Modulating Endoplasmic Reticulum Stress.* Am J Respir Cell Mol Biol, 2019. **61**(6): p. 737-746.
149. Listenberger, L.L., et al., *Triacylglycerols accumulation protects against fatty acid-induced lipotoxicity.* Proceedings of the National Academy of Sciences, 2003. **100**(6): p. 3077.
150. Ricchi, M., et al., *Differential effect of oleic and palmitic acid on lipid accumulation and apoptosis in cultured hepatocytes.* J Gastroenterol Hepatol, 2009. **24**(5): p. 830-40.
151. Bononi, A., et al., *Germline BAP1 mutations induce a Warburg effect.* Cell Death Differ, 2017. **24**(10): p. 1694-1704.
152. Park, C.M., J.E. Lee, and J.H. Kim, *BAP1 functions as a tumor promoter in prostate cancer cells through EMT regulation.* Genetics and molecular biology, 2020. **43**(2): p. e20190328-e20190328.
153. Kumar, R., et al., *BAP1 has a survival role in cutaneous melanoma.* The Journal of investigative dermatology, 2015. **135**(4): p. 1089-1097.
154. Qin, J., et al., *BAP1 promotes breast cancer cell proliferation and metastasis by deubiquitinating KLF5.* Nature communications, 2015. **6**: p. 8471-8471.
155. Neviere, Z., et al., *[Malignant mesothelioma and constitutional BAP1 gene mutations].* Rev Mal Respir, 2019. **36**(2): p. 241-248.

156. Chen, X.X., et al., *BAP1 acts as a tumor suppressor in intrahepatic cholangiocarcinoma by modulating the ERK1/2 and JNK/c-Jun pathways.* Cell Death Dis, 2018. **9**(10): p. 1036.
157. Webster, J.D., et al., *The tumor suppressor BAP1 cooperates with BRAFV600E to promote tumor formation in cutaneous melanoma.* Pigment Cell Melanoma Res, 2019. **32**(2): p. 269-279.
158. Lee, H.J., et al., *The Tumor Suppressor BAP1 Regulates the Hippo Pathway in Pancreatic Ductal Adenocarcinoma.* Cancer Res, 2020. **80**(8): p. 1656-1668.
159. Deng, R., et al., *BAP1 suppresses prostate cancer progression by deubiquitinating and stabilizing PTEN.* Mol Oncol, 2021. **15**(1): p. 279-298.
160. Nishikawa, Y., et al., *Transdifferentiation of mature rat hepatocytes into bile duct-like cells in vitro.* Am J Pathol, 2005. **166**(4): p. 1077-88.
161. Michalopoulos, G.K., L. Barua, and W.C. Bowen, *Transdifferentiation of rat hepatocytes into biliary cells after bile duct ligation and toxic biliary injury.* Hepatology, 2005. **41**(3): p. 535-44.
162. Hill, M.A., et al., *Kras and Tp53 Mutations Cause Cholangiocyte- and Hepatocyte-Derived Cholangiocarcinoma.* Cancer research, 2018. **78**(16): p. 4445-4451.
163. Chang, L., et al., *The SWI/SNF complex is a mechanoregulated inhibitor of YAP and TAZ.* Nature, 2018. **563**(7730): p. 265-269.
164. Yimlamai, D., et al., *Hippo pathway activity influences liver cell fate.* Cell, 2014. **157**(6): p. 1324-1338.
165. Hu, J., et al., *Targeting mutant p53 for cancer therapy: direct and indirect strategies.* Journal of Hematology & Oncology, 2021. **14**(1): p. 157.
166. Reinhardt, H.C., et al., *p53-deficient cells rely on ATM- and ATR-mediated checkpoint signaling through the p38MAPK/MK2 pathway for survival after DNA damage.* Cancer Cell, 2007. **11**(2): p. 175-89.
167. Yu, H., et al., *Tumor suppressor and deubiquitinase BAP1 promotes DNA double-strand break repair.* Proc Natl Acad Sci U S A, 2014. **111**(1): p. 285-90.
168. Ismail, I.H., et al., *Germline mutations in BAP1 impair its function in DNA double-strand break repair.* Cancer Res, 2014. **74**(16): p. 4282-94.
169. Peña-Llopis, S., et al., *BAP1 loss defines a new class of renal cell carcinoma.* Nat Genet, 2012. **44**(7): p. 751-9.
170. Sabbatino, F., et al., *Case Report: BAP1 Mutation and RAD21 Amplification as Predictive Biomarkers to PARP Inhibitor in Metastatic Intrahepatic Cholangiocarcinoma.* Front Oncol, 2020. **10**: p. 567289.

171. Rathkey, D., et al., *Sensitivity of Mesothelioma Cells to PARP Inhibitors Is Not Dependent on BAP1 but Is Enhanced by Temozolomide in Cells With High-Schlafen 11 and Low-O6-methylguanine-DNA Methyltransferase Expression.* J Thorac Oncol, 2020. **15**(5): p. 843-859.
172. LaFave, L.M., et al., *Loss of BAP1 function leads to EZH2-dependent transformation.* Nature medicine, 2015. **21**(11): p. 1344-1349.
173. Yamagishi, M. and K. Uchimaru, *Targeting EZH2 in cancer therapy.* Curr Opin Oncol, 2017. **29**(5): p. 375-381.
174. Schoumacher, M., et al., *Uveal melanoma cells are resistant to EZH2 inhibition regardless of BAP1 status.* Nat Med, 2016. **22**(6): p. 577-8.

Acknowledgements

An incredible journey that started 4 years ago culminated in the writing and finalizing of the thesis. During the course of this thesis, I received immeasurable support from friends, families and colleagues, without which, this moment may never have been actualized.

First and foremost, my sincerest gratitude goes to **Prof. Dr Tschaharganeh** for giving me the opportunity to carry out this amazing project in his laboratory. I appreciate the unique insights he provided, the scientific freedom afforded me to pursue my ideas and most importantly the support to grow in all facets of my professional life. I would also like to thank the members of my thesis advisory committee: **Prof Michael Boutros**, **Prof Volker Lohmann** and **Prof Mathias Heikenwaelder** for their helpful comments, valuable suggestions and scientific support and encouragement during the course of this thesis. I would also like to reiterate my appreciation for Prof Michael Boutros for being part of and chairing my thesis defence committee. I would also like to say thank you to **Prof Peter Angel** and **Dr Wilhelm Palm** for happily accepting to be part of my PhD defence committee.

I would like to specially thank **Prof Mathias Heikenwaelder** for providing scientific support in the form of providing help for IHC staining and providing unrestricted access to the enzyme measurement machine. Your energy and intrinsic motivation helped make this project come to a successful end. I am also thankful to **Prof Britta Bruegger** for helping out with quantifying of the lipidome and answering all my questions regarding lipidomics analysis enthusiastically. Special gratitude to the **CMCP** facility of the pathology institute for their help with tissue processing and IHC stainings.

The successful completion of this project is also down to having amazing colleagues. Many thanks to a colleague turned friend, **Leonardo** for being there all through our 4 years PhD marathon together. Our engaging discussions, your friendly mien and your disposition towards connecting with other has been an unforgettable highlight during my PhD. Thank you for being the fabric that connects the lab together. Special mention to **Aga** for her unparalleled support and kindness during the PhD. Your willingness to help out at all times stands you out as an excellent person, I am indeed grateful. Many thanks to **Yalda** for being there at all times and her calm dispositions towards issues. Having you as an office mate and engaging in stimulating discussions, occasional hangouts and trying out your Persian delicacies is a definite highlight of my PhD.

Special mention to all members of the Tschaharganeh lab for your useful feedbacks and engaging discussions during the course of the thesis. Special thanks to **Kai** and **Lio** for

their technical support and assistance. I would also like to thank **Lena** for her endless support with mice related work.

My appreciation goes to all my friends who have provided material and immaterial support during this thesis. **Dotun**; a friend turned brother, thanks for being there at all times. **Ehis**; your presence even from a distance has been a source of assurance. My genuine appreciation also goes to my family for their unconditional love and support, from my kid Bro **Ayodeji** to big sis **Taiwo** and everyone too numerous to mention.

Finally, I would like to thank my wife **Onyinyechi**, my jewel of inestimable value for her love, kindness and support. Your multifaceted support and contribution are impossible to quantify with words. You coloured my world with your presence and helped me finish the PhD with flourish. Thank you.

Supplementary Data

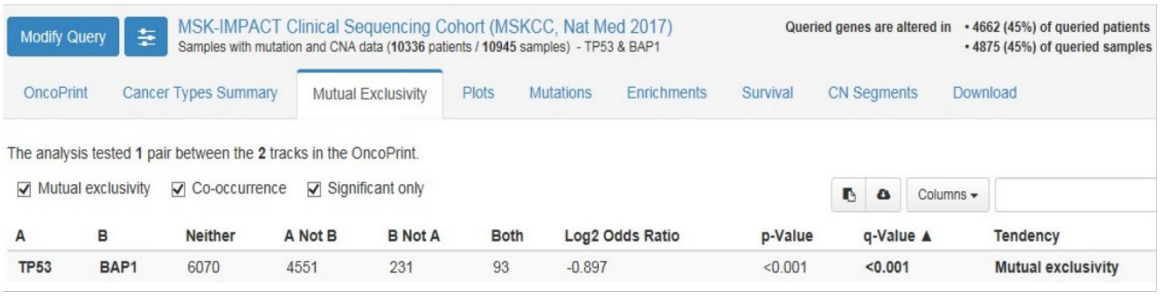

Supplementary figure A: *BAP1* and *TP53* mutations are mutually exclusive in human malignancies. cBioPortal analysis showing mutual exclusivity between BAP1 and TP53 mutations in a MSK-IMPACT (Top) and TCGA hepatocellular carcinoma cohort (Down)